Clara Picareta Branco

Bachelor in Environmental Engineering Sciences

Phosphorus Recovery from Wastewater:

State of the Art Based Design, Sizing and Parametrization of a Crystallization Reactor

Dissertation submitted in partial fulfillment of the requirements
for the degree of

Master of Science in
Environmental Engineering, Sanitary Engineering Profile

Adviser: Professor Doutor Pedro Santos Coelho
Assistant Professor
NOVA University of Lisbon

Co-adviser: Doutor Pedro Póvoa
Asset Management, IT and Innovation Director
Águas do Tejo Atlântico

Examination Committee

Chairperson:
Rapporteurs:

Members:

FACULDADE DE CIÊNCIAS E TECNOLOGIA
UNIVERSIDADE NOVA DE LISBOA

December 2020

Clara Picareta Branco

Bachelor in Environmental Engineering Sciences

Phosphorus Recovery from Wastewater:

State of the Art Based Design, Sizing and Parametrization of a Crystallization Reactor

Dissertation submitted in partial fulfillment of the requirements
for the degree of

Master of Science in
Environmental Engineering, Sanitary Engineering Profile

Adviser: Professor Doutor Pedro Santos Coelho
Assistant Professor
NOVA University of Lisbon

Co-adviser: Doutor Pedro Póvoa
Asset Management, IT and Innovation Director
Águas do Tejo Atlântico

Examination Committee

Chairperson:
Rapporteurs:

Members:

FACULDADE DE CIÊNCIAS E TECNOLOGIA
UNIVERSIDADE NOVA DE LISBOA

December 2020

Phosphorus Recovery from Wastewater: State of the Art Based Design, Sizing and Parametrization of a Crystallization Reactor

Aos meus pais, António e Paula,

por todo o amor e dedicação.

Acknowledgements

The conclusion of the present thesis and thereby, of this academic chapter of my life, could not be done without my expression of gratitude towards all the people who helped me to make it possible.

I would first like to thank my adviser, Professor Pedro Coelho, for having accepted my advising request. For having trust in me, and for all the thorough examinations, advice, and encouragement, thank you. More than your guidance in this thesis, I wish to show my gratitude to all your humanity and counseling along these last years. More than technical knowledge I hope I have, if not learned, at least always kept in mind the two of your major lessons: to think and to keep it simple.

I would also like to pay my special regards to my co-advisor, Doctor Pedro Póvoa. I want to express my gratitude for your patient and pragmatic support and for the immense opportunity I was given. Furthermore, thank you for encouraging me not to be afraid of failing and to go further. I am also indebted to Catarina Pécurto and the operators at Chelas WWTP, for all the interest they showed and their practical advices and support. Being impossible to thank each one individually, I also would like to recognize the invaluable assistance that all the people working at Águas do Tejo Atlântico provided me during my research.

To my family. To my parents, whose investment in my education ultimately resulted in this thesis. This accomplishment is as much yours as it is mine. Thank you for letting me learn what took me three years to realize – that, when given the chance, you should pursue what fulfills you. Upmost, I am everlastingly grateful for giving me that chance twice. To my sister, whose academic commitment and perfectionism has always been an inspiration since I was a child. Thank you for protecting me and for all your help.

To the family I chose and which chose me. To Maria, the most enthusiastic and strong person I know. To Catarina, my forever Erasmus companion and partner in the most humorous disasters. To Ana, for bringing such lightness into my life. To Bea, for being my wastewater buddy and for being the most tolerant person I know. To Simone, the most hard-working one. For all your love and support, thank you. All of you are a source of inspiration to me.

At last, to my boyfriend Gonçalo. You ease my life's less gracious moments and enhance the joyful ones, like no one else. Love is surely the best means to face whatever may come. Your eagerness to do and be better is not only inspirational as it is contagious. For all the above, and for continuously broadening my horizons, thank you. Words will always fail to express my gratefulness that our paths have crossed and of having you in my life.

To all of you, thank you for making me believe that where there is a way, there is a will, no matter the direction.

''Life can multiply until all the phosphorus has gone, and then there is an inexorable halt which nothing can prevent.'' (Asimov, 1974, p. 164)

ABSTRACT

Phosphorous (P) is an essential element for all living organisms. There is no workaround or another element that can be substituted for it. Concurrently, phosphate rock is being increasingly consumed to produce P fertilizer to support global food production. Being a non-renewable and irreplaceable resource, phosphate rock depletion comprises P-scarcity and food security concerns. Potential geopolitical instability of countries producing phosphate also plays a major role in P-scarcity.

While on the one hand, the responsible management of P helps grow the crops needed to feed a growing planet, on the other hand, excess P discharged into water bodies may cause eutrophication and water quality problems related with. Therefore, continuous efforts have been made to decrease P discharge by means of wastewater treatment techniques.

Removing P from wastewater, especially through biological processes, may, however, carry associated problems in wastewater treatment plants (WWTP) as there is a potential for P resolubilization in their sludge handling system. P resolubilization results in P-rich internal streams and increases the P load to be treated. Hence, under favorable conditions, the P resolubilization may involuntarily precipitate struvite, which is usually responsible for clogging pipes and damaging the WWTP equipment.

Interestingly, struvite crystallization is one of the most promising recovery techniques to mitigate or even solve the aforementioned problems in WWTP. Recovering P in the form of struvite, under controlled circumstances, not only prevents unintentional struvite formation and P load increase, as it also produces a slow release fertilizer with a market value. Furthermore, this P-recycling enhances the P-security and the P-loop closure.

Against this background, one of the goals of this dissertation was the designing and sizing of a crystallization reactor that recovers P from wastewater in the form of struvite. Applying an existing methodology to obtain a struvite solubility limit curve, which is of paramount importance for the control parameters of the reactor, was another objective. Other aims were also to understand the fundamental principles of struvite crystallization and to review the struvite recovery technologies most commonly implemented worldwide at full-scale.

The designing and sizing of a crystallization reactor was accomplished in this thesis and the rationale behind it was extensively described. To this end, the technologies review carried out was an invaluable support. As for the fundamental principles of struvite crystallization, they were described comprehensively here, and this allowed to understand the need of a solubility curve for the control parameters of the reactor. Accordingly, such a curve, referring to Chelas WWTP centrate, was determined: a 2nd order polynomial curve fitted the experimental data through an R^2 of 0.96. Consequently, the applied methodology was proven to work with this centrate. Moreover, the application of this procedure allowed to make explicit some important aspects that happen to be not available in the literature. These aspects were also described here.

Keywords: Phosphorus, Wastewater, P-recovery, Struvite precipitation, Reactor, Solubility curve

RESUMO

O fósforo (P) é um elemento essencial a todos os organismos vivos, sem substituto possível. Concomitantemente, o consumo da fosforite intensificou-se como consequência da crescente necessidade de obter fertilizantes para a produção global de alimentos. A fosforite é um recurso não-renovável e insubstituível pelo que a sua potencial exaustão suscita justificadas preocupações ao nível da escassez de P e da segurança alimentar. Adicionalmente, a potencial instabilidade geopolítica dos países produtores de fosfatos desempenha um papel importante na escassez do P.

Se, por um lado, a gestão responsável de P é fundamental na produção agrícola que tem de acautelar o crescimento demográfico global, por outro, a descarga de P, em excesso, em corpos de água, pode causar fenómenos de eutrofização, bem como os consequentes problemas em termos da sua qualidade. Têm sido, por isso, feitos vários esforços no sentido de limitar esta descarga através de técnicas de tratamento de águas residuais.

Contudo, a remoção de P da água residual pode originar problemas nas estações de tratamento de águas residuais (ETAR), especialmente nas que efetuam remoção de nutrientes biologicamente. O tratamento da fase sólida pode potenciar a ressolubilização de P, o que pode resultar em fluxos internos ricos em P e no aumento da carga de P a tratar. Sob condições favoráveis, a ressolubilização de P pode ainda causar a precipitação espontânea de estruvite. que usualmente causa obstrução e danos nas tubagens e equipamentos das ETAR.

Porém, ao mesmo tempo, a recuperação de P na forma de estruvite, em condições controladas, não só previne a incrustação de estruvite e reduz a carga de P a tratar, como permite a produção de um fertilizante de libertação lenta com valor comercial. A cristalização de estruvite é, por isso, uma das técnicas de recuperação mais promissoras. Para além disso, esta reciclagem de P permite aumentar a segurança do P e fechar o seu ciclo.

Neste enquadramento, um dos objetivos desta dissertação foi o desenho e dimensionamento de um reator que permite recuperar P a partir de água residual, na forma de estruvite. A aplicação de uma metodologia existente para obter uma curva limite de solubilidade, que é crucial ao controlo do reator, foi outro objetivo. Adicionalmente, compreender os princípios fundamentais da cristalização da estruvite e elaborar uma revisão de literatura sobre as tecnologias de recuperação de P mais implementadas à escala real foram outros dos objetivos.

Um dos resultados desta dissertação foi o desenho e dimensionamento do reator, cuja justificação foi detalhadamente apresentada. Para o efeito, a revisão de tecnologias realizada foi uma ferramenta auxiliar crucial. No que diz respeito aos princípios fundamentais da formação de estruvite, estes foram descritos de forma extensiva, o que permitiu compreender a necessidade de uma curva de solubilidade para os parâmetros de controlo do reator. Deste modo, determinou-se uma curva de solubilidade, referente às escorrências da desidratação da ETAR de Chelas: uma curva polinomial de 2ª ordem ajustou-se aos dados experimentais através de um R^2 de 0.96. Por conseguinte, a aplicabilidade desta metodologia foi validada para as escorrências em estudo. Para além disso, a aplicação deste procedimento permitiu explicitar alguns aspetos importantes que se encontram omissos na revisão de literatura efetuada. Esses aspetos foram também descritos nesta dissertação.

Palavras-chave: Fósforo (P), Água residual, Recuperação de P, Precipitação de estruvite, Reator, Curva de solubilidade

Contents

List of Figures

List of Tables

Acronyms

ATP - Adenosine Triphosphate

BEPR - Biological Excess Phosphorus Removal

BNR – Biological Nutrient Removal

BOD – Biochemical Oxygen Demand

BPR – Biological Phosphorus Removal

BWB - Berliner Wasserbetriebe

CFD - Computational Fluid Dynamics

CSTR - Continuous Stirred Tank Reactor

DAWWTP - Durham Advanced Wastewater Treatment Plant

DNA - Deoxyribonucleic Acid

EBPR - Enhanced Biological Phosphorus Removal

EDP – Energias de Portugal

ETAR – Estação de Tratamento de Águas Residuais

EU – European Union

FBR – Fluidized Bed Reactor

IAP - Ion Activity Product

ID - Identification

IUPAC - International Union of Pure and Applied Chemistry

LIWWTP - Lulu Island Wastewater Treatment Plant

MGD – Million Gallons per Day

MLD – Megalitres per Day

OECD - Organisation for Economic Co-operation and Development

PAOs - Phosphate Accumulating Organisms

PES - Polyether Sulfone

PHA - poly-β-hydroxyalkanoate

PVC - Polyvinyl Chloride

RNA - Ribonucleic Acid

ROI - Return of Investment

SIMTEJO - Saneamento Integrado dos Municípios do Tejo e Trancão

SR – Sales Revenue

SLR - Surface Loading Rate

SRF – Struvite Recovery Facility

SS – Suspended Solid

SSR – Supersaturation Ratio

UBC - University of British Columbia

UK – United Kingdom

US – United States of America

VFAs - Short Chain Volatile Fatty Acids

WASSTRIP - Waste Activated Sludge Stripping to Remove Internal Phosphorus

WWTP - Wastewater Treatment Plant

CHAPTER 1

INTRODUCTION

1.1 Context

1.1.1 The Dissipative Nature of Phosphorus

Life absolutely requires phosphorus (Daneshgar et al., 2018). There is no workaround or another element that can be substituted for it (Ashley et al., 2011). The biochemist Isaac Asimov further emphasized the irreplaceability of phosphorus and its importance for all biological systems by naming it "life's bottleneck" (Asimov, 1974).

As a matter of fact, biochemically, phosphorus (P) is the basis for all life on our planet (Lehninger, 1973). It is actually a vital component of all living organisms (Daneshgar et al., 2018).

At the molecular level, P is a building substance of DNA and RNA in the form of phosphate ion (orthophosphates) PO_4^{3-} (Daneshgar et al., 2018). As Lehninger (1973) stated, adenosine triphosphate (ATP) is the primary carrier of chemical energy in cells by transferring phosphate groups from energy-yielding to energy-requiring processes. Phospholipids contribute to the formation of cell membranes (Lehninger, 1973).

Besides being a crucial biological element, phosphorus is also an indispensable fertilizer constituent (Scholz et al., 2013). In plants, phosphorus is essential for cell growth and, consequently, fundamental to the growth of fruit, seed development and ripening (Johnston, 2000). Therefore, it has no replacement in food production (Misselhorn et al., 2010).

In the biosphere, animals obtain phosphorus from food, namely, plants or lower trophic-level animals (Johnston, 2000). Plants, in turn, obtain phosphorus from soils (Ashley et al., 2011). Their roots draw from soil the soluble inorganic form of phosphorus, known as orthophosphates, dissolved in soil solution (Johnston, 2000).

Soil phosphorus is either added through fertilizers, manures or organic residues; or is naturally derived from weathered bedrock (Cordell & White, 2014). Bedrock containing phosphorus has taken tens of millions of years to form (Broecker, 1976; Filippelli, 2011; Pierrou, 1976).

From a geochemical point of view, the long-term global phosphorus cycle has four major components: (i) tectonic uplift and exposure of phosphorus-bearing rocks to weathering; (ii) physical erosion and chemical weathering of rocks, producing soils and providing dissolved and particulate phosphorus to rivers; (iii) riverine transport of phosphorus to flood plains, lakes, and oceans; and (iv) sedimentation of phosphorus associated with organic and mineral matter and burial in sediments (Ruttenberg, 2003). According to Ruttenberg (2003), the cycle begins anew with the uplift of sediments into the weathering regime.

For atoms that end up on the seafloor, it takes 10–100 million years before they become re-exposed by tectonic uplift (Scholz, 2019). In contrast, land-based cycling of organic P has rapid turnover times of just around 4 days to 100 years (Smil, 2000).

Indeed, in terrestrial ecosystems in its pre-agricultural age, weathered P atoms cycled many times before erosion and runoff transported particulate and soluble phosphorus to the ocean, or it became unavailable as a result of lithification or leaching processes (Scholz, 2019). To be precise, myriads of small-scale, land-based cycles move phosphates present in soils to plants and then return a large share of the assimilated nutrient back to soils when plant litter, dead microorganisms, and other biomass are mineralized and their elements become available once again for autotrophic production (Smil, 2000). Figure 1.1, which illustrates the natural phosphorus cycle, highlights the aforementioned.

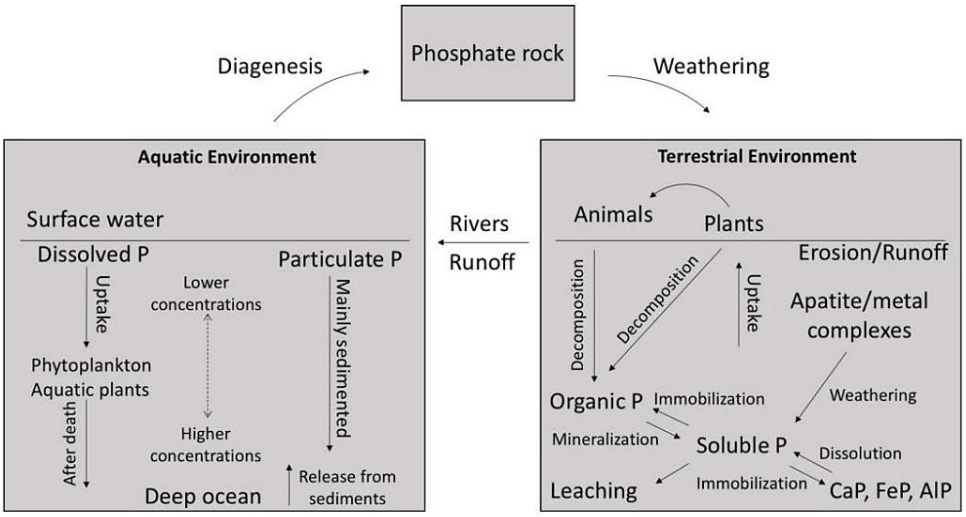

Figure 1.1 - Natural phosphorus cycle in aquatic and terrestrial environments (Daneshgar et al., 2018, based on Filippelli, 2011; Pierrou, 1976).

Nonetheless, terrestrial ecosystems have been fundamentally changed by agricultural activity, particularly the arable land covering approximately 10% of Earth's terrestrial area (Scholz et al., 2014; Smil, 2000). On agricultural land, a larger number of phosphorus atoms do not cycle a single time (Scholz, 2019).

Furthermore, the introduction of mineral phosphorus fertilizer, mainly sourced from mined phosphate rock, enabled the phosphorus which is lost from the soil when crops are harvested to be more easily replaced (Schröder et al., 2010). Actually, food could not be produced at current global levels without the use of processed mineral fertilizers (Cordell & White, 2014). The use of mineral fertilizers led, in general, to less recycling of waste products, for instance, manure and food residues (Schröder et al., 2010).

It should be also noted that, while P flow from food via human excreta typically found its way back to land in the past, presently it more often ends up in water bodies via wastewater from

urban centres or as sludge in landfills (Cordell & White, 2014). This is of major importance since close to 100% of phosphorus eaten in food is excreted (Jönsson et al., 2004), mainly through urine (70%), but also through faeces (30%) (Hruska, 2017).

Moreover, global estimations suggest that about one third of mineral fertilizers are lost by runoff and erosion annually, with phosphorus eventually ending up in the oceans sediment (Scholz et al., 2014; Schröder et al., 2010).

Thus, today, on a human timescale, phosphorus flows have a dissipative nature (Scholz, 2019): P predominantly flows in a one-way direction through the global food system from mines to the oceans via agriculture, at rates over three times the natural flow (Bennett et al., 2001; Lavelle et al., 2005).

1.1.2 Drivers for Phosphorus Recovery

Phosphorus is distributed around the world mostly in the form of minerals contained in sedimentary rocks - phosphate rocks reserves (Daneshgar et al., 2018). Notwithstanding, the availability of high-quality deposits that are *de facto* economically exploitable is not homogeneously worldwide distributed (Daneshgar et al., 2018). The majority of global phosphate rock reserves that are commercially recoverable are located in China, the United States and Morocco/Western Sahara (Rosemarin et al., 2009). Such uneven distribution exists because the combination of physical and chemical conditions associated with coastal upwelling zones, along with geological sea-level changes, is not only essential for the formation of the sedimentary deposits, as it is also rare (Daneshgar et al., 2018).

Additionally, phosphate rock is an irreplaceable, non-renewable resource (Cordell et al., 2009), whose global demand is rising due to a growing world population and increasing food demand (Ridder et al., 2012). It is noteworthy that about 90% of global phosphate rock demand is used for food production (OECD, 2015).

The future trend of phosphate rock production and consumption and, consequently, the question of whether (and when) it will be totally depleted in the future, is currently a controversial issue among researchers (Daneshgar et al., 2018). By the one hand, as global population is expected to grow drastically, demand for phosphorus will increase due to the unavoidable need to produce more food (Daneshgar et al., 2018). On the other hand, there is still a huge amount of phosphate resources unexploited because of the lack of feasible and not over-expensive methods to extract them (Daneshgar et al., 2018).

Both sides of the debate, however, recognize that phosphorus scarcity is not dependent solely on the rate of the resources depletion (Daneshgar et al., 2018). Other factors, which lead phosphate rock to have highly variable value, are also of great importance. These factors include potential geopolitical instability of supplier countries, market price and the time and effort it takes to extract phosphate rock (Daneshgar et al., 2018). For instance, in response to the growing phosphate demand, several producing countries have taken measures to restrict the export of phosphate rock in order to ensure sufficient availability to meet their own needs in the future (Ridder et al., 2012). In 2008, China, imposed a 135% tariff to discourage exports and protect domestic supplies (OECD, 2015). Securing a stable supply of phosphate is, therefore, of paramount importance (OECD, 2015).

For all the aforementioned, P-scarcity constitutes a driving force for recovering P. Figure 1.2 outlines the main uses and points of loss (known as 'sinks') of P. Bubble size represents the amount of phosphate lost.

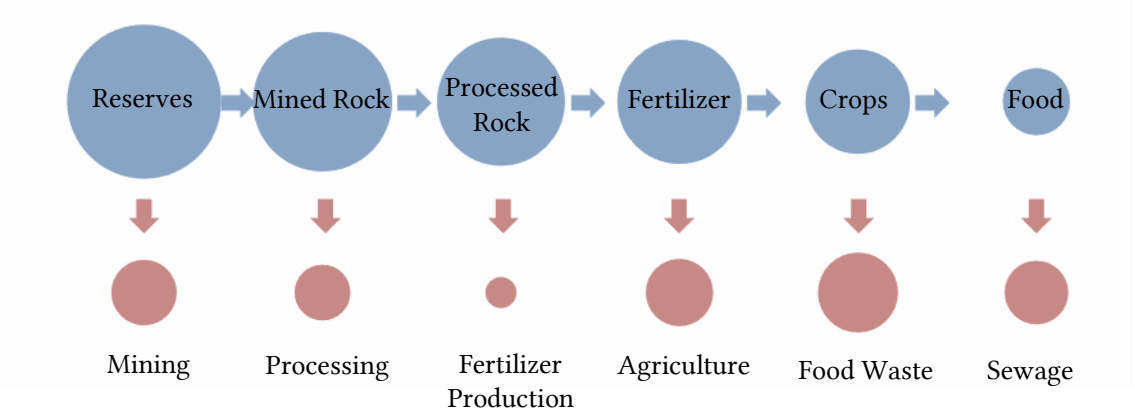

Figure 1.2 - Simplified overview of the main uses and sinks in phosphate use (Ridder et al., 2012).

Figure 1.2 is presented here to illustrate that there are many ways to reduce phosphorus lost, either by recovering it or improving its efficient use.

Paradoxically, although phosphorus is essential to sustaining life, it is also a pollutant (Britton & Baur, 2010). Over time, most of the mined phosphorus enters the ecosystem as waste, leading to excessive nutrient levels in water bodies (Britton & Baur, 2010). This overstimulates algae growth, causing eutrophication, killing off natural aquatic species by consuming too much oxygen in the water, and damaging waters for consumption and recreation (Britton & Baur, 2010). The increasing accumulation of nutrients discharged into the environment was cited by the Millennium Ecosystem Assessment in a 2005 report as one of the most significant environmental challenges facing the planet (Britton & Baur, 2010).

The prevention of phosphorus eutrophication includes the control of this nutrient load in water bodies. The control of P inflow from point sources to aquatic systems has been done by providing urban areas with sewage collection and wastewater treatment systems. In sensitive areas, nutrient removal is required as part of a more advanced treatment in wastewater treatment plants and the plants must comply with stringent discharge limits.

In fact, another main driving force for P-recovery is related to several serious problems plaguing the secondary wastewater treatment plants, especially those that are designed for removing nutrients biologically. These problems have enormous costs associated and render the compliance with nutrient discharge limits harder. Opportunely, these problems can be solved or alleviated through the recovery of P in the form of phosphate salts from streams rich in phosphorus. Struvite is a phosphate salt, constituted by equal molar concentrations of magnesium, ammonia and phosphate, that has been gaining increasing interest.

Crystallization of struvite has been pointed out as a promising technology that can be used to prevent and mitigate the problems associated to wastewater treatment plants using biological nutrient removal processes. Struvite forms spontaneously in wastewater treatment plants and, although uncontrolled formation is a nuisance and the formed struvite has no market value, controlled production of struvite can be applied to recover phosphorus from wastewater.

When the theoretical knowledge on struvite formation is exploited in a practical engineering process, it is possible to economically extract struvite from wastewater in commercial quantities. This has been generally done by precipitating struvite in a dedicated reactor, instead of allowing its spontaneous formation. Several technologies that recover P from wastewater in

the form of struvite have been developed, proven and applied in wastewater treatment plants at full-scale. The obtained struvite is a slow release fertilizer with market value. Moreover, its purity can sometimes be higher than of phosphate rocks. Recovering P in the form of struvite not only allows wastewater treatment plants that remove nutrients to operate smoothly, but also enables the plants to move towards circular economy, since they are able to produce a fertilizer with market value. Circular economy can thus, also be indicated as one of the driving forces for P-recovery.

To sum up, one of the main drivers for P-recovery is P scarcity. Mitigation of problems associated with secondary wastewater treatment plants (especially those using biological nutrient removal processes), and the attainment of a product that has a market value and plays a role in moving towards a circular economy and in closing the P-loop, are also driving forces for recovering P, namely in the form of struvite obtained from wastewater.

1.2 Motivation

The present thesis was conducted in a partnership between "Faculdade de Ciências e Tecnologia and Águas do Tejo Atlântico".

Águas do Tejo Atlântico is responsible for the management and operation of the multi-municipal wastewater sanitation system in Greater Lisbon and the West, in Portugal. The company aims to collect, treat and dispose of domestic and urban wastewater on a regular, continuous and efficient basis, from approximately 2.4 million inhabitants.

Spontaneous struvite scaling is a well-recognized problem in wastewater treatment plants (WWTP). Struvite scaling in the inner walls of piping can narrow the cross section of the flow within the pipe, leading to reduced treatment capacity and higher energy costs to move water through the wastewater treatment process (Antoniewicz, 2018). The gradual accumulation of struvite in pipes, equipment and fittings also leads to high costs due to replacement of parts and the downtime associated (Forrest et al., 2008). Figure 1.3 illustrates a few examples of struvite scaling in a pipeline, heat exchanger and outside of a centrifuge (from left to right). The pictures above represent the pipeline and equipment in the absence of struvite formation, whereas the images beneath depict them after struvite was formed.

Figure 1.3 - Struvite formation in a pipeline, heat exchanger, and outside of a centrifuge (from left to right) (Shanghai Shenglin, n.d.; Struvite Removal, 2020; theapexsolution, 2012).

Recovering phosphorus from wastewater in the form of struvite is a technology that allows to mitigate or even solve the aforementioned problems, and whose adoption should therefore be considered. Furthermore, recovering phosphorus in the form of struvite allows to obtain a fertilizer with market value, promoting the shift towards circular economy.

Removing phosphorus from wastewater in the form of struvite and supporting the adoption of this technology by Águas do Tejo Atlântico provide the motivation for the present thesis.

1.3 Objectives and Outline

With this motivation in view, this thesis aims at contributing the first preparatory steps towards the adoption of this technology, having in view the Chelas wastewater treatment plant, operated by Águas do Tejo Atlântico.

Against this background, this dissertation has the following main goals:

1. To systematically review the fundamental principles of struvite crystallization.
2. To review the struvite recovery technologies most commonly implemented worldwide at full-scale, which have been proven and are commercially established.
3. To design and size a reactor to remove phosphorus from wastewater in the form of struvite.
4. To apply an already existing methodology to obtain a struvite solubility limit curve which is of paramount importance for the control parameters of the reactor.

The accomplishment of these objectives provides the guidelines for the construction of the reactor, already initiated at the time of submitting this thesis, to be installed and operated in Chelas WWTP.

To pursue the aforementioned aims, the rest of the present document is structured as follows:

. Chapter 2: In this chapter, the fundamental principles of struvite crystallization are presented.

. Chapter 3: The biological P removal mechanism is described in this chapter. Also, Chapter 3 delves into the reasons that make it an opportunity for P-recovery in WWTP, more precisely, in the form of struvite.

. Chapter 4: A review, regarding the operation principles of the struvite recovery technologies more commonly implemented at full-scale, is presented here.

. Chapter 5: The rationale behind the sizing of the reactor is detailed in this chapter. The reactor dimensions and specifications are also determined and presented in Chapter 5.

. Chapter 6: In this chapter, a struvite solubility limit curve, for a centrate sample, taken from the centrifuge of Chelas WWTP, is determined by making use of an already existing methodology. A discussion of the obtained results as well as the completion of the methodology is included in this chapter.

. Chapter 7: The final remarks about this dissertation are presented in this chapter. Future developments based on this work are also discussed.

Appendixes B and C exhibit the reactor's photographs during and after construction, respectively.

CHAPTER 2

FUNDAMENTAL PRINCIPLES OF STRUVITE CRYSTALLIZATION

This chapter aims to understand and describe the fundamental principles of struvite crystallization. Based on this acquired theoretical knowledge, it will then be possible to, later on, perceive how these principles can be exploited in practical engineering processes that recover struvite from wastewater in WWTP.

Therefore, Chapter 2 consists of a literature review that addresses struvite's general characteristics and the chemical principles behind its crystallization. Struvite's crystallization mechanism, including the principles and concepts of struvite nucleation and crystal growth, is also discussed in this chapter. Additionally, several factors influencing struvite crystallization are reviewed here.

This literature review is organized in five sections. Section 2.1 describes struvite's properties and characteristics. Section 2.2 explains the chemical principles behind struvite precipitation with focus on struvite's chemical reaction and its solubility product constant. Section 2.3 delves into the mechanisms of struvite crystallization. Section 2.4 examines the parameters proved to have the most influence on struvite crystallization, with emphasis on crystallization from wastewater. At last, the major outcomes of Chapter 2 are outlined in section 2.5.

2.1 Struvite Characteristics

Magnesium ammonium phosphate hexahydrate, or struvite, as it is more commonly called, is a white to yellowish crystal (Chirmuley, 1994; Li, Huang, et al., 2019). Struvite is a crystal which is formed with an equal molar concentration of magnesium, ammonium, and phosphate combined with six water molecules ($MgNH_4PO_4 \cdot 6H_2O$) (Rahman et al., 2014).

The crystal consists of PO_4^{3-} (tetrahedral), $Mg(6H_2O)^{2+}$ (octahedral), and NH_4^+ (tetrahedral) groups which are held together by hydrogen bonds, as Figure 2.1 (a) depicts (Whitaker & Jeffery, 1970). Magnesium is located in the centre, with a hydration shell of six water molecules (only five shown in Figure 2.1 (a)). Struvite crystallizes as an orthorhombic structure, i.e., straight prisms with a rectangular base (Le Corre et al., 2009) – see Figure 2.1 (b).

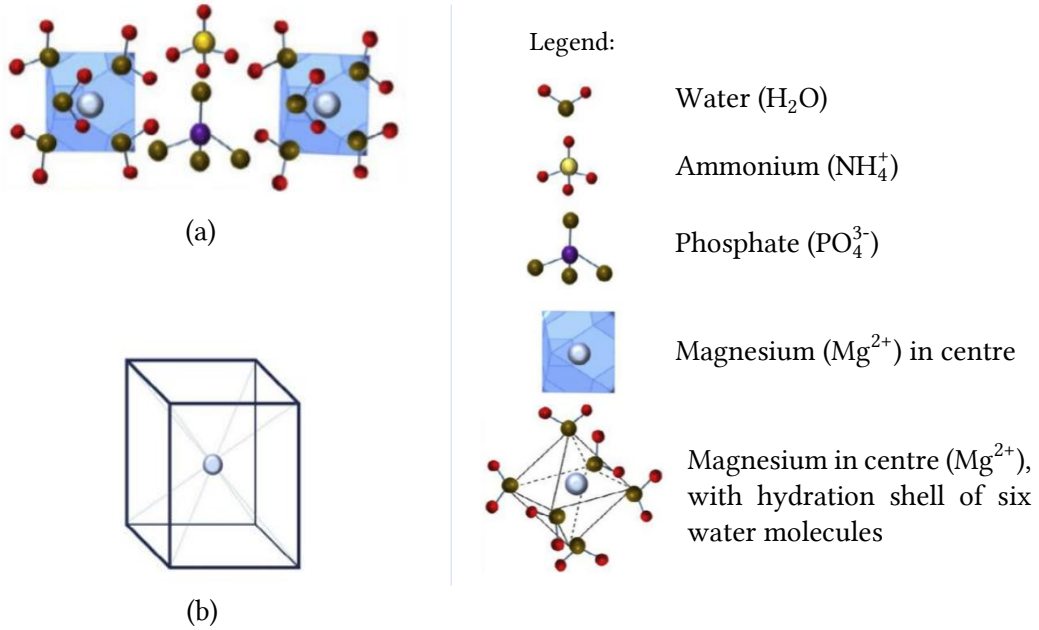

Figure 2.1 - Struvite crystal structure: (a) arrangement of ionic groups and (b) orthorhombic geometry of struvite crystal (adapted from Whitaker & Jeffery, 1970).

The crystal has a molecular weight of 245.43 $g.mol^{-1}$ and a density of 1.711 $g.\ cm^{-3}$ (Borgerding, 1972; Chirmuley, 1994). It is highly insoluble under neutral and alkaline conditions, but highly soluble at acidic pH (Chirmuley, 1994; Tansel et al., 2018). Struvite has a low solubility in water of about 160 mg per litre at 25°C (Chirmuley, 1994).

Struvite occurs as white crystalline powder, but can also occur in other forms such as large single crystals or very small crystals, as Figure 2.2 illustrates (Münch & Barr, 2001).

Figure 2.2 - Struvite's various forms: (a) white powder (van Loosdrecht & Brdjanovic, 2014), (b) large crystals (Pinfa, 2019) and (c) small crystals (Rempel, n.d.).

Struvite crystals form spontaneously in various biological media (Le Corre et al., 2009). For instance, it has been found in rotting organic material such as guano deposits and cow manure (B. Omar et al., 1994). In these cases, struvite is produced through the microbiological combination of ions from bacterial metabolisms with magnesium and phosphorus already present in the media (B. Omar et al., 1994). Struvite also forms in aqueous systems with high ammonia and phosphate level, such as wastewater (Tansel et al., 2018). Scale formation of struvite is frequently found in wastewater treatment plant facilities (Bayuseno et al., 2020).

Struvite is a phosphate mineral and also an effective fertilizer (Li, Huang, et al., 2019; Rahman et al., 2014). It has the advantages of being composed of primary macronutrient (nitrogen and phosphorus) and secondary macronutrient (magnesium); and of being a slow-release fertilizer (Gaterell et al., 2000). Overapplication of struvite does not burn plant roots due to its slow releasing characteristics, which is common with traditional ammonium–phosphate fertilizers (Min et al., 2019). In addition, there is the possibility of lower rates of application and a decrease of fertilizer loss due to run-off (associated to struvite's low-solubility in water) (Min et al., 2019).

Furthermore, struvite can also be used as a raw material for chemical industry (Li, Boiarkina, et al., 2019) .

2.2 Chemical Principles of Struvite Precipitation

2.2.1 Struvite's Chemical Reaction

Struvite structure is generally accepted to be $MgNH_4PO_4 \cdot 6H_2O$. The general reaction's pathway lacks, however, agreement (Forrest et al., 2009).

Equation (2.1) represents the general reaction pathway involving struvite formation that is most commonly observed (Forrest et al., 2009; Liu et al., 2012). This view is shared by many researchers such as Nelson et al. (2003), and Doyle and Parsons (2002) (Liu et al., 2012).

$$Mg^{2+}(aq) + NH_4^+(aq) + PO_4^{3-}(aq) + 6H_2O(l) \rightleftharpoons MgNH_4PO_4 \cdot 6H_2O(s) \quad (2.1)$$

Struvite does not precipitate as an amorphous solid cake mass but in the form of crystals (Crutchik & Garrido, 2011). However, the phenomenon produces a rapid decrease in the pH of the solution (Rahaman et al., 2006). This may suggest that the dominant form of P in the operating pH range for struvite crystallization is primarily HPO_4^{2-} or $H_2PO_4^-$, rather than PO_4^{3-}. (Liu et al., 2012). In that case, the convenient chemical reaction pathway for struvite formation proceeds according to equation (2.2) or (2.3), respectively, in which protons are generated (Liu et al., 2012). Besides Liu et al. (2012), researchers such as Rahaman et al. (2006), Babić-Ivančić et al. (2002), and Saidou et al. (2009) also support this view.

$$Mg^{2+}(aq) + NH_4^+(aq) + HPO_4^{2-}(aq) + 6H_2O(l) \rightleftharpoons MgNH_4PO_4 \cdot 6H_2O(s) + H^+(aq) \quad (2.2)$$

$$Mg^{2+}(aq) + NH_4^+(aq) + H_2PO_4^-(aq) + 6H_2O(l) \rightleftharpoons MgNH_4PO_4 \cdot 6H_2O(s) + 2H^+(aq) \quad (2.3)$$

Regardless of the reaction's pathway preferred, many different side reactions also act concurrently to struvite formation (Forrest et al., 2009). These include the interactions of each of its various components and are summarized in Table 2.1 (Forrest et al., 2009).

Table 2.1 - Competing reactions in struvite formation in a distilled water system

Ionization Equation	Reference
$MgOH^+ \rightleftharpoons Mg^{2+} + OH^-$	(Morel, 1983)
$NH_4^+ \rightleftharpoons H^+ + NH_3$	(Snoeyink & Jenkins, 1980)
$H_3PO_4 \rightleftharpoons H_2PO_4^- + H^+$	(Martell & Smith, 1989)
$H_2PO_4^- \rightleftharpoons HPO_4^{2-} + H^+$	(Martell & Smith, 1989)
$HPO_4^{2-} \rightleftharpoons PO_4^{3-} + H^+$	(Martell & Smith, 1989)
$MgH_2PO_4^+ \rightleftharpoons H_2PO_4^- + Mg^{2+}$	(Morel, 1983)
$MgHPO_4^+ \rightleftharpoons HPO_4^{2-} + Mg^{2+}$	(Taylor et al., 1963)
$MgPO_4^+ \rightleftharpoons PO_4^{3-} + Mg^{2+}$	(Childs, 1970)
$H_2O \rightleftharpoons H^+ + OH^-$	(Martell & Smith, 1989)

These thermodynamic equilibria (Table 2.1) further relate to the solution's pH through the concentration of H^+ and OH^- (Ali & Schneider, 2008). The speciation of struvite's constituents is therefore pH dependent (Doyle & Parsons, 2002). In wastewater, many other different species are present which may indirectly influence struvite equilibrium – e.g., carbonate, sulphate, and metals that precipitate phosphates, such as calcium and aluminium (Babić-Ivančić et al., 2002; Nelson et al., 2003).

2.2.2 Solubility and Solubility Product Constant, K_{sp}

Any solid, no matter how seemingly insoluble, is water-soluble to some extent (Mines Jr, 2014). Accordingly, the concentration of any solid substance is limited by the amount of it that can dissolve in water (Davis & Masten, 2016). Solubility can be defined as the quantity expressing the maximum concentration of a solute that can exist in a solvent at thermodynamic equilibrium at a specified temperature and pressure (Haynes, 2016). Any solid with a solubility of less than 0.1 M is said to be sparingly soluble (Robinson & Woollard, 1982).

Consider equation (2.4) that represents the general reaction of a sparingly soluble ionic solid dissolving into its constituent ions (Flowers et al., 2016). Equation (2.4) is usually referred to as the solubility equilibrium. Dissolution takes place when the ions at the surface of the solid migrate into the solvent (Mines Jr, 2014). Simultaneously, the ions in the solution will redeposit on the surface of the solid and this is known as precipitation (Mines Jr, 2014).

$$A_aB_b(s) \underset{\text{Precipitation}}{\overset{\text{Dissolution}}{\rightleftharpoons}} aA^{x+}(aq) + bB^{y-}(aq) \qquad (2.4)$$

The solubility dynamic equilibrium occurs when these two opposing processes proceed at a constant rate (Ojha & Prabhakar, 2013). At that point, the resulting solution contains the maximum amount of solute that will dissolve in the solvent. This is the condition at which the solution is considered saturated (Chang & Goldsby, 2012). Thus, solubility can be defined also as the amount of solute required to make a saturated solution at a given condition (Myerson & Schwartz, 2002). The solubility product constant, K_{sp}, is the equilibrium related to such a heterogeneous system, i.e., the equilibrium constant for the reaction in which a slightly soluble ionic compound dissolves to release its constituent ions to the solution (Girard, 2005; Michałowska-Kaczmarczyk & Michałowski, 2015).

Formally, it is correct to write an equilibrium constant expression involving the concentration of the solid, as represented in equation (2.5), where [.] indicates molar concentration (Robinson & Woollard, 1982).

$$K' = \frac{[A^{x+}(aq)]^a[B^{y-}(aq)]^b}{[A_aB_b\ (s)]} \quad (2.5)$$

In heterogeneous equilibrium, the concentration of a solid remains constant and independent of parameters such as pressure, temperature and solvent's volume (Tro, 2015). Its concentration does not change no matter what amount it is present because a solid does not expand to fill its container (Tro, 2015). Consequently, its concentration depends only on its density, which is constant as long as some solid is present (Tro, 2015). For that reason, $[A_aB_b\ (s)]$ does not affect chemical equilibria and it is excluded in the expression of the equilibrium constant. The new constant so defined is the aforementioned solubility product constant - K_{sp} (Robinson & Woollard, 1982).

K_{sp} can be expressed in molarities, and its value is calculated as outlined in equation (2.6*)* (Chang & Goldsby, 2012). It is the product of the molar concentrations (mole/L) of the constituent ions (obtained by dissolution), each raised to the power of its stoichiometric coefficient in the equilibrium (equation (2.4)) (Chang & Goldsby, 2012).

$$K_{sp} = [A^{x+}]^a[B^{y-}]^b \quad (2.6)$$

The value of K_{sp} indicates the solubility of an ionic compound - the smaller the value, the less soluble the compound is in water (Chang & Goldsby, 2012). K_{sp} is more commonly referred to as pK_{sp}, the negative log of K_{sp} (Forrest et al., 2009).

Furthermore, K_{sp}'s value is of great use to predict when the dissolved solute comes out of solution (Chang & Goldsby, 2012). In industrial and laboratory preparations, one can adjust the concentrations of ions until the ion product, Q, exceeds K_{sp} (Chang & Goldsby, 2012). The solution will then be supersaturated, and, in time, some solute will come out as crystals, until equilibrium is reached again (Chang & Goldsby, 2012). Q has the same form as K_{sp} except for the fact that the concentrations of ions are not equilibrium concentrations. (Chang & Goldsby, 2012).

Therefore, and recalling struvite's ionic composition and its proposed reaction's pathways, when Mg^{2+}, NH_4^+, and $H_nPO_4^{n-3}$ (n=0, 1 or 2) exist in solution, and the product of their concentrations (Q) is larger than struvite's K_{sp}, the crystal may precipitate (Zhang et al., 2017). K_{sp}'s calculation formula, according to the reaction's pathway described by equation (2.1), is depicted in equation (2.7) (Zhang et al., 2017).

$$K_{sp} = [Mg^{2+}][NH_4^+][PO_4^{3-}] \quad (2.7)$$

It is, however, relevant to allude to the fact that the state of supersaturation is a necessary but not sufficient condition for the generation of particles within a homogeneous phase (Tai et al., 2006). As reported by Tai et al. (2006), if the solution is homogeneous, a supersaturated solution may last forever without a disturbance. This issue will be further addressed in section 2.3.

It is also noteworthy that K_{sp}'s value is accurate for any pH (Doyle & Parsons, 2002). The reason for that is the following - even though pH influences the quantity of struvite's constituent ions, K_{sp} is independent of the initial concentrations of reactants and products (Lodish et al., 2000).

At this point, and since the concepts of solubility and supersaturation are now established, the notions of precipitation and crystallization deserve further consideration. Both precipitation and crystallization refer to unit operations that generate a solid from a supersaturated solution (Khopkar & Ranade, 2019). Precipitation is defined as the sedimentation of a solid material (a precipitate) from a liquid solution, in which the material is present in amounts greater than its solubility in the liquid (IUPAC, 1997). On the other hand, IUPAC (1997) designates

crystallization as the formation of a crystalline solid from a solution, melt vapour or a different solid phase, generally by the lowering of the temperature or by evaporation of a solvent.

These two definitions share, however, some overlap (Delegard & Peterson, 2019). For instance: "a crystallization process, as achieved by lowering of the temperature or by evaporation of a solvent" would cause precipitation, i.e., "the sedimentation of a solid material" (Delegard & Peterson, 2019). Moreover, precipitation can sometimes give origin to crystalline solids besides non-crystalline ones (Stumm & Morgan, 1996).

The exact distinction between the two terms relies on the procedures that foster their respective occurrence (Delegard & Peterson, 2019). Precipitation is understood more narrowly as the process in which the mixing of two clear solutions results in a solid from the mixture, whereas crystallization is obtained generally by lowering the temperature or by evaporation of a solvent (Delegard & Peterson, 2019). Notwithstanding, some authors (Khopkar & Ranade, 2019) indicate the speed of the process and the size of the solids particles produced as the differentiation criteria between crystallization and precipitation. Precipitation refers to a rapid solid formation that can origin small crystals or amorphous solids (Khopkar & Ranade, 2019).

Ultimately, the general IUPAC nomenclature should be followed where appropriate, e.g., you can never crystallize to give an amorphous solid (Toyokura, 1993). Nonetheless, this nomenclature runs the risk of crystallization and precipitation ending up ambiguous (Toyokura, 1993). For simplification purposes, and since struvite precipitates in the form of crystals, and both precipitation and crystallization share the basic steps (supersaturation, nucleation, and growth), the terms will be used interchangeably in this dissertation (Crutchik & Garrido, 2011). This is in line with Jones (2002) and Toyokura (1993), who consider crystallization as the precipitation of crystals from solution.

2.2.3 K_{sp}'s Limitation

So far, the equilibrium constant for ionic systems has been expressed in terms of the concentration of its reagents. Although this is very convenient as it turns the reading straightforward, it is not a strictly accurate concept (Robinson & Woollard, 1982). More advanced equilibrium theory shows that the true constants should be expressed in terms of the chemical activities of the reagent species, rather than the concentrations concept (Robinson & Woollard, 1982).

Consequently, the aforementioned, is a limitation inherent to the solubility product concept, as K_{sp} is a function of the reagents concentrations (Robinson & Woollard, 1982). For this reason, K_{sp}, as expressed in (2.6), is more rigorously called apparent or concentration solubility product and is given the symbol K_c (Bhuiyan et al., 2007). To overcome this limitation, another equilibrium constant, the activity solubility product, K_{so}, should be considered (Doyle & Parsons, 2002).

2.2.4 Activity Solubility Product, K_{so}

Before defining the activity solubility product, K_{so}, ionic strength and ionic activity concepts deserve previous consideration.

In electrolytic environments such as wastewater, there exist a lot of strong interactions between ions (Tomašić & Zelić, 2018). For that reason, and as stated by Tomašić and Zelić (2018), the behavior of any ion is subjected to the influence of the surrounding ones. Due to the interactions

between ions, many of them behave less actively than they would alone (Tomašić & Zelić, 2018). Consequently, these ions appear to be less concentrated than they are. Such "effective" concentration of a species in a mixture is called the ionic activity of the ion, α or a (Tomašić & Zelić, 2018).

The ionic activity α_i, of a particular ion i, is dimensionless and relates to its molar concentration [i], through the respective, also dimensionless, activity coefficient γ_i, as illustrated in equation (2.8) (Zhang et al., 2017).

$$\alpha_i = \gamma_i \times [i] \tag{2.8}$$

In infinitely dilute solutions (ideal solutions), ions react independently from each other (Belessiotis et al., 2016). In that circumstance, the activity coefficient, γ_i, is very close to 1, and, therefore, the activity equals the molar concentration of the ion (Freiser & Freiser, 1992; Zhang et al., 2017). However, as the concentration increases, ions start to interact between them, and the activity coefficient decreases (Belessiotis et al., 2016). One should also keep in mind that the activity coefficients of undissociated solutes will be affected by the total solution composition. (Freiser & Freiser, 1992; Tomašić & Zelić, 2018).

The activity and activity coefficient were both defined as dimensionless. Therefore, for equation (2.8) to be correct, [i] must be normalized to its concentration in some arbitrary, but clearly defined standard state $[i^\theta]$ – see equation (2.9) (Benjamin & Lawler, 2013; MacIntyre, 1976).

$$\alpha_i = \gamma_i \times \frac{[i]}{[i^\theta]} \tag{2.9}$$

The typically chosen standard state for any substance in solution is concentration, $[i^\theta]$, at 1 M, at a specific temperature (Moore et al., 2010). Thereupon, considering $[i^\theta] = 1$, equation (2.8) can be used to determine the activity of a solute. Regarding pure solid and liquid phases, by definition, $\frac{[i]}{[i^\theta]} = 1$ (Anderson, 2005; Benjamin & Lawler, 2013). This arises from the fact that the standard state of a solid or liquid is usually the solid or liquid itself, respectively (Zumdahl, 2007). When referring to pure solid and liquid phases, γ_i is also 1, and so, the activity is also 1 (Anderson, 2005; Benjamin & Lawler, 2013).

Activity coefficients further relate to the ionic strength of the solution, denoted by I. Ionic strength is a measure of the intensity of the electrical field created in a solution by an ionic activity. I is defined as half of the sum of terms obtained by multiplying concentration [i], of a constituent i present in the solution, by the square of its valence z - see equation (2.10) (Belessiotis et al., 2016; Tsobanoglou & Schroeder, 1985). Ionic strength of wastewaters may vary from 0.0 to 0.2 mol/L, which differs according to the dissolved solids concentrations (Türker & Çelen, 2010).

$$I = \frac{1}{2} \Sigma ([i] \times z_i^2) \tag{2.10}$$

Equation (2.11) represents the simplified empirical relationship between γ_i and I, for aqueous solutions at 25 ºC, valid for I values less than 0.1 mol/L (Türker & Çelen, 2010). Here, z is again the valence of the ion.

$$-\log \gamma_i = 0.5 \times z_i^2 \times \frac{\sqrt{I}}{1 + \sqrt{I}} \tag{2.11}$$

Reached this point, a solubility product that considers the influence of ionic strength and the ionic activity - the activity solubility product - may, at last, be defined (Doyle & Parsons, 2002).

Equation (2.4) is presented here again to recall the equilibrium reaction of a sparingly soluble ionic solid (product) dissolving into its constituent ions (reagents).

$$A_aB_b(s) \underset{\text{Precipitation}}{\overset{\text{Dissolution}}{\rightleftharpoons}} aA^{x+}(aq) + bB^{y-}(aq) \tag{2.4}$$

The activity solubility product, K_{so}, can be expressed as the quotient of the multiplication of the reagents' activities by the activity of the product – see left side of equation (2.12) (Févotte et al., 2011). Because A_aB_b is a solid substance, its activity is 1 (Zumdahl, 2007). As a result, K_{so} is defined as the product of the ionic activities of the species involved in the equilibrium each raised to the respective stoichiometric number as represented in equation (2.12) (right side) (Févotte et al., 2011). Only when the value of each of the activity coefficients ($\gamma_{A^{x+}}$, $\gamma_{B^{y-}}$) is 1, K_{sp} can represent K_{so} (Zumdahl, 2007).

$$K_{so} = \frac{\alpha_{A^{x+}}^{a} \times \alpha_{B^{y-}}^{b}}{\alpha_{A_aB_b}} = (\gamma_{A^{x+}} \times [A^{x+}])^{a} \times (\gamma_{B^{y-}} \times [B^{y-}])^{b} \tag{2.12}$$

Along these lines, and recalling the general reaction pathway for struvite formation (equation (2.1)), the equilibrium constant (K_{so}) for struvite can be obtained according to equations (2.13) and (2.14) (Bhuiyan et al., 2007).

$$Mg^{2+}(aq) + NH_4^+(aq) + PO_4^{3-}(aq) + 6H_2O(l) \rightleftharpoons MgNH_4PO_4 \cdot 6H_2O(s) \tag{2.1}$$

$$K_{so} = \alpha_{Mg^{2+}} \times \alpha_{NH_4^+} \times \alpha_{PO_4^{3-}} \tag{2.13}$$

$$K_{so} = (\gamma_{Mg^{2+}} \times [Mg^{2+}]) \times (\gamma_{NH_4^+} \times [NH_4^+]) \times (\gamma_{PO_4^{3-}} \times [PO_4^{3-}]) \tag{2.14}$$

The solution ionic strength I is employed to determine the activity coefficient γ_i of each component ion (Mg^{2+}, NH_4^+ and PO_4^{3-}) (Fattah et al., 2009). Ionic strength can be calculated through equation (2.10), based on the ionic concentration of each species and its respective charge. The ionic strength of the solution can also be determined based on conductivity measurements using a conversion factor (Fattah et al., 2009).

Both K_{sp} and K_{so} refer to equilibrium. It should be stressed that the activities considered in equations (2.12) to (2.14) are those and only those occurring once the equilibrium is reached (Burgot, 2017). Likewise, for struvite precipitation to occur, K_{sp} needs to be exceeded, i.e., the ion activity product (IAP) of the ions in reaction needs to exceed K_{sp} to obtain a supersaturated solution (Bhuiyan et al., 2007). More simply, if $\frac{IAP}{K_{so}} > 1$, the solution is supersaturated and struvite may form (Bhuiyan et al., 2007). Similarly, IAP has the same form as K_{so}, except for the fact that the K_{so} refers to equilibrium conditions.

K_{so} is also commonly referred to as pK_{so}, the negative log of K_{so} (Doyle & Parsons, 2002).

From equations (2.12) and (2.6), it comes that K_{so} relates to K_{sp} through equation (2.15) (Bhuiyan et al., 2007).

$$\prod_{i=1}^{n} \gamma_i = \frac{K_{so}}{K_{sp}} \tag{2.15}$$

2.2.5 K_{so}'s Limitations

When taking ion activities and ionic strength into consideration, K_{so} brings undoubtedly further precision to struvite's solubility determination. However, one should be aware that K_{so} is pH specific (Doyle & Parsons, 2002).

Slight variations in the pH result in a change in the speciation of the struvite's constituents. In turn, speciation affects the conditions for struvite precipitation (Bhuiyan et al., 2007). As Bhuiyan et al. (2007) elaborated:

> The proportion of ammonium ion (NH_4^+) present in solution depends on its equilibrium with ammonia (NH_3) and varies markedly with pH. Due to the triprotic nature of the orthophosphoric acid, several orthophosphate species exist in aqueous solution, resulting in a variable proportion of PO_4^{3-} with pH of the solution. Hydrolysis of the magnesium ion leading to the formation of $MgOH^+$ is significant only at higher pHs. In the presence of phosphate and ammonia, magnesium forms a number of complexes depending on pH and concentration of the species in solution. (p. 1021)

Consequently, any variation in the composition of water results in differences in ionic strength and ion activity (Doyle & Parsons, 2002). Consequently, K_{so} and the struvite precipitation potential change correspondingly. Thereupon, as highlighted by Doyle & Parsons (2002), the solubility of struvite also varies with pH. Since wastewater composition varies from one water treatment plant to another, every wastewater is likely to have a distinct K_{so} value at a specific pH (Doyle & Parsons, 2002).

A fundamental problem of predicting struvite precipitation is predicting the equilibrium characterization, or in other words, to define the actual species present in the solution (Bhuiyan et al., 2007). The difficulty arises from the fact that all the three reaction ions - Mg^{2+}, NH_4^+, and PO_4^{3-} - exhibit complex equilibria in aqueous solution (Bhuiyan et al., 2007).

From a practical point of view, the predicted K_{so} value depends on the experimental precision, and on the thermodynamic method used to calculate the equilibrium constant values, at different temperatures, for all the equilibrium relations involved during the precipitation of struvite (Hanhoun et al., 2011). Table 2.1 expresses the side equilibrium relations involved in struvite precipitation. The conventional technique for determination of the K_{so} value of a reaction involves either the formation of precipitate or the dissolution of a previously formed crystal in distilled water (Bhuiyan et al., 2007).

Published values of the value of pK_{so} for struvite at 25 ºC range from 9.41 to 13.36 (Bhuiyan et al., 2007). The reasons that explain the discrepancies in the reported solubility product values include: (i) using approximate solution equilibria to determine K_{so}, (ii) neglecting the effect of ionic strength, (iii) variation in the presence of both organic and inorganic complexes, as well as dissolved species formed between the principal constituents of struvite, and (iv) selection of different chemical species for calculations (Andrade & Schuiling, 2001). Naturally, widely varying experimental methodologies and conditions, with respect to pH, temperature and ionic strength, also contribute for much of the discrepancies that exist between these reported values. (Bhuiyan et al., 2007).

To conclude, the determination of K_{so} is intricate and time-consuming, as it requires several calculations and constants (Bhuiyan et al., 2007). To overcome this drawback, one uses a solubility product in terms of the total analytic concentrations of magnesium, ammonium, and phosphate – the equilibrium conditional solubility product, $P_{s_{eq}}$ (Bhuiyan et al., 2007).

2.2.6 Equilibrium Conditional Solubility Product, $P_{s_{eq}}$, and Supersaturation Ratio, SSR

Before defining the equilibrium conditional solubility product, $P_{s_{eq}}$, some remarks should be considered about analytical concentrations.

Solutions that consist of magnesium, ammonium and phosphate form not only ions but also complexes (Ohlinger et al., 2000). The total analytical concentrations of the constituents of struvite, Mg, NH_4, and PO_4, denoted by $C_{T_{Mg}}$, $C_{T_{NH_4}}$, $C_{T_{PO_4}}$, respectively, are the sum of the dissolved concentrations of their complexes and free ions, as expressed in equations (2.16) to (2.18) (Ali et al., 2005; Ali & Schneider, 2008).

$$C_{T_{Mg}} = \left[Mg^{2+}\right]+[MgOH^{+}]+[MgH_2\ PO_4^{+}]+[MgHPO_4]+[MgPO_4^{-}] \tag{2.16}$$

$$C_{T_{NH_4}} = [NH_4^{+}] + [NH_3] \tag{2.17}$$

$$C_{T_{PO_4}} = [H_3PO_4] +[H_2PO_4^{-}]+ \left[HPO_4^{2-}\right]+\left[PO_4^{3-}\right]+[MgH_2\ PO_4^{+}]+[MgHPO_4]+[MgPO_4^{-}] \tag{2.18}$$

The ionization fractions of Mg, NH_4 and PO_4 can be defined by the quotient of free ion concentration and the total concentration of each chemical component – see equations (2.19) to (2.21) (Bhuiyan et al., 2007).

$$f_{Mg} = \frac{\left[Mg^{2+}\right]}{C_{T_{Mg}}} \tag{2.19}$$

$$f_{NH_4} = \frac{[NH_4^{+}]}{C_{T_{NH_4}}} \tag{2.20}$$

$$f_{PO_4} = \frac{\left[PO_4^{3-}\right]}{C_{T_{PO_4}}} \tag{2.21}$$

Finally, the equilibrium conditional solubility product, $P_{s_{eq}}$, describing the conditional equilibrium for any given pH level, can then be expressed as a function of the activity solubility product (K_{so}), the ionization fraction (f_i) and the activity coefficient (γ_i) for the respective species (Bhuiyan et al., 2007; Forrest et al., 2009) – equation (2.22).

$$P_{s_{eq}} = \frac{K_{so}}{f_{Mg} \times f_{NH_4} \times f_{PO_4} \times \gamma_{Mg^{2+}} \times \gamma_{NH_4^{+}} \times \gamma_{PO_4^{3-}}} = C_{T_{Mg}} \times C_{T_{NH_4}} \times C_{T_{PO_4}} \tag{2.22}$$

Notwithstanding, the determination of $P_{s_{eq}}$ as a function of the measured equilibrium concentrations ($C_{T_{Mg}}$, $C_{T_{NH_4}}$, and $C_{T_{PO_4}}$) is more straightforward – see equation (2.23) (Fattah, 2004).

$$P_{s_{eq}} = C_{T_{Mg}} \times C_{T_{NH_4}} \times C_{T_{PO_4}} \tag{2.23}$$

Since $P_{s_{eq}}$ can be derived directly from measured total concentrations, speciation or activity calculations become redundant in estimating maximum dissolved total concentrations (Ronteltap et al., 2007).

Because the $P_{s_{eq}}$ value is determined for a specific matrix, it is valid for this matrix only (Stumm & Morgan, 1996). $P_{s_{eq}}$ will vary with pH, ionic strength and temperature of the solution (Mavinic et al., 2007). Thus, equilibrium conditional solubility product refers to solubility at a specific set of conditions, a conditional solubility (Turovskiy & Mathai, 2006)

Plotting $P_{s_{eq}}$, calculated as a function of measured analytical equilibrium concentrations vs. pH, establishes a struvite solubility limit curve for a specific ionic strength, temperature and solution composition (Bhuiyan et al., 2007). This curve is of great use since it can be applied to predict struvite's precipitation (Bhuiyan et al., 2007). It is possible to maintain the ionic strength of the solution relatively constant while varying the pH by using adequate buffers (Ellis & Morrison, 1982; Elving et al., 1956).

This simple method of drawing such curves using the experimentally determined equilibrium total concentrations for a range of pH values was used by researchers such as Adnan et al., 2003, and Britton et al., 2005 (Bhuiyan et al., 2008). In the studies carried out by the aforementioned researchers, a sufficient amount of struvite crystals was placed in different jars containing the solution in study, at different pHs. This ensured that some solid-phase struvite remained at equilibrium. It was assumed that the crystals would not affect the solubility determination for a 24 h equilibrium (Adnan, Koch, et al., 2003; Britton et al., 2005).

Figure 2.3 exemplifies a plot of a struvite's solubility curve, representing the equilibrium between struvite's solid phase and its dissolved constituent ions, in aqueous solution, for different pH values.

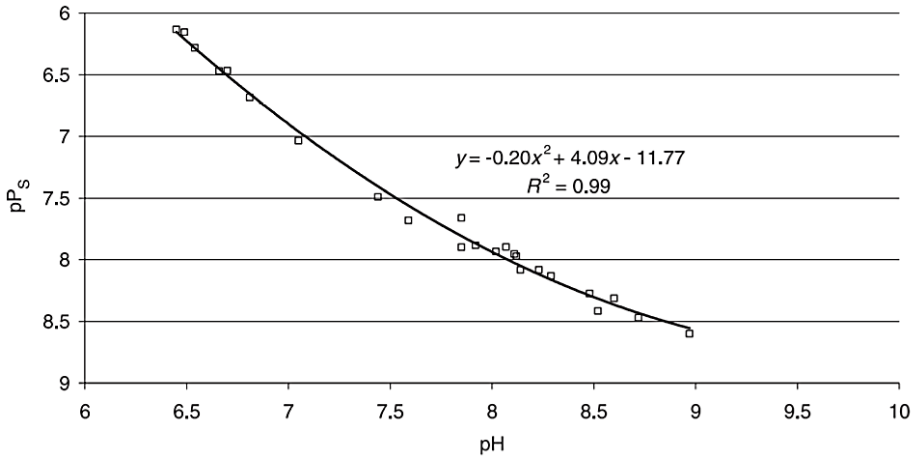

Figure 2.3 - Struvite $P_{s_{eq}}$ in digester supernatant as a function of pH (Britton et al., 2005).

P_s represents the conditional solubility product of a sample in study in non-equilibrium conditions and pP_s is the negative logarithm of P_s (Britton et al., 2005). A fluid with a pP_S above the equilibrium curve is supersaturated for struvite (Britton et al., 2005). The higher above the curve is a pP_s point, the higher the precipitation potential. (Ohlinger et al., 2000). To relieve supersaturation and move towards equilibrium, the solution crystallizes and the concentrations of struvite's concentration in solution decrease until pP_s intersects the equilibrium curve (Adnan, Koch, et al., 2003; Ohlinger et al., 2000).

As Figure 2.3 suggests, increasing pH until about 9.5 leads to an increase in pP_s, which translates in a decrease in P_s, and therefore, a decrease in struvite's solubility (Daegi Kim et al., 2016). This coincides with the optimum pH for precipitation (Booker et al., 1999). At pH values greater than 9.8, volatilization of free ammonia from the solution decreases both the rate of formation and yield of struvite (Booker et al., 1999).

Even though $P_{s_{eq}}$ is extremely useful in predicting struvite precipitation, it has the following disadvantage. Using the conditional solubility values for describing a struvite crystallization system renders the comparison between studies more difficult, since any changes in wastewater composition change its inherent $P_{s_{eq}}$ value (Iqbal et al., 2008).

Lastly, the supersaturation ratio (SSR), as a measure of the potential of precipitation, may be defined in terms of the equilibrium conditional solubility product, $P_{s_{eq}}$, and of a calculated conditional solubility product P_s - see equation (2.24) (Fattah, 2012).

$$SSR = \frac{P_s}{P_{s_{eq}}} \tag{2.24}$$

Theoretically, any value greater than 1 indicates that the solution is supersaturated, and that struvite's formation is possible. Crystallization may occur until the SSR value reaches 1 – value at which the system is in equilibrium (Adnan, Koch, et al., 2003). For values of SSR<1, the system is undersaturated and precipitation won't occur – this is the case of any point located below the solubility curve in Figure 2.3.

Another very important application of SSR consists in defining the metastable zone of the crystallization process (Adnan, Koch, et al., 2003). The characteristics of the metastable zone (i.e. its width limits) define the optimum mode of crystallization for a given process. Section 2.3 will further explore the definition of the metastable zone.

2.3 Mechanisms of Struvite Crystallisation

2.3.1 General Principles of Crystallization Processes

Crystal formation is a complex process of purification of a solute (liquid or solid) leading to the development of a solid phase made of regular structures named crystals (Le Corre et al., 2009). For struvite crystallization to occur, a supersaturated solution, which is not in equilibrium, is required (Adnan, Koch, et al., 2003). According to Pastor et. al (2008), supersaturation is the driving force for all crystallization processes. Supersaturated solutions induce crystallization by a combination of nucleation and crystal growth (Myerson & Ginde, 2002).

Nucleation and crystal growth are, indeed, the two chemical processes through which struvite crystal development occurs (Rahman et al., 2014). Nucleation determines the initial formation of crystals and crystal growth determines their subsequent size (Jones, 2002). The relation of the degree of nucleation to crystal growth controls the product crystal size and size distribution (Ali & Schneider, 2005).

2.3.2 Nucleation

The primary step in struvite crystallization is nucleation - the phase separation or the birth of new crystals (Myerson & Ginde, 2002; Rahman et al., 2014). When the solubility of the solution is exceeded and the solution becomes saturated, Mg^{2+}, NH_4^+, and PO_4^{3-} molecules start to associate and form aggregates (clusters) (Myerson & Ginde, 2002) that grow by accretion in a favorable pH (Rahman et al., 2014).

Crystal clusters, of only a few nanometres in size (Jones, 2002), form stochastically, consuming energy from the supersaturated solution (Ali & Schneider, 2005). This energy is supplied by a thermodynamic driving force in the supersaturated solution (Ali & Schneider, 2005). This driving force is given by the change in chemical potential between supersaturation and equilibrium states (Vedantam & Ranade, 2013). Continuous collision of the clusters forms stable nuclei (Ali & Schneider, 2005).

Two energy barriers must be overcome to create a new stable nucleus in a supersaturated solution: (i) an energy barrier to form a new surface and (ii) an energy barrier to form the volume of the crystal (Wagh & Martini, 2017). Wagh & Martini (2017) termed the total energy that must be overcome to form a nucleus as the activation free energy. Nucleation may also be induced by agitation - mechanical energy input enhances the nucleation process (Myerson & Ginde, 2002). A stable nucleus is a nucleus that has achieved a critical size, and thus will continue to grow (Wagh & Martini, 2017).

Mechanisms of nucleation can be classified in primary or secondary nucleation (Myerson & Ginde, 2002). Myerson & Ginde (2002) established the following distinction criteria: primary nucleation occurs in the absence of crystalline surfaces, whereas secondary nucleation or surface secondary nucleation involves the active participation of these surfaces.

There are two types of primary nucleation: the homogeneous primary process, which causes the spontaneous occurrence of crystals in highly purified or highly supersaturated solution; and the heterogeneous primary process, where crystal formation occurs due to the presence of foreign particles or impurities, which function as substrates (Le Corre et al., 2009). Figure 2.4 represents a simple scheme of the different mechanisms of crystallization.

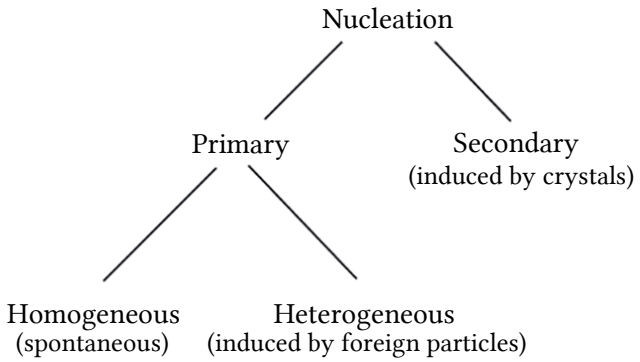

Figure 2.4 - Mechanisms of struvite crystallization (Mullin, 2001).

In turn, secondary nucleation mechanism requires an already existing suspension of crystallized particles, preferably, of the same species as the solid that will further crystallize (Rahman et al., 2014). Secondary nucleation occurs mainly due to the collision of larger particles with the crystallizer internals or with other crystals leading to formation of crystal fragments (Vedantam & Ranade, 2013). Nucleus form on the surface of these particles (Rahman et al., 2014) and are latter detached from them by the shear exerted by the fluid or by shocks undergone by the particles (Regy et al., 2002). Secondary nucleation can be defined as the generation of new crystals by crystals already present in the suspension (Doran, 2013).

Among the different nucleation mechanisms, homogeneous primary nucleation requires the highest supersaturation level to spontaneous development, followed by heterogeneous primary nucleation and surface secondary nucleation, respectively (Rahman et al., 2014). A foreign substance present in a supersaturated solution is generally known to reduce the energy required

for nucleation (Myerson & Ginde, 2002). “Parent crystals” in secondary nucleation also have a catalysing effect on the nucleation phenomena (Myerson & Ginde, 2002). In an unseeded crystallization process, primary nucleation triggers the formation of the first-formed crystals and remains the main nucleation mechanism, throughout the entire process, due to the high supersaturation values (Vedantam & Ranade, 2013).

2.3.3 Crystal Growth

After nucleation has been achieved - i.e., solute molecules have formed the smallest sized particles possible under the conditions present - crystal growth follows (Myerson & Ginde, 2002). The previously developed nuclei grow substantially more until they form detectable crystals (and beyond) (Le Corre et al., 2009).

Crystals grow by the advance of the individual faces present on the crystal (Garside et al., 2002), in a layer-by-layer fashion (Myerson & Ginde, 2002). In general, each face will grow at a different rate and the relative growth of different faces determines crystal habit or shape (Garside et al., 2002). The linear growth velocity of a face is usually defined as the rate of growth of a face in the direction normal to the face (Myerson & Ginde, 2002).

Growth of crystals from solution involves the two following consecutive major processes. Firstly, there is the mass transport from the solution to the crystal surface by diffusion through the liquid phase, by convection (fluid motion) or by a combination of both mechanisms (Garside et al., 2002; Jones, 2002; Mullin, 2003). Then, a surface reaction in which the growth units are integrated into the crystal lattice occurs, also named as the surface reaction process (Garside et al., 2002; Jones, 2002; Mullin, 2003).

Primarily, when a crystal is grown in solution, it takes the solute from it, thus reducing the concentration of the solution around it (Rudolph, 2015). To allow the crystal to keep growing, fresh solute concentrations must be withdrawn from the bulk of the solution, and lead molecules must move toward the crystal face of the growing crystal (Rudolph, 2015). This motion of the solute is referred to as the mass transfer process (Arend & Hulliger, 1989).

Ensuing processes occurring on the surface of the crystal may be grouped together under the general title of surface integration (Arend & Hulliger, 1989). These processes can be subdivided into these subsequent stages: (i) first, adsorption of the growth unit coming from solution into the crystal surface; (ii) release of part of its solvation shell, after which the growth unit diffuses into the adsorption layer until it is either incorporated into the lattice or leaves the adsorption layer and returns to the solution (Jones, 2002). A solvation shell is the interaction interface between the solvent and the compound or biomolecule that constitutes the solute (Garrett & Grisham, 2008). At last (iii), if the growth unit reaches a point where it can be built into the lattice, the crystal surface loses the remaining of its solvation shell before final lattice incorporation (Jones, 2002). Figure 2.5 illustrates the aforementioned surface reaction process.

A kink site is a spot of the crystal surface where the attachment of a growth unit to the three surfaces of the crystal is possible (Myerson & Ginde, 2002). In agreement with Myerson & Ginde (2002), from an energetic point of view, a kink site is more favorable than other sites where the growth unit is attached only to both the surface and to a growing step of the crystal, or attached solely to the surface of a growing layer. For that reason, it is easier for molecules to grow in a layer-by-layer fashion (Myerson & Ginde, 2002).

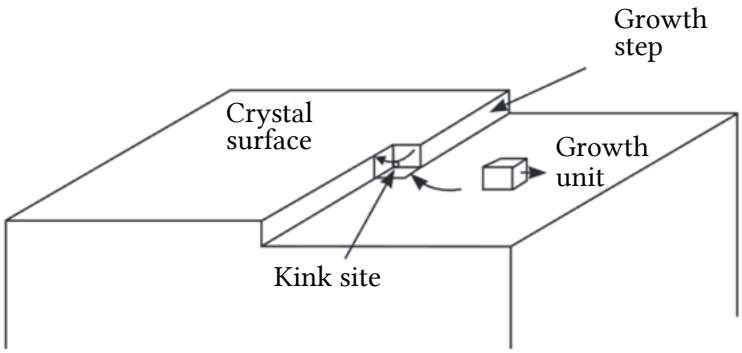

Figure 2.5 - Attachment of a growth unit into a kink site (Jones, 2002).

The growth of stable nuclei is an energy-releasing process (Mullin, 2001; Myerson & Ginde, 2002), since energy is released per growth unit upon the crystallization of a new "slice" of thickness. (Hartman & Perdok, 1955). One should note that neither the diffusion step nor the surface reaction process will, however, proceed unless the solution is supersaturated (Jones, 2002).

In addition to nucleation and crystal growth, important secondary processes, such as agglomeration and breakage of crystals, also occur during crystallization (Jones, 2002). Furthermore, after nuclei have formed and crystals have grown to reach a state of equilibrium, further reorganization of molecules might occur within or between crystals (Wagh & Martini, 2017). These arrangements result in changes in size, number and shape of crystals and often occur during storage over days, weeks or years (Wagh & Martini, 2017). Such recrystallization is usually detrimental to product quality but can conveniently be avoided or delayed by manipulating process conditions.

2.3.4 Induction Time

A period of time usually goes by between the achievement of supersaturation and the appearance of crystals - this is called the induction time (Mullin, 2003). Jones (2002) defined the induction time as the sum of the nucleation time and the growth time (time required to grow to a detectable crystal size).

A highly supersaturated solution has a shorter induction time, whereas relatively lower supersaturation is characterized by a longer or even infinite induction time (Ali & Schneider, 2005). According to I. Ali & Schneider (2005), one disadvantage of infinite induction time is the redissolving of induced crystals in solution due to high-energy consumption from a relatively low driving force. To overcome this drawback, seed materials may be preliminary added (Münch & Barr, 2001). Suitable seeds act as diffusive media and enhance crystal growth by layering of newly born clusters onto the surface of the seeds and govern crystal growth (Ali & Schneider, 2005, 2006). The presence of seed crystals generally reduces the induction period, but does not necessarily eliminate it (Mullin, 2001).

In a study carried out by I. Ali & Schneider (2005), seeds of struvite proved to be more effective for struvite crystallization due to the similarity of lattice structure, than quartz sand borosilicate glass grindings. The similarity of lattice structure between seed and mother crystal stimulates the integration process of newly born crystals onto the seed surface (Ali & Schneider, 2005).

2.3.5 Metastable Zone

When solutions are supersaturated they do not necessarily crystallize spontaneously (Wertman et al., 2019). By spontaneous crystallization, one means crystallization without the preliminary addition of seed crystals (Rudolph, 2015), i.e., when crystallization arises out of a homogeneous solution.

For spontaneous crystallization to occur, the activation free energy required for nucleation must be firstly overcame (Wertman et al., 2019). This means that supersaturating a homogeneous solution by some degree will not necessarily result in crystallization (Myerson & Ginde, 2002), namely if the energy requisite for nucleation is not fulfilled (Wagh & Martini, 2017). Recall that the state of supersaturation is a necessary but not sufficient condition for the generation of particles within a homogeneous phase (Tai et al., 2006).

The thermodynamically metastable zone is defined as the critical zone of solution supersaturation where crystallization is not governed by nucleation (Ali & Schneider, 2005), as no appreciable nucleation occurs here (Bhamidi et al., 2017). Ostwald (1897) first introduced the term metastable supersaturation to classify supersaturated solutions in which primary nucleation would not occur (Mullin, 2001).

As a consequence, in the metastable zone, if preliminary crystals are not present, nuclei do not appear (Nienow & Paul, 2016). Only by further increasing the supersaturation, a certain degree of supersaturation will be reached at which primary nucleation occurs: the metastable limit – see Figure 2.6 (Ulrich & Strege, 2002). The boundary between the metastable and oversaturated zones is the absolute limit of the metastable region where phase separation must occur immediately (Myerson & Ginde, 2002).

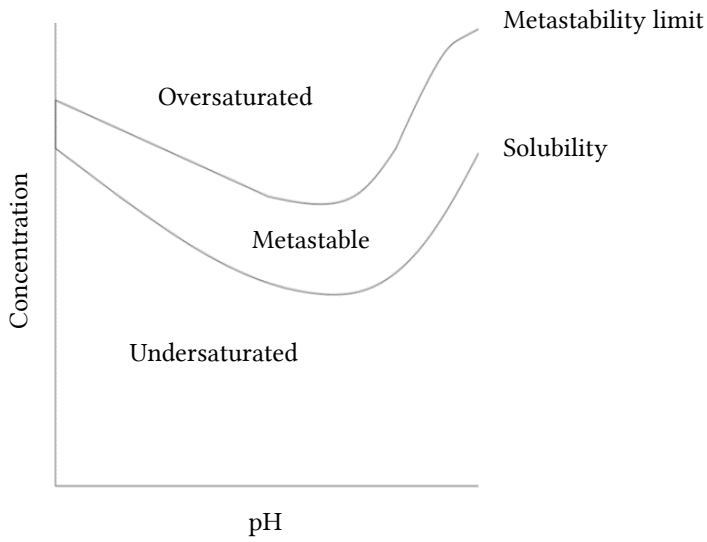

Figure 2.6 - States of a solution during the crystallization process (adapted from Stumm and Morgan, 1996).

Nonetheless, if crystals seeds of the solute are placed in any supersaturated solution, the solution becomes heterogeneous and crystal growth may occur on the seeds (Myerson & Ginde, 2002). Under these circumstances, crystallization may be induced in the metastable zone, but only through solution seeding (Rudolph, 2015). Additionally, the presence of placed crystals may give rise to secondary nucleation (Nienow & Paul, 2016).

Even though secondary nucleation is possible within the metastable zone, that typically happens at higher supersaturations, near (but below) the metastable limit (Wertman et al., 2019). The closer the solution concentration is to the metastable limit, the likelihood of secondary nucleation is increased (Wertman et al., 2019). Yet, crystal growth is the dominant mechanism when the concentration is close to the solubility (Wertman et al., 2019).

Figure 2.6 can be divided in three distinct zones:

i. The **undersaturated or stable zone** – here the system is always homogeneous (Tai et al., 2006). Even if crystals are initially present, they will dissolve (L. Wang et al., 2016). Therefore, in this zone, crystallization is impossible (Mullin, 2001). This is in line with the aforementioned solubility curve plot, where a system underneath the curve is undersaturated and SSR<1 (Adnan, Koch, et al., 2003) – recall subsection 2.2.6, Figure 2.3. At an SSR value equal to 1 the system is in equilibrium, which corresponds to the solubility curve in figure 2.6.
ii. The **metastable zone**, where the solution is moderately supersaturated and growth of existing crystals continues until the solution reaches the solubility curve (Myerson & Ginde, 2002). For growth to occur it is imperative that crystal seeds are placed in the solution (Mullin, 2001), otherwise crystallization will not occur. Subsequently, nuclei may be generated by the secondary mechanism but only if sufficient energy is given to the crystal surface (Tai et al., 2006).
iii. The **oversaturated zone** or the also called unstable zone in which primary nucleation occurs (Tai et al., 2006). Here, primary and secondary nucleation are the pre-eminent mechanisms of crystallization (Wertman et al., 2019). As a consequence, crystallisation can be rapid and abundant without the addition of crystal seeds (Le Corre et al., 2009).

Knowledge of the metastable zone width represents valuable information in a crystallization process (Ali & Schneider, 2005). According to I. Ali & Schneider (2005), the former plays a crucial role in maintaining product quality.

Studies carried out by Britton et al. (2005) and Adnan et al. (2003), have shown that the metastable zone is ideal for the growth of large size crystals of struvite (>1 mm diameter). The referred metastable zone lies within a range of SSR values between 3 and 5 (Adnan, Mavinic, et al., 2003; Britton et al., 2005).

Metastable limits define acceptable operating conditions for the minimization of uncontrolled nucleation (Mullin, 2003). At concentrations greater than the metastable limit, vast numbers of tiny crystals (nuclei, of the order of 1 to 10 μm), also known as fines, form during primary nucleation (Nienow & Paul, 2016; Ulrich & Strege, 2002; Vu et al., 2003). The generation of an excessive number of small crystals reduces the growth of large crystals (W. Omar & Ulrich, 1999). As stated by Omar & Ulrich (1999), the resulting average sizes are usually too small.

Additionally, even though operating at high levels of supersaturation beyond the metastable limit implies higher growth rates, the outcome is of poorer quality due to mother liquid incorporation that occurs in these conditions. If, on the one hand, high levels of supersaturation result in inferior crystal quality, on the other hand, slow growth rates, at supersaturation levels close to the solubility curve, lead to high purity crystals at the cost of very long retention times of the product in the solution (W. Omar & Ulrich, 1999).

Long retention times are not desirable for economic reasons (Ulrich & Strege, 2002). With this in view, a compromise between product quality and economic efficiency has to be acknowledged at the industrial scale (Ulrich & Strege, 2002). As a rule of thumb, industrial crystallization should be achieved by operating approximately in the middle of the metastable zone (Hofmann, as cited in Ulrich & Strege, 2002).

Measurement of the metastable width has traditionally been performed in situ at the laboratory scale by detecting nuclei formation by turbidity or by the small temperature increase associated with the heat of formation (Nienow & Paul, 2016). Although struvite formation is an endothermic reaction (Crutchik & Garrido, 2016), there is a heat release involved with attaching molecules to clusters during nucleation (ter Horst et al., 2011).

2.4 Conditions and Parameters Influencing Struvite Crystallization

2.4.1 Supersaturation

Supersaturation is an inclusive parameter which considers the effect of several other parameters (struvite constituent ions, ionic strength, pH and temperature) (Shaddel et al., 2019). From a practical point of view, the regulation of supersaturation is achievable in the process fluid by adjusting the concentration of struvite constituent ions or by adjusting the pH of the bulk solutions (Rahaman et al., 2008).

Supersaturation is the main driving force for the crystallization process (Shaddel et al., 2019) since it is the main factor that causes the nucleation of struvite crystals (Darwish et al., 2016). It is also the main parameter that governs the morphology and the size of the precipitated struvite (Abbona & Boistelle, 1979; Martí et al., 2008).

Struvite morphologies (struvite precipitated from wastewater) observed at low supersaturations (SSR=1–3) show a well-faceted (polyhedral) structure with a bipyramidal appearance and generally free of major defects (Shaddel et al., 2019). Increasing the supersaturation beyond SSR=3 initiates the transition between well-faceted crystals to hopper crystals (Shaddel et al., 2019). As the supersaturation is increased (SSR>5.8), the area of the crystal planes becomes smaller and it eventually disappears at higher supersaturation (Shaddel et al., 2019). Further increases in supersaturation result in the formation of needle-like and dendritic crystals with high aspect ratios - poor quality crystals (Shaddel et al., 2019). The transition exhibited by the crystals from polyhedral to dendritic morphologies is induced by changing growth mechanisms as a result of the increasing supersaturation (Shaddel et al., 2019).

Crystal size and size distribution are also strongly influenced by supersaturation due to its strong effect on the nucleation rate (Shaddel et al., 2019). High supersaturation values (SSR>3) give origin to an increase of fine particles (Shaddel et al., 2019). These smaller particles result from boosted nucleation rates that produce higher number of particles, which then consume the remaining supersaturation by crystal growth (Mehta & Batstone, 2013). The rapid nuclei formation swiftly depletes the ion concentration preventing subsequent crystal growth (Durrant et al., 1999). The rapid rate of nucleation for higher supersaturation is due to a higher driving force for mass transfer from liquid to crystal phase (Ariyanto et al., 2014). On the other hand, lower supersaturation values (SSR=1–3) result in large size crystals with a lower content of fine particles (Shaddel et al., 2019). As a general trend, the particle sizes' decrease with the increase of the initial supersaturation and a more homogenous size distribution is obtained for the particles crystallized at lower supersaturations (Shaddel et al., 2019). Therefore, lower supersaturation levels can be considered for process optimization (Shaddel et al., 2019).

Both nucleation and crystal growth rates raise with supersaturation (Shaddel et al., 2019). Accordingly, the reaction times for completing the precipitation shorten under high supersaturation (Shaddel et al., 2019). Bouropoulos and Koutsoukos (2000) and Ohlinger et al. (1999) reported that the induction time preceding the onset of crystallization is inversely proportional to the supersaturation ratio. Figure 2.7 quantitatively illustrates the increase in growth rate and the decrease in induction time as a function of supersaturation in an experiment carried out by Bouropoulos and Koutsoukos (2000). An increase of SSR from 1.13 to 3.33 shortened the induction time by around 20 fold and increased more than 55 times the crystal growth rate (Le Corre et al., 2009).

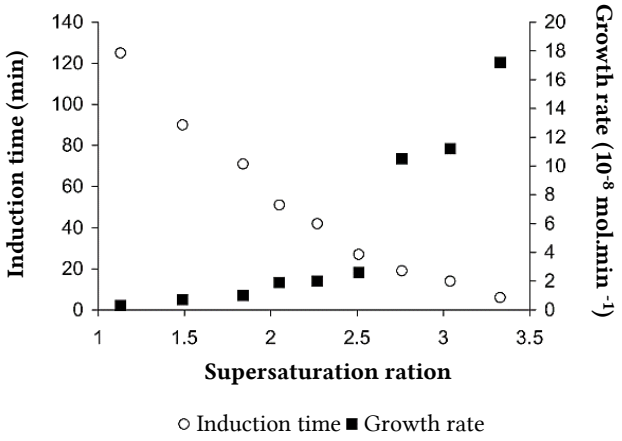

Figure 2.7 - Effect of supersaturation ratio on the induction time and growth rate of struvite at pH 8.50, 25°C (adapted from Bouropoulos & Koutsoukos, 2000).

2.4.2 pH

Several authors have studied the effects of pH on struvite crystallisation and it clearly appeared that it mostly affects the solubility constant (Le Corre et al., 2009). The general acceptable notion about struvite solubility is that it decreases with increasing pH (Ohlinger et al., 1998). However, as pH continues to rise above a pH of about 9, the solubility of struvite begins to increase again, due to the volatilization of free ammonia (Booker et al., 1999; Snoeyink & Jenkins, 1980). Thus, a high initial pH can be limiting in the sense that it causes the transformation of NH_4^+ ions into gaseous ammonia (NH_3). This reduces the nitrogen concentration and affects the molar ratio Mg:N:P (minimum value 1:1:1) necessary to form struvite (Booker et al., 1999; Snoeyink & Jenkins, 1980).

Struvite precipitation has been noted to occur over a wide pH range (7–11) but with varying precipitation potential (J. Wang et al., 2005). Booker et al. (1999) and Stratful et al. (2001) defined in their respective studies a pH range for which the precipitation rate of struvite is optimum. Removal of Mg^{2+}, NH_4^+ and PO_4^{3-} by precipitation of struvite is maximum within the pH range of about 8.5 to 9.5 (Booker et al., 1999).

Naturally, pH also has a significant influence on supersaturation (Li, Huang, et al., 2019). Struvite precipitation is indirectly influenced by the pH of the solution as the supersaturation increases with the increase of pH, until a certain pH value (Darwish et al., 2016). The strong influence of pH on supersaturation results from its deterministic effect on phosphate and ammonia speciation in solution (Shaddel et al., 2019). The increase of pH shifts the equilibrium reactions of struvite constituents, which consequently increases the supersaturation with

respect to struvite (Shaddel et al., 2019). At pH greater than 10, struvite crystallization is inhibited not only due to NH_4^+ volatilization, but also due to the formation of other compounds such as $Mg_3(PO_4)_2$ and $Mg(OH)_2$ that consume Mg^{2+} and HPO_4^{2-} ions, and other amorphous compounds such as hydroxyapatite $Ca_{10}(PO_4)_6(OH)_2$ (Darwish et al., 2016).

As struvite precipitates, it triggers a release of protons ions in solution and consequent change in pH occurs during the nucleation process (Le Corre et al., 2005). The drop in pH is characteristic of the speed at which the first crystals of struvite occurs and is linked to the rate of struvite formation (Le Corre et al., 2005).

2.4.3 Foreign Ions

Ionic species other than Mg, P and N are considered foreign ions. (Li, Huang, et al., 2019). Theoretically speaking, impurities in solution from which a compound may precipitate can affect the growth rate of crystals due to blocking of active growth sites inhibiting the increase of crystal size (Jones, 2002). Although few authors have studied the influence of foreign ions on struvite crystallisation, it is known that the presence of calcium or carbonates ions in the media affects negatively the growth rate and can lengthen the induction time preceding the first occurrence of crystals (Koutsoukos in Le Corre et al., 2009). Le Corre et al. (2005) found that increasing the calcium concentration also may lead to the formation of an amorphous substance rather than crystalline struvite.

2.4.4 Molar Ratios

2.4.4.1 $Mg:NH_4^+:P$ Ratio

Theoretically, struvite may form at a Mg:N:P molar ratio of 1:1:1 (Darwish et al., 2016). In practice, the actual optimum ratio is usually different from the equimolar one due to the presence of other species that may form other products (Zhang et al., 2009). Therefore, optimum molar ratio should be individually contemplated for each case, to achieve the highest efficiency of struvite precipitation (Darwish et al., 2016).

2.4.4.2 Mg:P Ratio

For struvite to form, a Mg:P ratio over one is always required (Li, Huang, et al., 2019). However, it is difficult to determine an optimal Mg:P ratio under varying solution composition (Li, Huang, et al., 2019). Magnesium dosage in excess might be required when and if the usage of NaOH is considered for pH adjustment (Korchef et al., 2011). A pH elevation may increase the local saturation of undesired precipitates (i.e., newberyite, bobierrite and brucite), which compete with struvite for magnesium (Hutnik et al., 2011). On the other hand, excess magnesium may decrease struvite purity (Demeestere et al., 2001). A wide range of PO_4:Mg values have been applied for struvite precipitation from wastewater, but in most cases, the effective ratio was 1:1 or 1:1.2 (Rahman et al., 2011).

The Mg:P molar ratio further plays an important role in the compactness of the struvite produced – higher Mg:P values give origin to more “compact” crystals (Fattah et al., 2008). High magnesium concentrations also favour struvite crystal aggregation (Bouropoulos & Koutsoukos, 2000).

2.4.4.3 NH_4^+:P Ratio

NH_4^+ also participates to struvite precipitation: the supersaturation increases with the N:P molar ratio and the nucleation rate of struvite is speeded up (Capdevielle et al., 2013).

Additionally, NH_4^+ improves the buffer capacity of the solution (Capdevielle et al., 2013). The nucleation of struvite occurs at a lower pH than the one needed for the precipitation of calcium phosphate (Abbona et al., 1986). Consequently, struvite precipitation is favoured by a high concentration of NH_4^+ (Capdevielle et al., 2013). A stoichiometric excess of ammonium (30–80 ppm) has been reported to help drive the reaction to form relatively pure struvite (Stratful et al., 2001).

Moreover, the ammonium concentration influences the lateral growth and thickness of struvite crystals (Shaddel et al., 2019). Increasing the content of NH_4^+ affects the distribution of supersaturation around the growing crystal (Shaddel et al., 2019). Lower concentrations of NH_4^+ result in smoother top surfaces and less branching of the crystals (Shaddel et al., 2019).

2.4.5 Mixing Energy or Turbulence

At the optimum pH, the induction time is affected by the process fluid turbulence (Ohlinger et al., 1999). The induction time decreases as the mixing speed increases and the nucleation of struvite becomes rapid (Rahaman et al., 2008). Once the nuclei are formed, struvite crystal growth on the existing nucleation sites is primarily controlled by the mixing energy (Rahaman et al., 2008). Mixing enhances the mass transfer of solute to crystal and increases the crystal growth rate. (Li, Huang, et al., 2019). Growth rate is believed to be limited by low turbulence or low mixing energy (Ohlinger, 1999). Contrarily, excess mixing may lead to crystal breakdown (Rahaman et al., 2008).

2.4.6 Temperature

Reaction temperature has a significant effect on the solubility products of crystals (Fang et al., 2016). The effect of temperature on solubility shows a steady increase in solubility with increasing temperature until 50°C (Aage et al., 1997) – Figure 2.8. Maximum solubility was found to be at 50°C with solubility then falling (Doyle & Parsons, 2002).

As the solubility product is linked to the supersaturation state of the solution in which crystals may occur, the precipitation of struvite is more difficult to obtain at high temperatures (Le Corre et al., 2009)

Temperature is also known to affect crystal growth as it affects the relative rates of diffusion and surface integration (Le Corre et al., 2009). High temperature of crystallisation usually leads to diffusion-controlled growths, while low ones lead to surface integration controlled growths (Jones, 2002). Moreover, the rate of crystal growth often increases at high temperature and can affect crystal size shape and type (Le Corre et al., 2009). For an identical range of concentrations, struvite crystals adopted a dendritic form in a wider zone at 37° C than at 25° C (Babić-Ivančić et al., 2002). Also, for high magnesium concentrations, high temperature could affect the nature

of crystal formed, e.g., struvite transforming faster into newberyite than at lower temperature (Babić-Ivančić et al., 2002).

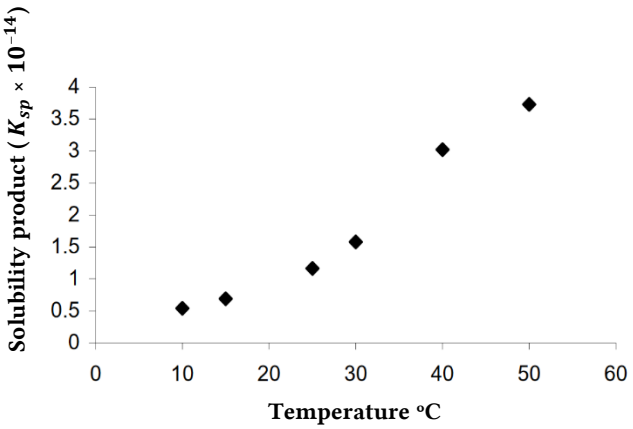

Figure 2.8 - Evolution of struvite solubility product on temperature according to Aage and Burns data (adapted from Aage et al., 1997).

2.4.7 Seeding

Seeding promotes crystal growth by enabling the crystallisation of small struvite particles on seeds (Le Corre et al., 2009). It helps to overcome the initial energy barrier for nucleation as seeds act as centres of secondary nucleation and subsequent crystallization is possible (Li, Huang, et al., 2019). Faster nucleation and better struvite product quality can be achieved through proper seeding (Li, Huang, et al., 2019). Kim et al. (2009) found that seeding concentration changed the crystallization mechanism - nucleation was the main mechanism at lower seed concentration and crystal growth was preferred at higher concentrations.

2.5 Summary

Struvite ($MgNH_4PO_4 \cdot 6H_2O$) is a white to yellowish crystal with enhanced fertilizing properties. Struvite forms with an equal molar concentration of magnesium, ammonium, and phosphate combined with six water molecules ($MgNH_4PO_4 \cdot 6H_2O$)

As a phosphate fertilizer, struvite stands out for its very slow nutrient release rate. Additionally, the crystal is sparingly soluble in water which reduces both the leaching tendency and the nutrient loss due to surface run-off. Usage of struvite as a raw material for chemical industry is also possible. Struvite crystals forms spontaneously in various biological media (e.g. guano deposits and cow manure) and in WWTP facilities.

Struvite's solubility is highly dependent on the pH of the solution from which struvite may crystalize. The reason for this is that pH influences the speciation of struvite's constituent ions- Mg^{2+}, NH_4^+, and PO_4^{3-}. Also, these ions exhibit complex equilibria in aqueous solution and may form several complexes by varying the solution pH. Therefore, the precipitation potential of struvite is also pH dependent.

Because of this pH dependency, the prediction of struvite precipitation from a solution can be complex and time-consuming. To overcome this difficulty, one uses an equilibrium conditional solubility product, $P_{s_{eq}}$, which can be determined in a practical manner by multiplying the total analytical concentrations of each of struvite's constituents - Mg, NH_4, and PO_4 - present in the solution. The total analytical concentration of a struvite's constituent is the sum of its respective complexes and free ions.

Plotting the negative log of $P_{s_{eq}}$, $pP_{s_{eq}}$, versus pH establishes a curve for that particular solution - the struvite solubility limit curve. The drawing of such curve requires the placement of a sufficient amount of struvite crystals in a few jars, each one containing the solution in study (naturally, each jar will be at a different pH). Analytical concentrations can then be measured. The resulting curve represents the equilibrium between struvite's solid phase and its dissolved ions, in aqueous solution, for a range of pH values. This equilibrium can be altered, by instance, by adding struvite's constituent ions into the solution or changing the pH solution. In that case, the conditional solubility product is designed P_s instead of $P_{s_{eq}}$.

A solution with a pP_s (-log (P_s)) above the equilibrium curve is supersaturated for struvite. The higher above the curve that a pP_s point resides, the higher the precipitation potential. To relieve supersaturation and move towards equilibrium, the solution crystallizes. By doing so, the concentration of struvite's constituent ions in solution decreases. Crystallization may occur until pP_s intersects the equilibrium curve. Supersaturation ration is the quotient between P_s and $P_{s_{eq}}$ and is a measure of the precipitation potential. For SSR>1 precipitation is possible and for SSR<1 it is not. The main disadvantage of using $P_{s_{eq}}$ is that it refers solely to the matrix in study, rendering the comparison between studies more complicated, since struvite formation potential is dependent on the solution composition and conditions (e.g., pH).

Even though supersaturation is the main driving force of crystallization processes, one should note that supersaturation of a solution is a necessary but not sufficient condition for struvite to crystallize from it. There are energy barriers that must be overcome for crystallization to occur. These energy requirements can be more easily achieved by seeding the solution. SSR values between 3 and 5 are considered ideal for the growth of crystals larger than 1 mm of diameter. For growth to occur at these SSR values, it is imperative that the solution is seeded.

Several parameters have been proved to have the most influence on struvite crystallization, namely, in crystal size and size distribution, and in crystal morphology. These are: supersaturation, pH, foreign ions, molar ratios (Mg:NH_4^+:P, NH_4^+:P, Mg:P), turbulence and temperature and solution seeding. SSR from 1 to 3 provide crystals of good quality in terms of morphology. Increasing SSR also reduces the induction time and enhances the growth rate (high SSR will however origin poorer crystals). Precipitation of struvite is maximum within a pH range of about 8.5 to 9.5. For pH >9 struvite solubility decreases, diminishing the precipitation potential. Foreign ions such as Ca, inhibit or difficult struvite's precipitation. For crystallization to occur, Mg:NH_4^+:P must be at least 1. Increasing mixing speed decreases the induction time and increases crystal growth rate. Nonetheless, excessive mixing energy may lead to crystal breakdown. Lower temperatures (10-20ºC) favour struvite precipitation. Seeding helps to overcome the initial energy barrier for nucleation to occur.

CHAPTER 3

BIOLOGICAL PHOSPHORUS REMOVAL

By far the most successful and widely used biological treatment technology is the activated sludge process (Oh et al., 2010). In municipal activated sludge wastewater treatment systems, the two main approaches utilised for phosphorus removal from wastewater are traditional chemical phosphorus removal and biological phosphorus removal (Blackall et al., 2002). A combination of these processes is also frequently used (Yeoman et al., 1988).

The present chapter aims to, firstly, describe thoroughly the biological P removal mechanism used in municipal activated sludge wastewater treatment systems, and secondly, delve into the reasons that make it an opportunity for P recover, more precisely, in the form of struvite. Therefore, Chapter 3 is organized in four major parts: section 3.1, sections 3.2 to 3.4, section 3.5 and section 3.6.

Section 3.1 briefly describes the differences between the two traditional technologies for P-removal from wastewater: chemical P removal and biological P removal. Furthermore, this section explains the main reasons why, currently, chemical phosphorus removal is being replaced by biological methods in municipal wastewater treatment.

Sections 3.2 to 3.4 focus on the biological P removal mechanism. Section 3.2 clarifies the biological phosphorus removal mechanism, whereas section 3.3 describes the most simple system configuration of biological P removal in municipal activated sludge wastewater treatment systems. Additionally, section 3.4 outlines the advantages and disadvantages of the biological phosphorus removal mechanism.

Section 3.5 discusses how a particular disadvantage – potential P release in anaerobic conditions, described in section 3.4 - can comprise an opportunity for P recovery in the form of struvite.

Concluding remarks regarding are presented in section 3.6.

3.1 Traditional Technologies for Phosphorus Removal from Municipal Wastewater

Both chemical and biological removal techniques work by fixing the phosphorus in the sludge (Le Corre et al., 2009) and are efficient in the sense that they achieve effluent concentrations of 1 to 2 $mg.L^{-1}$ (Parsons & Smith, 2008). From a P recovery perspective, the major drawbacks with these methods is, however, that the phosphorus is removed along with various other wastage products (Stratful et al., 1999).

Traditional chemical removal is brought about by adding metal salts that react chemically with soluble orthophosphates to form precipitates of insoluble metal phosphates (Morse et al., 1998). Iron (II), iron (III) and aluminium (III) are the types of metal precipitants most commonly used (Parsons & Berry, 2004). The metal salts may be added: (i) at the primary clarifier (pre-precipitation); (ii) directly to the mixed liquor, either in the aeration basin or upstream of the secondary clarifier (simultaneous precipitation); or (iii) after the secondary portion of the plant in the feed, to a tertiary solid–liquid separation process (post-precipitation) (Janssen, 2002). Multiple point addition may also be employed (Parsons & Berry, 2004).

These formed precipitates of insoluble metal phosphates are usually removed by solids separation processes (e.g., sedimentation, flotation or filtration) (Tchobanoglous & Burton, 1991) and are found incorporated in the resulting sludge (Le Corre et al., 2009). Whilst resulting precipitates may be rich in P, separation of chemically bonded phosphorus from the sludge requires elaborate and expensive operations to make it recoverable and reusable (Daneshgar et al., 2018). Chemical precipitation renders the precipitates difficult, if not impossible, to be recycled in an economical and industrial manner (de-Bashan & Bashan, 2004).

On the other hand, the biological phosphorus removal process is based on the principle that some types of bacteria, present in the microbial biomass in activated sludge, are able to accumulate large amounts of soluble orthophosphate, beyond its anabolic requirements (Janssen, 2002; Wentzel et al., 2008). The orthophosphate is stored in the bacteria cells in the form of insoluble polyphosphate (polyP) (de-Bashan & Bashan, 2004). Biological phosphorus removal is realized by creating favorable conditions for the growth of these bacteria, which results in the enrichment of P in the sludge (Mulkerrins et al., 2004). The biological phosphorus removal mechanism is rather elaborate - further explanation will be provided in section 3.2.

Ultimate elimination of phosphate from the system is achieved by the wastage of P-rich excess sludge (McGrath & Quinn, 2004). Recovered phosphorus is naturally biologically bound and can be released into solution under certain conditions (Morse et al., 1998). Thus, from a recovery point of view, the EBPR is a much more promising option – phosphorus is concentrated in such way in the activated sludge that its recovery is relatively easy (Janssen, 2002). Sludges from biological phosphorus removal are higher in plant available P and make better agricultural fertilisers (Stratful et al., 1999). Biological phosphorus removal may also be expressed as enhanced biological phosphorus removal (EBPR) or biological excess phosphorus removal (BEPR) (Wentzel et al., 2008).

While both chemical and biological phosphorus removal techniques can produce adequately low levels of P in treated wastewater (Blackall et al., 2002), the latter is seeing increased used in

comparison to the former (Grady et al., 1999). Besides the easier management and significantly higher reuse potential of produced sludges, EBPR offers other advantages. These benefits are almost all linked to the total absence or very limited dosing of chemicals (Blackall et al., 2002). They include eliminating chemical usage costs and decreasing the quantity of waste sludge that must be processed (Grady et al., 1999).

As a matter of fact, dosing chemicals during chemical phosphorus removal results in the major following drawbacks: higher chemical costs than those of biological phosphorus removal systems; and a significant increase in sludge production, which results in a higher sludge treatment and disposal costs (Bowker & Stensel, 1987). These shortcomings comprise the main reasons why, currently, chemical phosphorus removal is being replaced by biological methods in municipal wastewater treatment (Haandel & Lubbe, 2015; Stratful et al., 1999). Nonetheless, chemical phosphorus removal can still be useful, for instance if the activated sludge system does not have enough capacity for complete BPR (Haandel & Lubbe, 2015). Metal salt addition for phosphorus removal is a reliable, well documented P removal technique and also has its benefits (Haandel & Lubbe, 2015). These benefits are: (i) controls required for P removal are fairly simple and straightforward; (ii) chemical usage requirement is basically dependent on total phosphorus concentration of wastewater and required effluent levels; (iii) P removal is relatively easy and inexpensive to install in existing facilities, and effluent P levels can be controlled by metal salt dosages to maximum efficiency levels (Haandel & Lubbe, 2015).

When relating to chemical precipitation, the BPR also has its disadvantages (Janssen, 2002). As soon as the BPR mechanism is considered, both advantages and disadvantages of the EBPR will be afterward considered in depth.

3.2 Biological Phosphorus Removal Mechanism

Enhanced biological phosphorus removal may be defined as the biological uptake of phosphorus by selected microorganisms present in the activated sludge system, in considerable excess of that required for their balanced microbial growth (Greenberg et al., 1955; Janssen, 2002). These selected microorganisms are collectively referred to as phosphate accumulating organisms (PAOs) as they are able to store large amounts of soluble orthophosphate in the form of insoluble polyphosphates (polyP) in intracellular reserves (Wentzel et al., 2008). PolyP consists of a linear chain of phosphate groups linked together by high-energy phosphoanhydride bonds and ranges in length from three to greater than 100 orthophosphate groups (Kulaev, 1979). The stored polyphosphate is considered as a phosphate or energy backup (Janssen, 2002).

The biological removal process capacity is inherently related to the fraction of the PAOs present in the activated sludge process, or the ability to increase their fraction in it (Janssen et al., 2002). Biological phosphorus removal is, therefore, accomplished by creating conditions favourable for the growth of PAOs, causing the activated sludge community to become enriched in them (Grady et al., 1999). The BPR process is primarily characterised by circulation of activated sludge through anaerobic and aerobic phases, coupled with the introduction of influent wastewater into the anaerobic phase (Wagner & Loy, 2002).

Figure 3.1 illustrates the reactions taking place in PAOs under anaerobic conditions through a simplified biochemical model. Initial anaerobic conditions are required for PAOs to gain a selective advantage over other bacteria, through their ability to take up substrate in the form of

short chain volatile fatty acids (VFAs) (e.g., acetate and propionate), and to convert these to a carbon storage polymer (McGrath & Quinn, 2004). For that purpose, VFAs must be available to trigger the development of PAOs (Morse et al., 1998). Volatile fatty acids are either a part of the readily biodegradable substrate in the influent or are formed from it by fermentation in the anaerobic zone by facultative aerobic bacteria (fermenting organisms) (Wiesmann et al., 2007). PAOs take up VFAs from the bulk liquid and store them internally by linking them together to form complex long chain carbon molecules of poly-β-hydroxyalkanoates (PHAs), a carbon storage polymer (Wentzel et al., 2008).

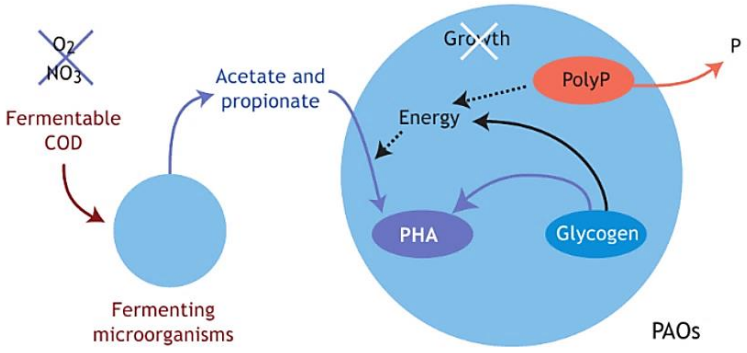

Figure 3.1 - Simplified biochemical model for PAOs under anaerobic conditions (Wentzel et al., 2008).

Most of the energy required for the VFAs uptake and later PHAs synthesis comes at the expense of hydrolysis of another biopolymer – polyP (Wentzel et al., 2008). PolyP is previously stored in the cells by PAOs microorganisms (Wentzel et al., 2008). When polyP is hydrolysed, i.e., broken down to orthophosphate for energy supply, orthophosphate is released to the extracellular medium, being carried into the liquid phase (McGrath & Quinn, 2004). The absence of nitrate in the anaerobic phase is critical for polyP utilisation during PHA formation, since nitric oxide exhibits an inhibitory effect on enzymes that play an essential role in the degradation of polyphosphate (Wentzel et al., 2008). Being a storage compound, glycogen also plays an important role in providing part of the energy required through its degradation (McGrath & Quinn, 2004; Wiesmann et al., 2007).

In contrast to PAOs, which store some of the substrate during the anaerobic phase (Wentzel et al., 2008), organisms other than PAOs have a lower or no availability to the substrate (acetate or VFA) under this condition (Janssen, 2002). Because oxygen and nitrate-N are absent, oxidation of organic matter cannot occur in the time provided, making it impossible for most species of heterotrophic bacteria to transport and store or metabolize organic matter (Grady et al., 1999). Rather, these heterotrophic bacteria only carry out fermentation reactions, resulting in the formation of volatile fatty acids (VFAs) (Grady et al., 1999). Thus, and even though there is no growth involved in the anaerobic phase of the process, the aforesaid will lend an advantage to PAOs to grow in relation to the non-PAOs in the aerobic phase of the activated sludge (Wentzel et al., 2008).

Once the activated sludge has circulated through an anaerobic phase, the circulation through an aerobic one must follow (Wagner & Loy, 2002). One should note that by the time the mixed liquor flows into the aerobic zone, VFAs are stored through the PAOs' polyP reserves (Grady et al., 1999). As a result, VFAs are unavailable to the other heterotrophic bacteria and, in aerobic conditions, only the slow biodegradable substrate is available to them (Grady et al., 1999). Under these circumstances, PAOs do not have to compete for substrate as the stored substrate in the polyP reserves is used exclusively by them (Grady et al., 1999).

Figure 3.2 depicts the reactions taking place in PAOs under aerobic conditions through another simplified biochemical model. In aerobic conditions, the carbon reserves previously stored as PHA by PAOs are oxidized with oxygen or nitrate (Janssen, 2002). The released energy is used by the PAOs: (i) for cell growth; (ii) for the synthesis of glycogen; and (iii) to take up the orthophosphate from the water phase and store it as polyphosphate in their cells (Wiesmann et al., 2007). By taking up orthophosphate and converting it to polyP, PAOs are able to replenish their internal polyP (McGrath & Quinn, 2004). In doing so, PAOs remove not only the formerly released orthophosphate by them during the anaerobic phase but also almost all the available orthophosphate from the surrounding oxygen rich environment (McGrath & Quinn, 2004). In other words, orthophosphate is taken up by PAOs to a higher level than that released by them in the anaerobic stage (Wiesmann et al., 2007).

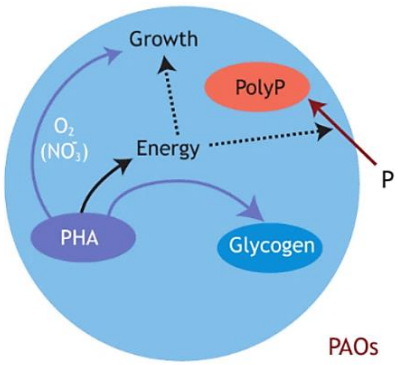

Figure 3.2 - Simplified biochemical model for PAOs under aerobic conditions (Wentzel et al., 2008).

Although PAOs are often present in significant numbers in totally aerobic suspended growth cultures, they only develop the ability to store large quantities of phosphate when they are subjected to alternating anaerobic and aerobic conditions (Lötter et al., 1986). This follows from their unique capability to store carbon at the expense of phosphate under anaerobic conditions and to store phosphate at the expense of carbon under aerobic conditions (Grady et al., 1999). By doing so, PAOs are adequately established and become predominant in the biomass community after several weeks (Wentzel et al., 2008). Phosphate uptake may not necessarily require an aerobic stage (McGrath & Quinn, 2004). Under anoxic conditions nitrate can provide an alternative electron acceptor for phosphate assimilation and intracellular polyP formation (Kuba et al., 1993).

The P uptake in the aerobic phase results in more phosphate being included in the cells than was released in the anaerobic zone, so the total phosphate concentration in solution is reduced (Kang et al., 2008). When the microorganisms are removed through settling and wasting, the contained phosphate is also removed (Kang et al., 2008). The net elimination of the process results from the bacterial cell growth and the removal of surplus sludge at the point when the phosphate is taken up to a higher level than that released in the anaerobic stage (Wentzel et al., 2008). Phosphorus is biologically bound in the resulting biological sludge and the P accumulated in the bacterial cells can be again released if anaerobic conditions are established afterwards (Daneshgar et al., 2018; Morse et al., 1998).

3.3 System Configurations of Biological Phosphorus Removal

The treatment objectives of a BPR activated sludge system are to remove organic matter and phosphorus from mixed liquor to required levels, and to develop a sludge that settles well enough to produce an effluent low in suspended solids after standard clarification (Randall et al., 1992).

The BPR process configuration is simple and requires only a small change from conventional activated sludge design (Randall et al., 1992). Instead of the biological reactor being a single conventional aeration basin, the influent wastewater should flow into an anaerobic stage, followed by an aerobic one, ensued by clarification and recycle of the settled sludge back to the anaerobic stage (Randall et al., 1992). Recycled sludge then mixes with the influent wastewater (Randall et al., 1992).

The return activated sludge is recycled to the anaerobic zone to build up the population of PAOs in the system and to be reconditioned for another EBPR cycle (Minnesota Pollution Control Agency, 2006). Figure 3.3 illustrates the basic configuration for a continuous flow system (Randall et al., 1992), which comprises the typical configuration of EBPR (Motlagh & Goel, 2014).

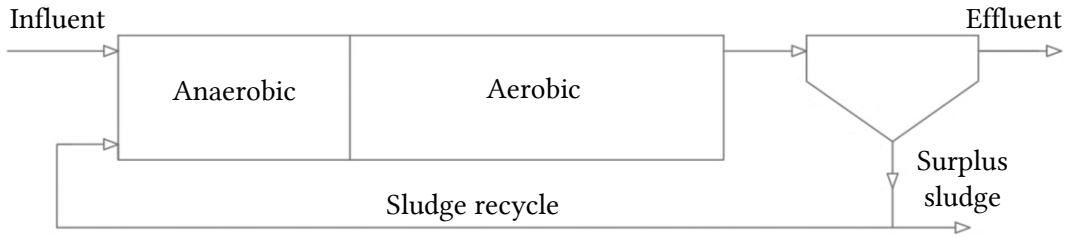

Figure 3.3 - Two-stage biological phosphorus removal system (adapted from Janssen, 2002).

Nonetheless, many other system configurations for application of the EBPR have been developed and implemented in practice (Janssen, 2002). The main difference between these systems is the way in which an anaerobic zone is maintained and protected against the introduction of nitrate (Haandel & Lubbe, 2015). Processes that remove both nitrogen and phosphorus incorporate anaerobic, anoxic and aerobic zones along with mixed liquor recirculation (Grady et al., 1999). Further discussion of other configurations rather than the one depicted in figure 2.11 is out of the scope of the present dissertation. More information about these can be found in the works carried out by Randall et al. (1992), Grady et al. (1999) and Haandel & Lubbe (2015).

3.4 Advantages and Disadvantages of the Biological Phosphorus Removal

Several advantages of the BPR process are coupled to the absence or limited presence of chemicals (Janssen, 2002) (chemical usage may be necessary in cases where there is loss of BPR

efficiency (Bowker & Stensel, 1987)). The advantages over chemical processes as well as BPR intrinsic advantages are summarized in Table 3.1. Disadvantages of the biological process are also discussed in Table 3.1.

Table 3.1 - Advantages and disadvantages of biological phosphorus removal processes (Bowker & Stensel, 1987; Janssen, 2002).

Advantages	Disadvantages
There is no chemical sludge production. Sludge quantities generated are comparable to the ones of conventional activated sludge systems. Chemical dosing, sludge handle and disposal costs are, therefore, significantly less compared to the chemical processes' ones.	**Dependence on wastewater composition.** The capacity of the activated sludge to enhance PAOs is dependent on the available amount of organically bound carbon, among other factors.
There is no deterioration of water dewaterability of the surplus sludge. In chemical methods, phosphate is conserved in the form of a metal phosphate with an adherent water fraction.	**Lower stability and flexibility.** Despite improved controlled possibilities, the quality of total effluent under significantly changing process conditions is less stable than in chemical processing methods.
Sludge is of better quality. Due to higher P content, surplus biological sludge constitutes a potentially attractive source for fertilization. Biologically bound phosphate acts as a "slow fertilizer". The relatively low release of phosphate increases fertilizer value and hence plant grow.	**Potential for phosphorus release in the sludge handling system.** Stored phosphate may be released from the BPR sludge as a consequence of anaerobic conditions in some sub-processes of the sludge treatment, e.g., anaerobic digestion. Dewatering of the BPR sludge then results in the recycling of the orthophosphate back to the main treatment.
Negligible extra implementation costs. Can be implemented directly at existing plug flow activated sludge plants with little or no equipment changes or additions provided that the plant has enough capacity.	**Demand of efficient solid separation processes.** Requires highly efficient secondary clarifier performance to achieve 1 mg/L of total P.
Possibility to simultaneous recover nitrogen. Phosphorus removal can be accomplished together with ammonia nitrogen or total nitrogen removal at virtually no additional operating costs with some of the processes' configurations.	**Somewhat limited to suspended growth systems.** Not easily retrofitted into fixed biological systems.

Although biological phosphorus removal has many advantages over chemical phosphorus removal, there is one disadvantage of the BPR process worth discussing in more detail. This disadvantage is the phosphorus release in the sludge treatment as a consequence of anaerobic conditions. This release does not occur for chemically precipitated phosphate (Haandel & Lubbe, 2015).

Often, excess sludge undergoes one or more sludge treatment steps, for instance, a gravitational thickening, possibly followed by sludge digestion and sludge dewatering (Janssen, 2002). At

WWTP using the BPR processes, these sludge treatment steps may release phosphate to the liquid phase as a consequence of exposure to anaerobic conditions (Haandel & Lubbe, 2015). Phosphate occurs not only because the release of biologically stored phosphate but also due to a long sludge age through a decay of cells (due to lysis) (Janssen, 2002). P release results in P-rich internal streams and increases the P load to be treated (Janssen, 2002).

Phosphate release always takes place during gravitational thickening of secondary BPR sludge (Janssen, 2002). The release is attributed to the hydrolysis of polyphosphate by PAOs under the anaerobic conditions developed within the thickener (Gutierrez et al., 2020). This P release is determined by the sludge retention time in the thickener and the polyphosphate content of the sludge (Janssen, 2002). Gravitational thickening of surplus BPR sludge, comprising a hydraulic retention time of one day, is already sufficient to convert about 50% of all polyphosphate into orthophosphate (Haandel & Lubbe, 2015). After two days, the conversion is almost complete (Haandel & Lubbe, 2015). Thickening of secondary excess sludge together with primary sludge, when both sludges have become highly anaerobic, will lead to increased phosphate release due to the presence of easily biodegradable organic matter in the primary sludge (Haandel & Lubbe, 2015; Jaffer & Pearce, 2004). Phosphate release due to cell lysis is in general not significant in a thickener (Haandel & Lubbe, 2015). When the sludge in the thickener is unstirred, the orthophosphate remains in the thickened sludge layer (Janssen, 2002). This phosphate will finally come free in the following sludge dewatering processes (Janssen, 2002). The phosphate will be transported by turbulence from the thickened sludge layer to the overflow water (Janssen, 2002).

Phosphorus' solubilisation will proceed through the sludge stabilization process (Jaffer & Pearce, 2004). During anaerobic sludge digestion, a complete degradation of polyphosphate to orthophosphate takes place due to high temperatures and long retention times (Janssen, 2002). A large part of the organic phosphorus contained in the organic sludge is also converted to orthophosphates because of the degradation of cells (Haandel & Lubbe, 2015; Janssen, 2002). Overflow water may consist of overflow after secondary thickening in a gravitational thickener, or may consist of the filtrate/centrate after dewatering of the digested sludge in a belt filter press/centrifuge (Janssen, 2002). Either way, it contains the same level of orthophosphate as the one present in the digester (Janssen, 2002).

When thickened or digested sludge is dewatered, all phosphate present in the liquid phase will be returned to the head of the activated sludge process (Haandel & Lubbe, 2015). The soluble phosphorus remaining in all of the return liquor streams increases the load on the secondary treatment and may represent a 25–45% recycle of the phosphorus load arriving at the works on a daily basis (Jaffer & Pearce, 2004). The negative effect of this internal phosphate loading on the effluent (i.e., reduction of BPR) varies in practical conditions according to the P uptake capacity of the sludge (Janssen, 2002). The balance of the received phosphorus load leaves the site in the dewatered sludge cake (Jaffer & Pearce, 2004). Some of this will still be in organic form, predominantly intercellular, arising from non-degraded cells from the activated sludge (Jaffer & Pearce, 2004). Some other will still be in soluble form in the liquid phase of the sludge cake (Jaffer & Pearce, 2004).

Furthermore, WWTP, especially those employing secondary treatment and anaerobic sludge digestion, suffer from accumulation of struvite on pipe walls and equipment surfaces of anaerobic digestion and post digestion processes (Fattah et al., 2008). This growth of "uncontrolled" struvite increases pumping and maintenance cost as well as reduces the overall capacity of the plant in lost hydraulic capacity (Fattah et al., 2008). Figure 3.4 illustrates a 6" pipe where part of the struvite has already been removed on the right side.

Figure 3.4 - Involuntary formation of struvite on pipe walls (on the left) (Jayne Products, n.d.).

This uncontrolled struvite formation that occurs in the treatment plant cannot be used as fertilizer as it is difficult to remove once formed in the pipes and pumps, and often requires the use of concentrated acid and hot water blasting (Fattah, 2014). Sometimes the extent of fouling is so severe that the replacement of pipework becomes the only feasible option (Doyle & Parsons, 2002). Annual costs for a mid-size treatment plant (25 MGD) related to struvite deposits can easily exceed US$100.000 (Benisch et al. as cited in Doyle & Parsons, 2002).

As a matter of fact, struvite precipitation is possible from sludge or water streams containing high concentrations of soluble phosphate (Korving et al., 2019) and these phosphate concentrations are typically found when a WWTP combines EBPR and anaerobic sludge digestion (Korving et al., 2019; Schipper, 2019).

The formation of struvite under such circumstances occurs due to the released phosphate from anaerobically digested biological sludge that may complex with metal ions (Haandel & Lubbe, 2015). Metal ions originate from wastewater and are brought together with the sludge to the digester (Janssen, 2002). In general, PAOs also contain a significant amount of Mg^{2+} as a result of adsorbing it as a compensation for the negative electrical charge of PO_4^{3-} (Haandel & Lubbe, 2015). During the breakdown of polyphosphates in the digester, these metals come free and they also play a role in the binding of phosphate (Jaffer & Pearce, 2004; Janssen, 2002). During sludge digestion, the released Mg^{2+} will precipitate with PO_4^{3-} as $Mg_2(PO_4)_3$ (Haandel & Lubbe, 2015). If NH_4^+ is present, as normally it will be since ammonia is produced from the break-down of proteins and bacteria (Münch & Barr, 2001), struvite is formed (Haandel & Lubbe, 2015). Combined with the high ammoniacal nitrogen concentrations and elevated soluble magnesium concentrations present in the digester, and the buffered pH of 7.3–7.5, the potential for struvite precipitation is large (Jaffer & Pearce, 2004).

Struvite scaling is also a prominent nuisance in digester supernatant recycle lines, especially at the elbows and the suction side of pumps (Borgerding, 1972). Borgerding (1972) gives four other factors that may be responsible, either singly or in combination, for producing suitable conditions for this:

i. Surface to volume ratio. In sludge storage units such as the digesters, the surface area to volume ratio is small, whereas in sludge supernatant pipelines is large. Therefore, a pipeline provides proportionately larger surface areas than a digester on which nucleation and crystallisation can occur. Furthermore, during the times of no flow (i.e., no sludge or supernatant withdrawal) the conditions are ideal for the settlement of formed struvite.

ii. Condition of interior surface of pipewalls. Rough pipelines provide better nucleation surfaces (joints in the pipes also serve the same purpose). Tests carried in PVC pipes showed the least growth and cast iron showed the thickest growth.
iii. Increase in energy. Vibrations and gentle stirring have been found to aid the formation of precipitates in supersaturated solutions. At wastewater treatment plants, vibrations occurring in centrifuges and pumps cause struvite to precipitate at these locations.
iv. Pressure changes in pipelines. Localised pressure decreases occur at bends in pipelines, pump suction lines or venturis causing the release of dissolved CO_2 at these locations. This in turn raises the pH. Struvite is highly insoluble at alkaline pH and therefore precipitation occurs at these locations.

The phenomenon of struvite scaling is not restricted to plants with biological nutrient removal (BNR) process followed by anaerobic digestion - industrial experience suggests that it can also occur on conventional non-nutrient removal sites (Jaffer & Pearce, 2004). The BNR process, however, will exacerbate any problem by increasing the amount of soluble phosphorus and magnesium in the digested sludge and liquors (Carliell-Marquet & Wheatley, 2002).

Even though this P-release from sludge treatment may at first sight seem like nothing more than an inconvenient, it constitutes, a possibility for phosphorus recovery. The following section will delve into the reasons that make this P release a potential opportunity for P recovery in the form of struvite.

3.5 Phosphorus Release from Sludge Treatment Processes - an Opportunity for Struvite Recovery

The fate of the intracellular phosphorus, once surplus activated sludge is wasted from the BNR process, is of key importance for the recovery of phosphorus (Jaffer & Pearce, 2004). The phosphorus that is incorporated into bacterial biomass in the EBPR process is released to the liquid phase during sludge treatment processes, such as gravity thickening , anaerobic digestion and dewatering (Haandel & Lubbe, 2015). If the soluble phosphorus remaining in all of the return liquor streams is returned to the head of the activated sludge process, most of the P is only recirculated and not removed (Münch & Barr, 2001).

On the one hand, several measures to prevent phosphate recycling from sludge treatment could be applied (Janssen, 2002). These measures include: choice of a different thickening process; controlled operation of a gravitational thickener; separated stabilisation of primary and secondary sludge; and active binding of orthophosphate via chemical precipitation (in general iron salts are added) (Janssen, 2002).

On the other hand, the rejected liquors (sidestreams) from digested sludge dewatering show high phosphorus, ammonium and magnesium concentrations, which make these streams very appropriate for recovering phosphorus as struvite in a crystallization process (Martí et al., 2010). BPR has the potential to be used to pre-concentrate phosphorus from dilute municipal wastewater (Stratful et al., 1999). The concentrated streams will then enable the crystallization process to work more efficiently (Stratful et al., 1999). The thickener supernatant could also be used in the crystallization process since polyP hydrolysis can take place in the gravity thickener. Remind that precipitation of struvite requires that its components are available simultaneously

in the molecular ratio 1:1:1 (Mg^{2+}:NH_4^+: PO_4^{3-}) (de-Bashan & Bashan, 2004). Normally, municipal wastewaters tend to be rich in ammonium, but deficient in magnesium, so supplementation of magnesium may be required for the reaction to occur (de-Bashan & Bashan, 2004). Besides, struvite is one of the most insoluble phosphorus that not only extracts phosphate but also, to a lesser extent, nitrogen from solution during its formation (Hobbs, 2004).

Although uncontrolled formation is a nuisance, controlled production of struvite can be applied to remove phosphorus from sidestreams, reducing the recirculated phosphorus and nitrogen load to the head of wastewater treatment (Münch & Barr, 2001). This enables EBPR plants to achieve very low levels of effluent P concentrations (Münch & Barr, 2001). Controlled struvite production is also beneficial to treatment plants by reducing maintenance costs due to struvite scale prevention, as well as providing extra revenue from the sale of the recovered struvite crystals as fertilizers (Fattah, 2012).

If phosphorus is removed only from the sludge water after dewatering the digested sludge, scaling problems within centrifuges, digesters and sludge liquors pipes before the actual controlled crystallization will probably still occur (Petzet & Cornel, 2012). In this context, addition of a magnesium source directly to digested sludge followed by aeration to trigger struvite precipitation within the digested sludge has also been proposed and applied (Petzet & Cornel, 2012).

3.6 Summary

From a recovery point of view, the EBPR is a more promising option than chemical P precipitation – phosphorus is concentrated in such way in the activated sludge that its recovery is relatively easy (Janssen, 2002). Sludges from biological phosphorus removal are higher in plant available P and make better agricultural fertilisers (Stratful et al., 1999).

The biological phosphorus removal process is based on the principle that some types of bacteria, present in the microbial biomass in the activated sludge, are able to accumulate large amounts of soluble orthophosphate. These microorganisms are called PAOs (Wentzel et al., 2008). Thus, the biological P removal is realized by creating conditions favorable for the PAOs.

An initial anaerobic zone allows the PAOs to take up VFAs into their cells and store them as PHA. The energy needed for this storage is obtained from the oxidation of an internal polyphosphate chain (polyP), stored just prior to this. This polyP oxidation results in the release of phosphate into the liquid phase. Accordingly, the anaerobic uptake of organic matter (VFAs) is inherently related to the prior accumulated polyphosphate (Wentzel et al., 2008; Wiesmann et al., 2007).

An aerobic zone must follow. Under optimal conditions no carbon source remains in the aerobic phase (Wentzel et al., 2008; Wiesmann et al., 2007). In aerobic conditions, the carbon reserves previously stored as PHA by PAOs are oxidized with oxygen or nitrate (Janssen, 2002). The released energy is used by the PAOs: (i) for cell growth; (ii) for the synthesis of glycogen; and (iii) to take up the orthophosphate from the water phase and store it as polyP in their cells (Wiesmann et al., 2007). By taking up orthophosphate and converting it to polyP, PAOs are able to replenish their internal polyP (McGrath & Quinn, 2004). In doing so, PAOs remove not only the formerly released orthophosphate by them during the anaerobic phase but also almost all the available orthophosphate from the surrounding oxygen rich environment (McGrath &

Quinn, 2004). Orthophosphate is taken up by PAOs to a higher level than that released by them in the anaerobic stage (Wiesmann et al., 2007).

By going through both anaerobic and aerobic conditions, PAOs are adequately established and become predominant in the biomass community after several weeks (Wentzel et al., 2008; Wiesmann et al., 2007). The PAOs are the only bacteria being able to store substrate in a first anaerobic reactor and to oxidize them in a second aerobic reactor. This is only possible by the enrichment of the Poly–P storage. This enrichment of PAOs, containing a high concentration of polyphosphate, leads to the establishment of biological phosphorus removal.

The net elimination of the process results from the bacterial cell growth and the removal of surplus sludge at the point when the phosphate is taken up to a higher level than that released in the anaerobic stage (Wentzel et al., 2008; Wiesmann et al., 2007). Phosphorus is biologically bound in the resulting biological sludge and the P accumulated in the bacterial cells can be again released if anaerobic conditions are established afterwards (Daneshgar et al., 2018; Morse et al., 1998).

In fact, one of the major inconveniences of using BPR is that the stored phosphate may be released from the sludge as a consequence of anaerobic conditions in some sub-processes of the sludge treatment, e.g., anaerobic digestion. Dewatering of the BPR sludge then results in the recycling of the orthophosphate back to the main treatment.

This P release may lead to uncontrolled struvite formation, a recognized problem in WWTP. As a matter of fact, struvite precipitation is possible from sludge or water streams containing high concentrations of soluble phosphate (Korving et al., 2019) and these phosphate concentrations are typically found when a WWTP combines EBPR and anaerobic sludge digestion (Korving et al., 2019; Schipper, 2019). These WWTP usually suffer from severe accumulation of struvite on pipe walls and equipment surfaces of anaerobic digestion and post digestion processes. Removal of this struvite scaling often requires the use of concentrated acid which inhibits the use of struvite as a fertilizer.

On the other hand, the rejected liquors (sidestreams) from digested sludge dewatering processes show high concentrations of struvite's constituents, which make these streams very appropriate for recovering P as struvite in a crystallization process. Although uncontrolled formation is a nuisance, controlled production of struvite can be applied to remove phosphorus from sidestreams. These controlled processes will: (i) prevent the costs of replacing/cleaning the equipment and pipes associated to involuntary struvite scaling in WWTP; (ii) increase the efficiency of BPR processes; and (iii) obtain a by-product of interest, e.g., a fertilizer.

CHAPTER 4

TECHNOLOGIES FOR STRUVITE RECOVERY FROM WASTEWATER

Under the double pressure from environmental pollution and the non-renewable nature of phosphate rock, methods for the effective and efficient P-recovery from waste streams are attracting an increasing interest (Li, Boiarkina, et al., 2019; Shih & Yan, 2016). Recycling P from sewage by-products in wastewater treatment plants (WWTP) is currently the major P-recovery route (Shih & Yan, 2016). The reason for that is the convenient accessibility of sewage (Shih & Yan, 2016). As a result, struvite crystallization has been recognized as one of the most promising techniques to recover phosphorus from wastewater (F. Wang et al., 2019).

The present Chapter 4 aims to describe the operation principles of a few struvite recovery technologies that have been proven and are commercially established. In particular, the technologies addressed here are the ones most commonly implemented at full-scale worldwide. These technologies are: Pearl from Ostara, Phosnix from Unitika, Phospaq from Paques and Airprex from Berliner Wasserbetriebe (BWB).

For that purpose, the present chapter is organized in four sections. Section 4.1 discusses the need for technologies that recover P from wastewater. It also overviews the companies currently recovering P from wastewater worldwide. Section 4.2 describes the most common targets for P recovery in WWTP. Section 4.3 reviews the struvite recovery technologies most commonly implemented at full-scale worldwide. Since these technologies can be classified into two major groups - precipitation in a continuous stirred tank reactor (CSTR) and precipitation in a fluidized bed reactor (FBR) – section 4.3 is divided in two subsections. Subsection 4.3.1 addresses the FBR technologies (Pearl and Phosnix), whereas subsection 4.3.2 describes the CSTR technologies (Phospaq and Airprex). Both the efficiencies and the product quality of all four processes are discussed in subsection 4.3.3. Further attention is devoted to the Pearl technology by considering its implementation at both pilot and full-scale in section 4.3.4. At last, Chapter's 4 concluding remarks are presented in section 4.4.

4.1 The Need for Phosphorus Recovery Technologies

Recovery and reuse of phosphorus from wastewater rather than disposing of it are now being regarded as a solution to the inherent drawbacks of phosphorus removal traditional techniques (Le Corre et al., 2009). The contemporary focus is, indeed, recycling phosphorus in lieu of eliminating it from wastewater (de-Bashan & Bashan, 2004).

The most important difference between phosphorus removal and phosphorus recovery is that the former aims to reduce the P content of the WWTP effluents, whereas the latter is focused on the phosphorus-containing by-products, which can then be reused for another purpose (Daneshgar et al., 2018).

Phosphorus can be recovered from wastewater, sewage sludge, as well as from the ash of incinerated sewage sludge, and can be combined with phosphorus removal in most cases (Cornel & Schaum, 2009). The phosphorus recovery rate from the liquid phase can reach 40 to 50% at the most (Cornel & Schaum, 2009). This upper boundary is mostly linked to the limited recoverable phosphorus found in the rejected dewatering stream after sludge digestion, which typically accounts for 15%-30% of total P, depending on sludge treatment processes (Koga, 2019). Recovery rates from sewage sludge and sewage sludge ash can reach up to 90% (Cornel & Schaum, 2009). Nonetheless, P-recovery from liquid phase is a less energy-intensive and environmentally friendly process according to Amann et al. (2018).

There are a couple of thermal, chemical, and biological technologies that are on the cusp of becoming economically competitive by substituting other – obviously unsustainable – pathways, such as disposing (phosphorus of) dried sewage in the incineration processes of cement production or coal-fired power plants (Scholz, 2019). Several studies indicated that P recovery by struvite crystallization had advantages over other technologies in terms of: purity, crystalline form, and dewatering characteristics of the product; efficiency of P removal, the presence of Mg in struvite, the ability to simultaneously remove ammonia: and lower evaporative N losses compared to other N rich fertilizers (Kumar & Pal, 2015; Muster et al., 2013; Parsons & Smith, 2008; Puchongkawarin et al., 2015).

The development of struvite-related technologies started in the late 1990s when many WWTP made a move to BNR for the main wastewater stream, switching away from iron or aluminium precipitation (Walker, 2017). Facilities with anaerobic digestion then began to face problems with struvite scaling in the sludge line. So, technologies to rectify this nuisance began to be explored (Walker, 2017). Indeed, the main driver for these technologies was not the recovery of phosphorus, but the ability to save operational costs that would be incurred from chemicals for controlling the struvite or unscheduled maintenance to deal with scaling (Walker, 2017). The fact that phosphorus could be obtained to produce fertiliser was a secondary driver, but helped the business case significantly (Walker, 2017). Figure 4.1 demonstrates that companies recovering phosphorus as struvite (either from centrate or digestate) are leading the way of phosphorus recovery (Walker, 2017).

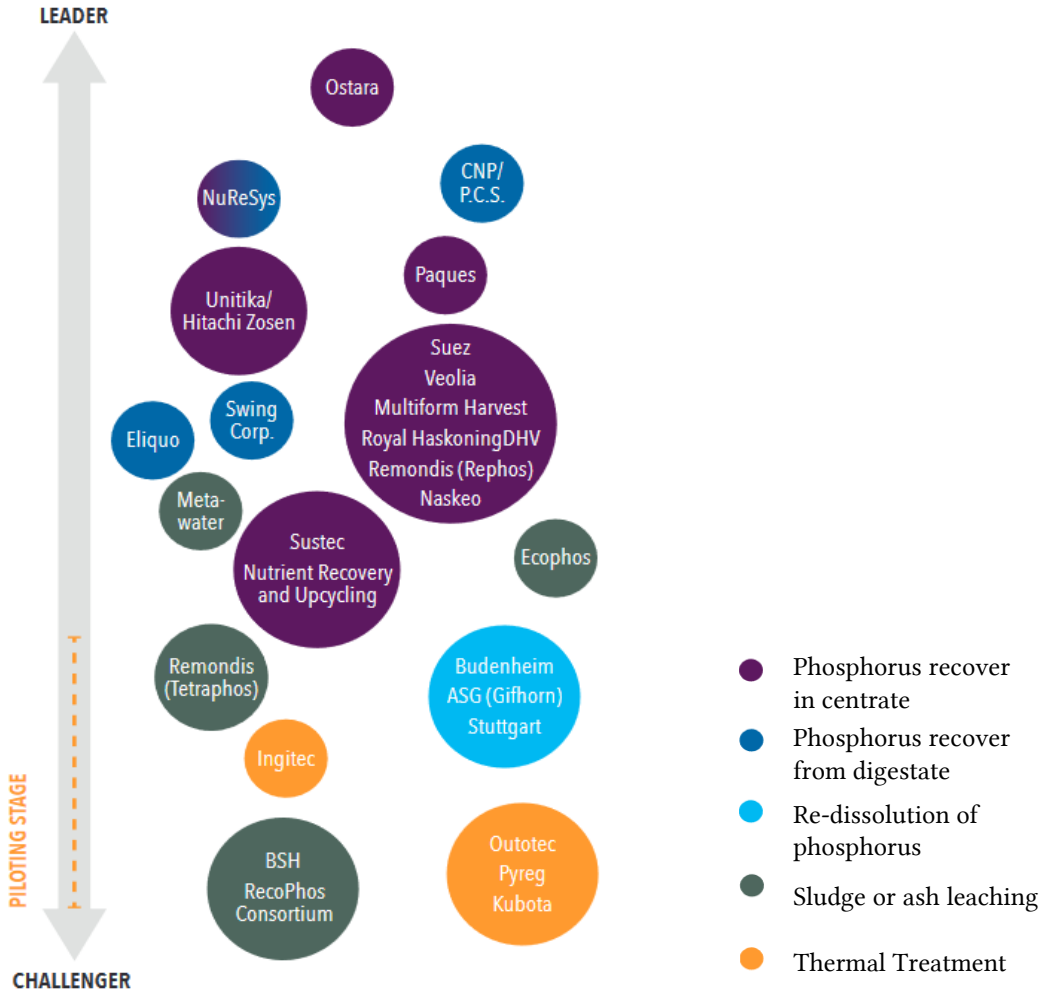

Figure 4.1 - Companies recovering phosphorus from wastewater (adapted from Walker, 2017).

More detailed information about P-recovery technologies can be found in the work carried out by Drizo (2019) and Ghosh et al. (2019). Also, a comparative technological, environmental and economic assessment of several P recovery technologies can be consulted in the work of Egle et al. (2016).

Struvite crystallization technologies can be classified into two major groups: precipitation in the continuous stirred tank reactor (CSTR) and precipitation in a fluidized bed reactor (FBR) (Ghosh et al., 2019; Muhmood et al., 2019). Pearl from Ostara and Phosnix from Unitika are currently the FBR technologies with the largest number of commercial installations operating or under construction worldwide (Kabbe & Rinck-Pfieffer, 2019), more specifically, 22 (Ostara, 2020a) and 8, respectively (Kabbe & Rinck-Pfieffer, 2019). In what concerns CSTR technologies, Phospaq from Paques and Airprex from Berliner Wasserbetriebe (BWB) are the most extensively applied technologies today. comprising 11 (Kabbe & Rinck-Pfieffer, 2019) and 13 installations (Centrisys Corporation, 2019; Kabbe & Rinck-Pfieffer, 2019), correspondingly (Kabbe & Rinck-Pfieffer, 2019).

The emerging crystallization of struvite is a promising alternative to phosphorus removal technologies (de-Bashan & Bashan, 2004; Le Corre et al., 2009). Struvite crystallization may serve as a catalyst for recovering phosphorus as a recyclable product from phosphorus concentrated wastewater streams (de-Bashan & Bashan, 2004; Le Corre et al., 2009).

Looking at the number of struvite projects being implemented in Japan, the EU and North America, struvite can be identified as a success story (Schipper, 2019). The precipitation of struvite from phosphate-rich sewage sludge water is well known and currently being practised in more than 40 full-scale installations world-wide (Schipper, 2019). Volume in Europe is approximately 1 kt P/year recovered as struvite at more than 20 WWTP and more than 40 full-scale installations worldwide (Nättorp et al., 2019).

Schipper (2019) highlighted the struvite technologies' beneficial effects at the WWTP level – a reduction of overall WWTP operating costs (opex). This primarily concerns the prevention of struvite scaling (which needs frequent and costly removal cycles) and reduced return loads for P and N in the sludge liquor recycled within the WWTP (Schipper, 2019). Some technologies also affect the sludge dewaterability (Schipper, 2019). They provide the biggest benefits due to better sludge dewatering and therefore an increase in dry matter content in sludge to be disposed of, saving on transport and processing cost (Schipper, 2019). Cost of struvite precipitation processes is in general compensated by their operational benefits (Nättorp et al., 2019).

Theoretical knowledge on struvite formation implies that, if involuntary crystallization in wastewater treatment environments conditions can be duplicated and exploited in a practical engineering process, there is potential to economically extract struvite from wastewater in commercial quantities (de-Bashan & Bashan, 2004). This might be done by precipitating struvite in a dedicated reactor, instead of allowing its spontaneous formation (Hao & van Loosdrecht, 2003; Münch & Barr, 2001; Stratful et al., 2001). Struvite is precipitated from an orthophosphate-rich process stream (concentration >100 mg P/L usually) (Nättorp et al., 2019), generally by adding magnesium and adjusting the pH (Korving et al., 2019). Due to the low magnesium concentration in most wastewater streams, magnesium addition is always required for struvite crystallization (Li, Huang, et al., 2019). Phosphorus concentrations should be above 50 mg/L in order to guarantee the economic viability of the process (Cornel & Schaum, 2009).

4.2 Hotspots for Phosphorus Recovery in WWTP

Side streams in WWTP of the EBPR type with anaerobic digestion consist of the most common targets for P recovery (Schipper, 2019). Reasons for that have been described in Chapter 3. Figure 4.2 depicts the most common targets for phosphorus recover.

Currently, the most applied option is the P recovery from the centrate/filtrate after dewatering (Kabbe & Rinck-Pfieffer, 2019). Struvite can be easily recovered from this side stream because of the low suspended solid (SS) content and viscosity compared to those of digested sludge (Koga, 2019).

Nonetheless, P recovery directly from the digested sludge prior to the dewatering process may comprise another option for struvite recover (Schoumans et al., 2015). The former has the advantage of improved separation during the dewatering process and lower maintenance as it prevents clogging of pipes and abrasion of the dewatering equipment (Nenov et al., 2016). Also, since both soluble P and struvite particles are recoverable in the digested sludge, it can be expected to recover more P here than from the liquid phase alone (Koga, 2019). However, because of the high SS content and viscosity, it is necessary to use a complete-mix reactor for recovering struvite from digested sludge (Koga & Hagino, 2016).

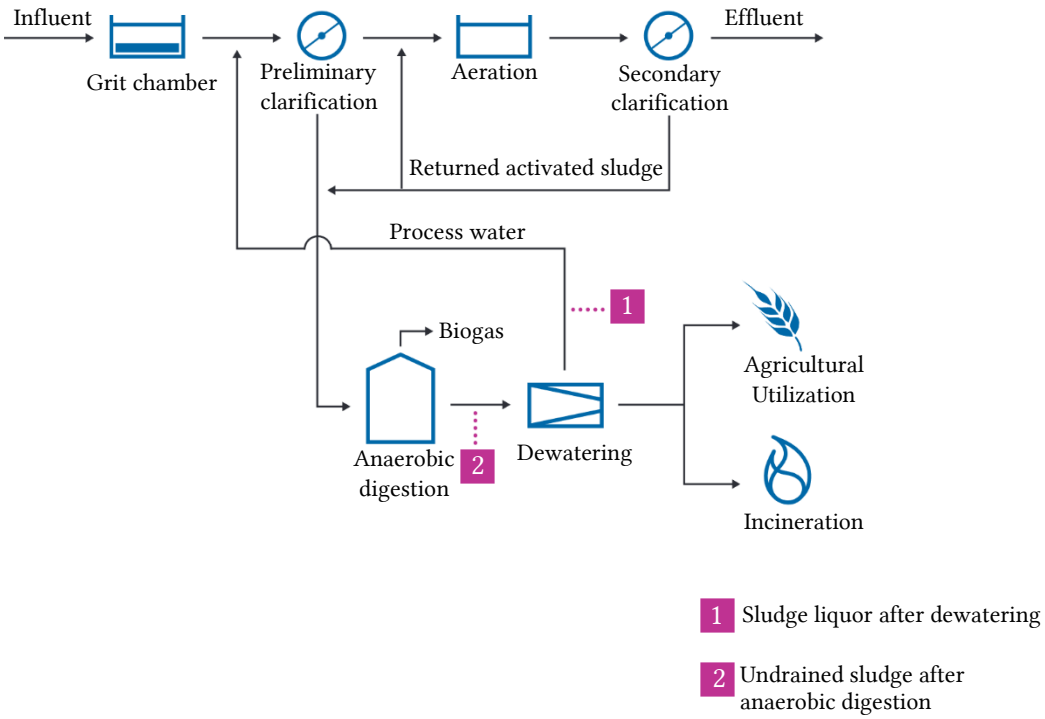

Figure 4.2 - Most common targets in the sludge treatment stream for phosphorus recover (adapted from Walker, 2017).

Second generation enhanced P recovery concepts include a waste activated sludge treatment step that biologically redissolves a part of phosphorus contained in the biomass prior to anaerobic digestion (Kabbe & Rinck-Pfieffer, 2019). The redissolved phosphorus can then be combined with the nitrogen and phosphorus present in the rich liquor of the dewatering procedure (Kabbe & Rinck-Pfieffer, 2019).

4.3 Review of the Available Technologies

4.3.1 Fluidized Bed Reactors (FBR)

4.3.1.1 Process Principles

The concept of fluidization can be visualized as follows: let us consider small, solid particles located in a vertical, packed bed – see Figure 4.3 (a) (Salmi et al., 2019). An assembly of solid particles becomes fluidized when the combined drag and body forces exerted on the particles by an upward-flowing fluid (gas or liquid) exceed the gravitational force holding the assembly together (Salmi et al., 2019; Yates & Lettieri, 2016).

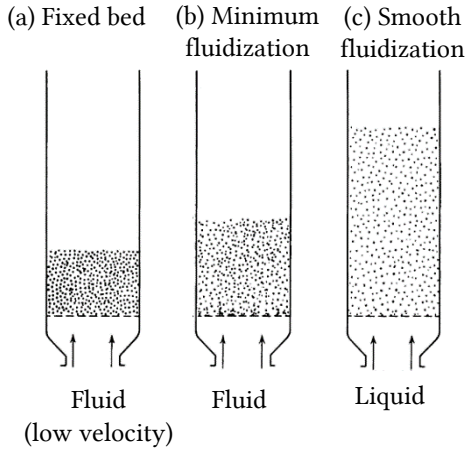

Figure 4.3 - Hydrodynamic behavior of a fluidized bed (adapted from Kunii & Levenspiel, 2012).

At this point, the bed expands and particles are suspended in the fluid (Salmi et al., 2019; Yates & Lettieri, 2016) - Figure 4.3 (b). The fluid velocity at which this occurs is termed the "minimum fluidization velocity" (U_{mf}) (Salmi et al., 2019) and its value is a function of the size, shape and density of the particles and the density and viscosity of the fluid (Yates & Lettieri, 2016).

In liquid-solid systems, an increase in flow rate above U_{mf} usually results in a smooth, progressive, expansion of the bed - Figure 4.3 (c) (Kunii & Levenspiel, 2012). Any particle that rises above the top of the bed due to transient nonuniformities in flow will encounter a local upward velocity that is less than the particle's terminal settling velocity and the particle will fall back into the bed (Grady et al., 1999). As the upward velocity of the fluid is further increased, ultimately, a point will be reached at which the local fluid velocity around the particles is equal to their terminal settling velocity (Grady et al., 1999). If the upward velocity is increased beyond that point, the upward drag forces on the particles will exceed the downward gravitational forces (Grady et al., 1999). Afterward, the particles will be carried away, and the bed will cease to exist (Grady et al., 1999).

Generally, gas-solid systems behave quite differently. With an increase in flow rate beyond minimum fluidization, large instabilities with bubbling and channelling of gas are observed (Kunii & Levenspiel, 2012). As stated by Kunii & Levenspiel (2012), at higher flow rates, agitation becomes more violent and the movement of solids becomes more vigorous.

Thus far, fluidization has been approached as a two-phase system: liquid-solid or gas-solid (Yates & Lettieri, 2016). Nevertheless, three-phase systems - gas-solid-liquid - should also be considered. In these systems, solid particles are fluidized by an up-flowing liquid, as a gas is being introduced separately at the base of the column (Yates & Lettieri, 2016). Thus, liquid and gas flow concomitantly upwards the column (Yates & Lettieri, 2016).

Fluidization is, in essence, a technique in which an assembly of solid particles is held in suspension by an upward-flowing liquid or gas, or both (Yates & Lettieri, 2016). A fluidized bed reactor is the vessel that is designed for the aforementioned interactions (McTigue et al., 2010). (Yates & Lettieri, 2016). Fluidized bed reactors are the most used technology at larger scale (Ghosh et al., 2019), as the design gives provision for sufficient reactive surface area and solution turbulence (Seckler et al., 1996). Also, FBR are compact due to short hydraulic time (Özkaya et al., 2019).

4.3.1.2 Pearl

Pearl is the core of Ostara's nutrient recovery solution (Gysin et al., 2018) and integrates into WWTP that operate EBPR (Ostara, 2017). This process is based on an up-flow fluidized bed reactor with multiple reactive zones or sections of increasing diameters from bottom to top, as illustrated in Figure 4.4 (Britton et al., 2009). Varying cross-sections give rise to different upward velocities in the crystallizer (Zamora et al., 2017).

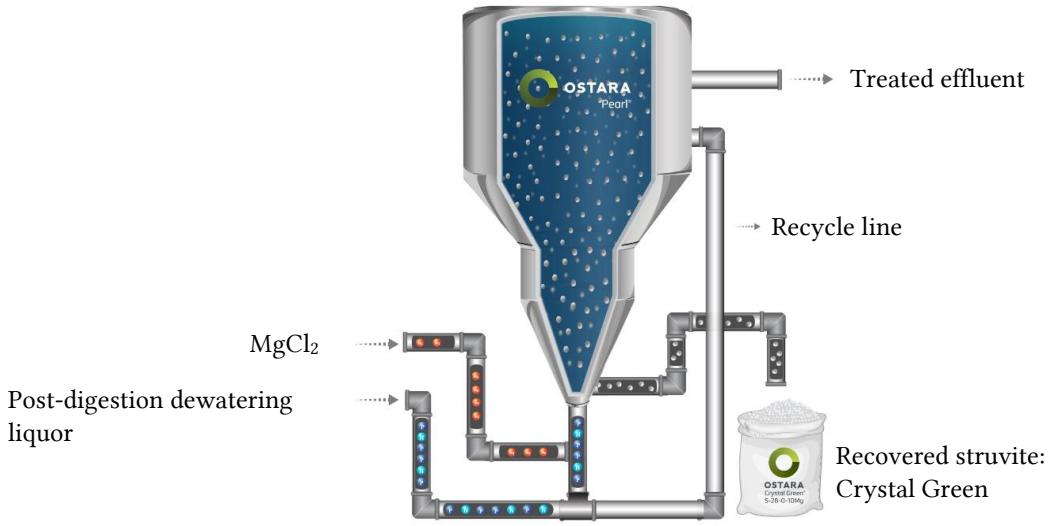

Figure 4.4 - Ostara's Pearl process (adapted from Lee, 2017).

The Pearl process comprises automatic chemical addition: soluble $MgCl_2$ salts (Jeyanayagam, 2018) are added to control ionic concentration and, when required, sodium hydroxide is added to adjust pH (Gysin et al., 2018). This allows operating the reactor at the desired SSR value at the bottom section (US Patent No. 7,622,047, 2009). Side-stream influent (post-digestion dewatering liquor) and chemicals are thereupon introduced into the bottom of the reactor, where struvite crystallization begins to occur (Gysin et al., 2018). Nucleation is achieved using already formed struvite micro-crystals which serve as seeds for pellet growth (Jeyanayagam, 2018; Jeyanayagam et al., 2012).

The solution velocity is maintained in such a way that all the particles in the crystal bed are fluidized in the solution (Rahaman et al., 2009). Since the fresh influent is pumped into the bottom of the reactor, the reactive solution contains the maximum supersaturation in this zone (Rahaman et al., 2009). Hence, as reported by Rahaman (2009), crystals at the bottom grow faster than those near the top of the reactor. High initial supersaturation in the vicinity of inlet ports of struvite reactor can favour nucleation over crystal growth at the onset of crystallization (Shaddel et al., 2019). Improving aggregation of the generated crystals in this stage is important. If this aggregation does not occur, distribution of the crystals in the space and time will reduce the chance of collision and aggregation in later stages (Shaddel et al., 2019). Moreover, improved aggregation contributes to better granulation and will further reduce the chance of product loss from reactor by wash out (Shaddel et al., 2019).

The treated effluent is discharged from the top of the reactor and returned to the WWTP for further treatment (Gysin et al., 2018). A portion of the treated effluent from the top of the reactor is returned to the bottom of the reactor in a recycle loop (Gysin et al., 2018). Pearl uses the recycle flow to control the up-flow velocity in the FBR (Jeyanayagam, 2018). Struvite

crystallization is thus controlled by a combination of magnesium dose, pH control (when needed) and by means of a treated effluent recycle (Britton et al., 2009).

The rationale behind the varying cross-sections of the reactor serves a double purpose: to sort the growing struvite particles through the column according to their weight and to maximize turbulence in the fluidized bed (Zamora et al., 2017). The high fluid velocity at the bottom of the reactor results in the washout of residual sludge solids (Britton et al., 2009). This contributes to a more pure struvite product free of organic material and pathogens (Britton et al., 2009). The Pearl process has the advantage of allowing large struvite pellets up to 8 mm in diameter to be kept in suspension at the bottom of the reactor without washing out fine crystal nuclei from the top of the reactor (Britton et al., 2009). Crystal retention time varies from 8 to 12 days (Koch et al., 2009).

The larger crystals at the bottom, once having achieved the desired size, are settled into the harvest zone, i.e., the bottom zone and are withdrawn from the reactor (Rahaman et al., 2009). Consequently, the smaller particles are allowed to move lower in the reactor where they will increase in size as they are exposed to higher concentrations of the reactants (Cullen et al., 2013). The product is dewatered, heat dried, sorted by size, and optionally stored in silos in a simple and fully automated process (Gysin et al., 2018). During harvest, the reactor will continue to be fed side-stream nutrients and perform nutrient removal without interruption or loss of efficiency (Gysin et al., 2018), as the finishing occurs automatically in batch-mode (Ostara, 2020b). Up to about 90% of the phosphates in the post-digestion dewatering liquor can be removed in the form of struvite pellets through the Pearl process (Desmidt et al., 2015; Jeyanayagam, 2018; Jeyanayagam et al., 2016). On average, Pearl facilities achieve a capital investment payback in 3–7 years and operate with over 95% uptime (Gysin et al., 2018).

The struvite recovered through Pearl technology - Crystal Green - is certified as fertiliser in the Canada, forty four US states, Taiwan, Puerto Rico, and the UK (Desmidt et al., 2015; Gysin et al., 2018). It complies with European fertilizer Regulation (EC) No 2003/2003 and meets the required limits for organic and inorganic constituents (Gysin et al., 2018). It is in the form of recovered phosphorus ready for reuse as a premium fertiliser directly from WWTP, with revenue to the plant guaranteed in a long-term offtake agreement (Ostara, 2020a). Crystal Green contains 28% available phosphorus and is sparingly water soluble, providing phosphorus, nitrogen and magnesium in a slow-release granule (Ryan et al., 2016). The granule dissolves in response to organic acids produced by the plant during root growth (Ryan et al., 2016) – it is root activated (Gysin et al., 2018). The low water solubility of Crystal Green minimizes P losses through runoff and distinguishes it from conventional phosphorus fertilisers, which are highly water soluble (Ryan et al., 2016). Crystal Green has been successful on high-value agricultural crops, turfgrass, golf and horticulture applications, including container or field-grown nursery stock (Ryan et al., 2016).

The Pearl process can also be used in conjunction with Ostara's other technology, Waste Activated Sludge Stripping to Remove Internal Phosphorus (WASSTRIP) (Ryan et al., 2016). WASSTRIP consists of a mixed tank maintained in an anaerobic condition (Gysin et al., 2018) that can be integrated into wastewater treatment systems to treat waste activated sludge upstream of thickening and anaerobic digestion (Ryan et al., 2016). WASSTRIP releases phosphorus from the stream (Prabesh, 2018). Subsequent sludge thickening diverts released

nutrients into thickening liquor, which the Pearl process recovers as depicted in Figure 4.5 (Gysin et al., 2018).

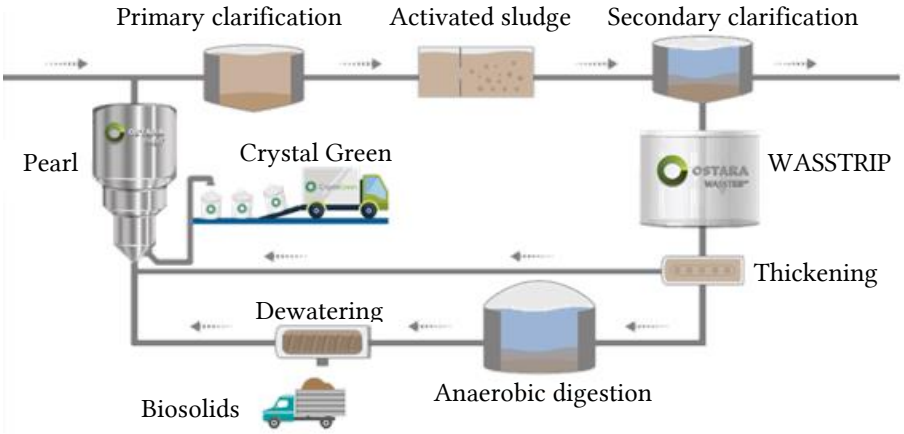

Figure 4.5 - Combination of Ostara's Pearl and WASSTRIP processes in a WWTP (adapted from Ostara, 2020a).

As the WASSTRIP liquor is low in ammonia, the stream needs to be combined with dewatering liquors in Pearl in order to precipitate struvite ((Gysin et al., 2018). This way, maximum phosphorus is provided to the Pearl reactor (Prabesh, 2018). As follows, the integration of both processes prevents struvite formation in the anaerobic digester (Ryan et al., 2016) . The inclusion of the WASSTRIP process not only increases struvite production by up to 60% (Jeyanayagam, 2018) but also reduces sludge production and improves sludge dewaterability (Gysin et al., 2018; Schauer & Laney, 2015). With WASSTRIP integration, the recovery may be up to 50% of total plant influent phosphorus (Ostara, 2020b).

4.3.1.3 Phosnix

The Phosnix process was set up by Unitika Ltd (Ryan et al., 2016) and is used in WWTP that use biological P removal (Ueno, 2004). It is based on a fluidized bed reactor comprising an air agitated column (Brett et al., 1997)– see Figure 4.6.

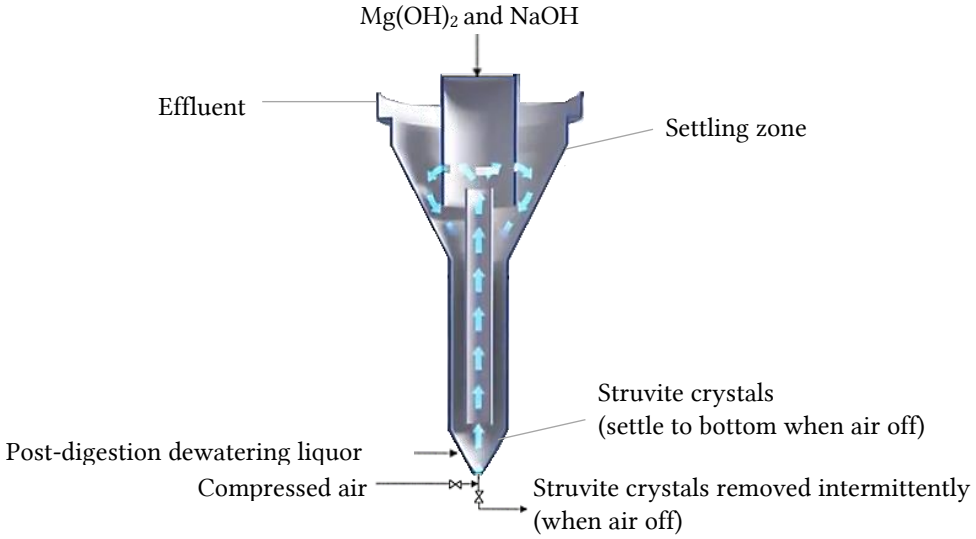

Figure 4.6 - Unitika's Phosnix process schematic (adapted from Hitachi Zosen Group Channel, 2019; Münch & Barr, 2001).

Dewatered liquor from anaerobic digestion is fed into the base of the FBR which contains a bed of granulated struvite as seed material to enhance crystal growth (Münch & Barr, 2001). The arrows in Figure 4.6 indicate the direction of the dewatered liquor flow (Hitachi Zosen Group Channel, 2019). The feed is then mixed with magnesium hydroxide and sodium hydroxide to achieve desired SSR and pH values, respectively (Ueno & Fujii, 2001). The correct stoichiometry and pH allow the nucleation and growth of struvite crystals (Stratful et al., 1999). The reactions occur at ambient temperature and pressure (Stratful et al., 1999). Complete mixing and suspension of the growing particles are assured by the air that is sparged into the base of the column (Münch & Barr, 2001).

The crystals grow until they sink into the base of the reactor where they are periodically removed. A retention time of 10 days allows the growth of pellets between 0.5 to 1.0 mm in size (Münch & Barr, 2001). The recovered product is then dewatered from the small amount of solution, which is lost when the crystals are removed, either by a filter bag system or natural drying (Münch & Barr, 2001). Smaller granules of the recovered struvite are returned to the reaction column to provide new seed material for the process to continue (Münch & Barr, 2001). The bell-shaped section at the top of the reactor also contributes to fines retention within the reactor (Jeyanayagam et al., 2012). The Phosnix system can recover up to 90% of the P-enriched side stream (Ryan et al., 2016).

The struvite obtained is registered as a fertilizer in the category of High Performance Complex Fertilizers (Ueno, 2004). The product has a N:P:Mg ratio of 5.3:13.3:11.5 (Thornton, 1998). It is sold to fertilizer companies as raw material for chemical fertilizers, that mix it with other inorganic and organic materials and adjust the proportion of nitrogen, phosphorus and potassium (Ueno, 2004). Unitika has been able to operate full-scale struvite reactors at a profit by successfully marketing their product (Münch & Barr, 2001). As mention by Münch & Barr (2001), despite the full-scale experience of this Japanese company, very little scientific knowledge has been published, and little detailed information about this process exists outside Japan.

4.3.2 Continuous Stirred Tank Reactors (CSTR)

4.3.2.1 Process Principles

A continuous stirred tank reactor (CSTR) is used to convert reactants into products (Alvarez et al., 1989). CSTR are open systems operating on a steady-state basis, where reactants are continuously introduced into the reactor through a feed stream (influent), while products are continuously removed through an exit stream (effluent) (Grady et al., 1999; Mousa & Dawood, 2015).

Any reactant carried into the reactor by the feed is dispersed evenly throughout the reactor without any time delay (Grady et al., 1999). Thus, samples taken from all parts of the reactor have the same composition (Grady et al., 1999. In addition, the effluent composition is the same as the reactor composition (Grady et al., 1999).

4.3.2.2 Airprex

Berliner Wasserbetriebe (BWB) developed the Airprex system (Ryan et al., 2016). The Airprex procedure unit is arranged immediately after the digestion and the basic precondition for the procedure is that the WWTP involved practice targeted biological phosphate elimination (Ortwein, 2018). Airprex is an aerated cylindrical continuous stirred tank reactor, with an inner

cylindrical zone mixed by air up flow and a settling zone between this inner cylinder and the outer cylinder, as depicted in Figure 4.7 (Desmidt et al., 2015; Kataki & Baruah, 2018).

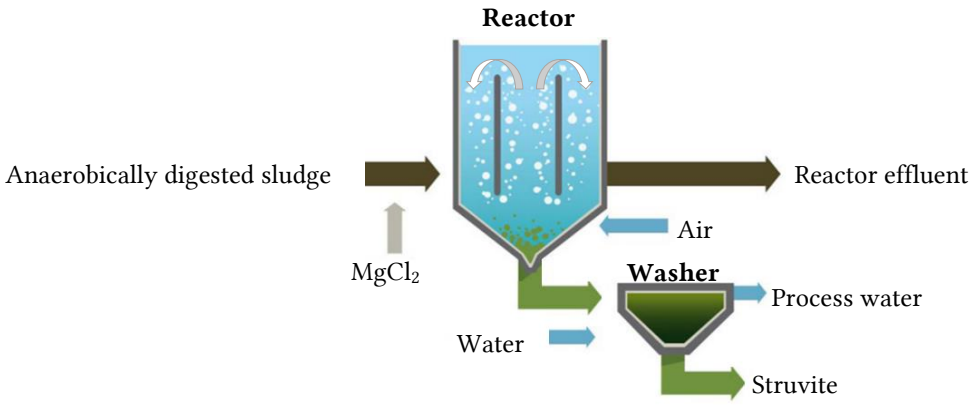

Figure 4.7 - Berliner Wasserbetriebe Airprex process schematic (adapted from Eliquo, n.d.; and SenUVK, n.d.).

After being introduced in the reactor, anaerobically digested sludge (Ryan et al., 2016) is intensively aerated in order to adjust pH by stripping CO_2 (Jeyanayagam, 2018). To induce struvite precipitation, additional magnesium ($MgCl_2$) is dosed (Jeyanayagam, 2018). Sludge is aerated in the inner cylinder and is then lifted upwards by air bubbles (Ghosh et al., 2019; Ortwein, 2018). After reaching the top, the sludge settles in the tranquil zone in the outer part of the reactor (Jeyanayagam, 2018). Continuous reactor mixing is provided by a specific circular flow regime induced by the air injection as illustrated by the white arrows in Figure 4.7. (Jeyanayagam, 2018). Hence, aeration serves a double purpose – it yields pH adjustment and provides an internal recycle flow between aerated and non-aerated zones (Desmidt et al., 2015).

The recycle allows the struvite crystals to grow until they reach a size from which they can escape from the recycle flow and settle (Desmidt et al., 2015). During the sludge retention time in the reactor (typically 6-8 h), struvite crystals are formed and settle by gravity into the conical bottom of the reactor (Jeyanayagam, 2018). Phosphate removals of the process are up to 90% (Desmidt et al., 2015). Beneficial side effects include a 2-4% increase in the dry substance content of the dewatered sludge and an up to 35% reduction in polymeric flocculants (Ortwein, 2018).

The settled struvite crystals are discharged at regular intervals and washed to remove residual sludge (Jeyanayagam, 2018). After washing out the organic contaminants, struvite is used as a valuable component in the production of fertilizers (processing to phosphoric acid) and fertilizers supplementation (Ortwein, 2018).

4.3.2.3 Phospaq

The Phospaq system was created by Paques and consists of an aerated CSTR with a separator, as illustrated in Figure 4.8 (Desmidt et al., 2015). Applications include side streams with high levels of P, typically due to EBPR treatment (Kataki & Baruah, 2018; Ovivo, n.d.-a). The side streams include centrate/filtrate and digester supernatant (Ovivo, n.d.-b)

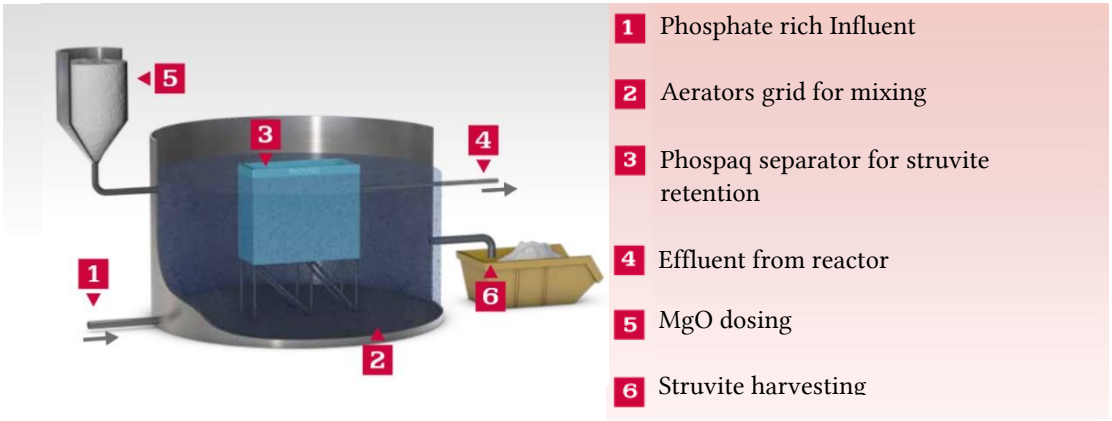

Figure 4.8 - Paques Phospaq process schematic (adapted from Paques, 2017).

Driessen et al. (2018), elaborated a complete description of the process:

> Magnesium is dosed as MgO, which simultaneously reacts with the present phosphate and ammonium of the P-rich influent and increases the pH to stimulate formation of struvite. Air is introduced to the reactor to (i) provide mixing of the struvite crystals formed, (ii) raise the pH by stripping CO_2, hence stimulating struvite formation and (iii) provide oxygen to oxidize BOD. The patented separator system at the top of the reactor is applied to retain the struvite and biomass in the system. (p.352)

As the crystals grow and become large enough to pass through the separator, the heavier crystals settle into the tank (to be withdrawn from the bottom), while the cleaned effluent leaves through the top of the separator (Ovivo, n.d.-a). Struvite is extracted from the bottom of the reactor and subsequently dewatered and dried resulting in a coarse powder (Driessen et al., 2018). The smaller crystals are kept in suspension in the reactor acting as nuclei for further crystallization of struvite (Driessen et al., 2018). Phosphorus recovery was reported to be up to 95% (Ryan et al., 2016).

Recovered struvite has a sand-like structure and is in compliance with EU standards for fertilizer (Ryan et al., 2016). It is exported to Germany for use as a raw material in the production of fertilisers or for mixing with other fertilisers to achieve desirable nutrient content (Ryan et al., 2016).

4.3.3 Phosphorus Removal Efficiencies and Quality of the Recovered Product

Table 4.1 summarizes the respective provider, type of reactor (FBR/CSTR), P source, recovered product, and maximum P removal efficiency (%), of each one of the Pearl, Phosnix, Airprex, and Phospaq technologies.

These are proven processes and demonstrate up to 90% removal efficiencies, except for the Phospaq technology. Phospaq possesses the highest P removal efficiency, namely up to 95%.

All technologies analysed here share the precondition that the WWTP involved practice targeted biological phosphate elimination and use anaerobic digestion. This precondition provides the best opportunity for P recovery in the form of struvite (de-Bashan & Bashan, 2004). Technologies' high efficiencies allow to recover around 20% of total plant influent phosphorus (Benisch et al., 2009; Cullen et al., 2013). When used in conjunction with other technologies (e.g., technologies implemented upstream of the anaerobic digester), the recovery may be up to 50%

of total plant influent phosphorus (Ostara, 2020b). Costs of struvite precipitation processes are in general compensated by their operational benefits (Nättorp et al., 2019) which enhance performance efficiency of waste treatment facilities (Shu et al., 2006).

Table 4.1 - Summary of the fundamental aspects of the Pearl, Phosnix, Airprex and Phospaq struvite recovery technologies

Technology name	*Developer*	*Type of reactor*	*P source*	*Recovered product*	*Max. P removal efficiency (%)*
Pearl	Ostara	FBR	Dewatering liquor	Ready for reuse as a premium fertilizer	90
Phosnix	Unitika	FBR	Dewatering liquor	Raw material for fertilizer production	90
Airprex	BWB	CSTR	Anaerobically digested sludge	Raw material for fertilizer production	90
Phospaq	Paques	CSTR	Dewatering liquor and digester supernatant	Raw material for fertilizer production	95

One of the principal interests of recovering phosphorus from wastewater as struvite is its potential use as a commercially viable product (Li, Boiarkina, et al., 2019). Therefore, the crystallization performance is quantified not only in terms of the P removal efficiency but also product quality (i.e. crystal size, morphology and purity) (Li, Boiarkina, et al., 2019).

Even though Phospaq holds the highest efficiency, its recovered product has a sand-like structure and it is used as a raw material in the production of fertilizers (Ryan et al., 2016). On the other hand, Pearl with a relatively lower P removal efficiency (less 5%) stands out for its ready to use recovered product – see Figure 4.9 (Ostara, 2020a).

Figure 4.9 - Crystal Green, the recovered product of Ostara (Ostara, 2020).

The most important criteria for the acceptability as a fertilizer are the concentrations of hazardous substances below the legal limits assumed and the plant availability of P from the recovery product (Günther et al., 2018). Struvite and polyphosphates generally show high plant availability, which is superior or at least comparable to mineral fertilizer (Satyaprakash et al., 2017). The slow heavy metal content of struvite can be explained by its specific structure, which prevents the placement of impurities, such as heavy metals, into the well-defined structure of crystal (Latifian et al., 2012).

4.3.4 Ostara's Pearl Technology Application

4.3.4.1 Pilot-scale Application

Because Ostara is a spin-off company of the research P-recovery group of the Canadian University of British Columbia (UBC) (Fattah, 2004; Rahaman et al., 2009), several pilot studies regarding the earlier development stages of the Pearl reactor are found in the literature. Among them, the study carried out by Fattah, (2004) is singled out here for its high P-removal as well as for its P-recover (in the form of struvite) values.

From January to June of 2004, a pilot-scale struvite crystallizer reactor was installed at the Lulu Island WWTP (LIWWTP), in British Columbia, to investigate the feasibility of P-removal from the post-anaerobic digestion dewatering centrate of the plant and subsequent P-recovery in the form of struvite pellets (Fattah, 2004).

LIWWTP is a secondary wastewater treatment plant that is operated by the Greater Vancouver Regional District of the Province of British Columbia (Fattah, 2004), with a flow capacity of 155 MLD and an average flow of 79 MLD in 2004 (Tailford, n.d.). According to Fattah, (2004):

> The plant consists of [primary treatment] and biological treatment that includes trickling filters, solid contact and secondary clarification. The sludge produced is managed through … sludge thickening, anaerobic digestion and biosolids dewatering. Solids removed from the primary settling tanks are thickened in a gravity thickener while those from the secondary process are thickened using a dissolved air flotation process. Sludge digestion is accomplished using a mesophilic anaerobic process (…). The digested sludge (…) is mechanically dewatered (…) in the centrifuge (…). (p.3)

The study consisted of two runs, run 1 (January - April 2004) and run 2 (June 2004) (Fattah, 2004). The phosphate concentration of the centrate varied throughout the study from 12 mg/L to 88 mg/L, considering run 1 and from 39 mg/L to 68 mg/L for run 2 (Fattah, 2004).

The crystallization process followed the aforementioned principles related to Pearl technology except for the recycling stream. An external clarifier was placed to store the effluent from the reactor and to trap the washed-out fine pellets and suspended solids from the reactor (Fattah, 2004). The clarifier had three distinct outlets: one for the recycle stream, another for the treated effluent and, finally, one for the sludge removal (see Figure 4.10). Therefore, a reactor, an external clarifier, storage tanks for LIWWTP centrate, magnesium feed and caustic were used. Pumps for the centrate, magnesium feed, caustic, recycle; and a pH controller were also needed (Fattah, 2004). The pH controller determined when and which amount of caustic had to be added to the reactor, so that the pH would be within ± 0.5 of a certain set value (Fattah, 2004).

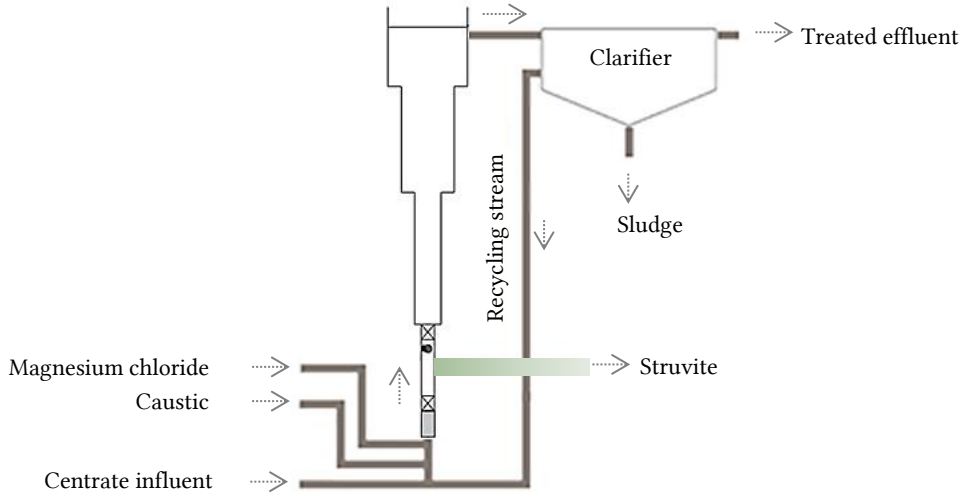

Figure 4.10 - Ostara's pilot-scale study process schematic (adapted from Bhuiyan et al., 2008).

Table 4.2 presents the reactor four distinct zones. A removable injection port below the harvest zone of 52.1 cm summed a total height of approximately 4.55 m. The reactor had a total volume of 91 L and was capable of handling total flows as high as 25 L/min (Fattah, 2004).

Table 4.2 - Dimensions of the reactor used in the pilot-study from Fattah (2004).

Section	Diameter (cm)	Height (cm)	Volume (L)
Harvest zone	7.6	74.9	3.42
Active zone	10.2	154.9	12.56
Fines zone	15.2	127.0	23.17
Seed hopper	38.1	45.7	52.12

Results showed that the reactor was capable of removing over 90% of phosphate (Fattah, 2004). Of these, Fattah (2004) reported that more than 85% were recovered as harvestable struvite pellets composed of nearly pure struvite (96% by weight). Also, phosphate concentration in the effluent could be lowered to 5 mg/L and sometimes as low as 2 mg/L depending on removal efficiencies (Fattah, 2004). Factors that affected phosphate removal were the operating pH, the reactor SSR, and the N:P and Mg:P molar ratios (Fattah, 2004).

4.3.4.2 Full-scale Commercial Application

Clean Water Service operates Durham Advanced Wastewater Treatment Plant (DAWWTP) with a flow capacity of 94,635 m^3/day, which serves Washington County (US) residents by providing tertiary wastewater treatment (Benisch et al., 2009). In May 2009, a commercial full-scale installation of the Pearl technology - a struvite recovery facility (SRF) - was installed at the plant (Baur, 2010).

DAWWTP consists of primary treatment and biological treatment (through activated sludge) (Pahren & Jakubowski, 1980; Schauer, 2015). followed by chemical (tertiary) clarification using alum and coagulant aids to reduce the phosphorus and solid content (Pahren & Jakubowski, 1980). The final steps are effluent filtration and disinfection (Schauer, 2015). After several years of chemical P removal, the plant was converted to EBPR with chemical backup (Benisch et al., 2009), The process was augmented with volatile fatty acids (VFA) from two-stage primary

sludge fermenters (Benisch et al., 2009). However, to meet the summer months strict P-discharge permit limit, alum had to be added in tertiary clarifiers (Cullen et al., 2013). As for the solid phase, Benisch et al. (2009) stated that: "Primary solids are pumped to the fermentation and thickening process, while waste activated and tertiary sludge are blended in an aerated storage tank before centrifuge thickening. Thickened primary, secondary and tertiary sludges are blended in a digester feed tank from where they are pumped to the digesters. Anaerobically digested sludge is dewatered with centrifuges" (p103). The centrate is further equalized in centrate storage tanks, and prior to the recycle return to the secondary treatment process, the centrate is sent to the phosphorus recovery process (Benisch et al., 2009).

Although BNR reduced chemical addition significantly, its side effects were evident by a rise of centrate phosphate concentration and, subsequently, an increase of recycled phosphorus (Benisch et al., 2009). The preceding side effects were accompanied by the problem of excessive struvite formation, which occurred in two forms: in centrate pipes and as struvite grit accumulation in digesters (Benisch et al., 2009). In view of alleviating the aforesaid issues and to make the BNR process more stable, as well as reducing the demand for VFA, the Pearl process was selected to remove phosphorus from the centrate (Benisch et al., 2009; Cullen et al., 2013).

The SRF consists of three Peal reactors designed to jointly treat a total of 454.000 m^3/d of sludge dewatering centrate with an average phosphate concentration of 400 mg/L in order to ensure that peak loads could be processed and to allow for future growth (Baur et al., 2010). The struvite recovery facility was built to recover a maximum of 200 kg/day of phosphorus which translates into a struvite production rate of 1500 kg/day (Baur et al., 2010). Each reactor is 9.5 m in height and its largest section has a diameter of 4.3 m, in a total of four different sections (Baur et al., 2010; Ostara, 2020b).

The reactors were seeded in April 2009 with struvite prills from the full-scale pilot unit in Edmonton, Canada, as seeding is only needed when starting up an empty reactor to reduce induction time (Cullen et al., 2013). After being discharged into storage tanks for equalization, the centrate is then fed to the reactors where crystallization occurs according to the Pearl process principles (Benisch et al., 2009). During a harvest, the largest particles are flushed out of the reactor through a harvesting mechanism and the product slurry is sent to a vibrating screen where water is removed (Benisch et al., 2009). The prills are then fed into a fluidized bed dryer to remove the surface moisture (Cullen et al., 2013). When the prills exit the dryer, they are sieved into four product sizes, ready to use with no additional processing (Cullen et al., 2013). Crystal Green ownership passes to Ostara when the super sacks containing the product are loaded on trucks and Ostara is responsible for its storage, marketing, licensing, sales and distribution (Cullen et al., 2013).

The struvite recovery facility removes 85% of soluble P-PO_4 and 15% ammonia from the sludge dewatering centrate while recovering 20% of the plant influent phosphorus load (Benisch et al., 2009; Cullen et al., 2013). When comparing the dewatering centrate contribution to the secondary treatment phosphate load before and after phosphorus recovery, the recycle load was reduced from 55% to 9%. (Benisch et al., 2009). In the first year of operations, 250,000 kg of struvite were produced, which represents 31,500 kg of phosphorus and 14,300 kg of ammonia removed from the system (Cullen et al., 2013). After two years of operation 455,000 kg of struvite had been recovered (Prabesh, 2018).

As reported by Cullen et al. (2013), the reduction of the phosphorus contained in the centrate recycle, occasioned by struvite controlled formation, lowered the P load to EBPR and made it more stable, which resulted in reducing alum usage by around 30%. Thus, the consequent reduction in dry solids tonnage is due to the reduction of phosphate as well as the reduction in chemical sludge production (Cullen et al., 2013). The daily rate of dry tons produced dropped

by around 10% comparing to previous production before the SRF was operational (Baur et al., 2010).

Benish et al. (2009) elaborated about the economics of P-recovery:

> The total cost of the P-recovery facility was $US 2.5 million. In order to reach a desired six-year return of investment (ROI), the combination of savings and income from the sales revenue (SR) of Crystal Green have to total $US 40,000/month assuming an annual interest rate of 5 %. By 2010, 35 t/month of product had been recovered. At 35 t/month, the required SR for the six-year ROI amounts to $US 1,150 without operation cost, overhead and profit. Operation and maintenance costs include energy ($US 0.08/kWh) for operation of the plant (~ $US 50/t of product), labour hours ($US 45/h), and magnesium chloride ($US 240/t). (p.112)

Because of the confidential nature of the public/private partnership, the exact information about the revenue generated from the sale of the product is not available (Benisch et al., 2009). Nonetheless, Cordell et al. (2011) reported that costs can be recovered in 3–5 years due to maintenance and capacity cost savings and fertilizer revenue. After this time, it can provide profit to the wastewater service provider (such as the municipality) (Britton et al., 2009).

To increase struvite production and to decrease struvite potential in the digestion system, the WASSTRIP process was implemented at full-scale in 2011 (Cullen et al., 2013). WASSTRIP doubled struvite production from previous years, with 70% of the phosphorus sent to the struvite reactors coming from WASSTRIP (Cullen et al., 2013). This resulted in overload of the existing reactors in the SRF which led to the suspension of WASSTRIP until the installation of a new Pearl reactor that would double the capacity of the SRF (Cullen et al., 2013).

4.4 Summary

Phosphorus release from sludge treatment processes in WWTP that combine biological P removal with anaerobic digestion offer the best opportunity for P recover from wastewater in the form of struvite. The conditions arisen under these circumstances are so highly prone to struvite formation that struvite occurs spontaneously and involuntarily in WWTP facilities.

Theoretical knowledge on struvite formation allows to duplicate the involuntary crystallization process in WWTP facilities and to explore the conditions under which this crystallization occurs., in practical engineering processes. This has been achieved by several technologies' developers by precipitating struvite in a dedicated reactor from an orthophosphate-rich process stream, and by adding magnesium and adjusting the pH. Phosphorus recovery can achieve typically 20% of total plant influent P. When combined with other technologies this recover may be up to 50% of total plant influent P.

The precipitation of struvite from phosphate-rich sewage sludge water is well known and currently being practised in more than 40 full-scale installations world-wide. Ostara is the market leader and stands out for the quality of its recovered product, a ready-to-use premium fertilizer. Because Ostara is a spin-off company of a research group of the University of British Columbia, several pilot studies regarding the earlier stages of Ostara's technology are available in literature. There is a lot of know-how with huge potential to be creatively transformed into innovation. Recycling value chains are already implemented worldwide and just waiting to be replicated (Kabbe, 2019).

CHAPTER 5

THE REACTOR AND THE COMPLEMENTARY CONSTITUENTS OF THE CRYSTALLIZATION SYSTEM

One of the main goals of the present dissertation is the sizing of a reactor to remove P from wastewater in the form of struvite. To profit from recent technological progress, rather than designing and sizing the reactor from scratch, the reactor was designed based on an already existing one. This chapter presents the sizing procedure of this reactor, and the complementary constituents of the chosen crystallization technology. For that purpose, this chapter is divided into three major sections - section 5.1, section 5.2 and section 5.3.

Section 5.1 presents the undertaking of learning how to design a reactor similar to the ones investigated by the UBC research P-recovery group. To learn how to design a similar reactor, data concerning the dimensions of the reactors is collected and analysed. For that purpose, patterns and proportions amongst the reactor's diameters and heights are sought. Both the lack of data related to the sizing procedure in the literature and the absence of consistent patterns amongst the UBC reactor's dimensions led to the need of replicating one of the reactors investigated by the UBC research P-recovery group. The selection of this reactor, amongst the various reactors studied by the UBC research P-recovery group, is also justified in section 5.1. Some modifications to the reactor are also described here.

Section 5.2 indicates the dimensions of the new reactor. Also, in this section, the sizing of the complementary constituents of the UBC crystallization system – the injection port, the external clarifier, the pumps and the tubing – is presented. The crystallization system as a whole is illustrated in Appendix A.

At last, section 5.3 presents the major findings and drawn conclusions of Chapter 5.

5.1 The rationale behind the sizing of the reactor

5.1.1 Data collection

The reactor designed in this dissertation is based on the pilot-scale reactors previously designed and tested by the UBC research P-recovery group. The underlying reason for founding the reactor design on the previously designed UBC reactors was to assess the applicability of these UBC reactors in recovering P from a Portuguese WWTP in the future. Also, proceeding this way has the advantage of benefiting from the UBC researchers' acquired knowledge. This approach was considered to be potentially more fruitful than starting the present P-recover study from scratch.

Indeed, a lot of experience and expertise has been gained through the years, since the UBC phosphorus recovery project started in 1999 (Adnan, 2002). For instance, some ideas of the reactor geometry were tested and discarded in the earlier phases of the UBC P-Recovery Project (Dastur, 2001). Also, according to Dastur (2001), even though the UBC P-Recovery Project produced P-removals of over 95% in the earlier stages, the form of the resulting crystalline material was extremely poor.

The main challenge in the design of a crystallization reactor is to predict the influence of crystallizer geometry, scale, feed characteristics and operating conditions on the process behaviour and product quality (Dastur, 2001). Since 2000, several pilot and bench-scale studies were carried out by the UBC P-Recovery Project and can be found in the literature (Lee, 2017). To profit from the progress obtain since then, the sizing of the reactor designed in this dissertation was determined, to a large extent, by exploiting the information present in these pilot and bench-scale studies carried out by the UBC P-Recovery Project. To this end, there was the need to firstly carry out a review of these studies. Both the process schematic and the reactor layout illustrated in Figure 5.1 are common to all the UBC studies under review here. Letters from A to D identify the sections of increasing diameters from bottom to top.

Recalling Ostara's Pearl Technology Application (section 4.3.4), namely its pilot-scale application (section 4.3.4.1), it is evident that the reactor layout and the process schematic represented in Figure 5.1 are identical to the ones used by Fattah (2004) (compare Figure 5.1 and Figure 4.10). The study carried out by Fattah (2004) comprises, indeed, one of the UBC studies considered in the review.

Each one of the different UBC studies considered in the review below analyzed a reactor which followed the concept of a fluidized bed reactor, whose functioning principles were aforementioned described in section 4.3.4. The UBC studies tested several controlling parameters such as the SSR, pH or magnesium dosage. Different flows entering the reactor were also tested (influent, NaOH, recirculation line).

The review of these UBC studies has the ultimate purpose of providing information that provides means to draw a reactor whose layout is identical to the one of Figure 5.1, and which is an outcome of overcoming several shortcomings in the past. Furthermore, each UBC study provides information regarding the operating conditions of the respective reactor, which can be used as a guideline for the future operation of the reactor designed in this dissertation. Thus,

the UBC studies were chosen as the foundation to design a reactor for two main reasons. Firstly, because Ostara, the leading company in recovering P, is a spin-off company of the UBC P-Recovery Project, which accomplished consistently good results in recovering P from wastewater. Secondly, because the UBC studies are in the form of dissertations which provide systematic and detailed information regarding the earlier phases of the Ostara technology. Such a large amount of information was not found in any other P-recover technology in the literature.

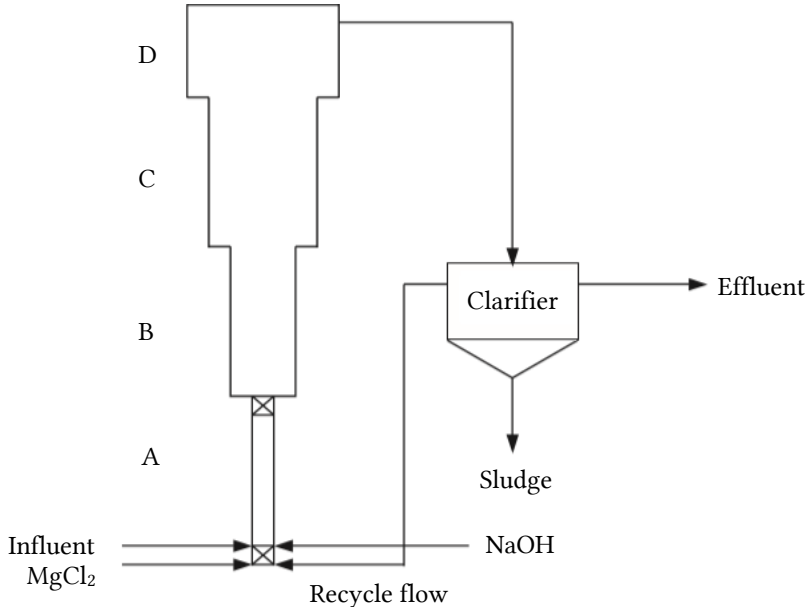

Figure 5.1 - Process schematic used by the UBC studies and layout of the reactors therein tested (adapted from Mavinic et al., 2007).

Table 5.1 outlines, for each UBC study reviewed in the present thesis, the respective key reactor's specifications and its efficiency indicators. These specifications and indicators will be further detailed and the reasons behind their selection clarified. For each study, respectively referenced in the rightmost column, Table 5.1 indicates the diameter ($Ø_s$) and the height (H_s) of each one of the constituent sections (A to D) of the reactor analysed. In the case of the studies carried out by Adnan (2002) and Huang (2003), each author designed and studied two reactors, distinguished as reactors A and B.

Observing Table 5.1, specifically, the relation between the diameter and the height of each reactor constituent section, it is noticeable that each reactor is different from the others and it has its own specific arrangement. Nonetheless, reactor B studied by Adnan (2002) and reactor B studied by Huang (2003) are identical, except for the difference of 1 cm between the diameter of section B. It is also noticeable that most of the reactors have identical section's diameters. This is the case of all the reactors reviewed in Table 5.1 except the following two: the reactor designed by Dastur (2001) and the reactor designed by Fattah (2004).

The survey of the dimensions of the reactors was an attempt to unveil the sizing procedure of the UBC reactor. As the sizing's principles and parameters lack in all UBC studies, surveying the dimensions of the reactors' sections could help identify patterns amongst them. The further analysis of the reactors' dimensions intends to identify patterns amongst (i) the proportion between the heights of its sections, (ii) the proportion between the diameters of its sections and at last, (iii) the proportion between the diameters and heights of its sections. If these patterns do exist (e.g., the heights of two adjacent reactor sections relate between themselves always through the same ratio), they can then be replicated when designing a new reactor. From a practical point of view, this attempt was considered the most viable one since the sizing criteria were not found in the literature. Furthermore, it is important to recall that the formation of

struvite pellets in the reactor is not only a chemical process but also a physical one. Additionally, each UBC dissertation operated its specific reactor, testing different influents and operational parameters, which adds extra complexity in the disclosure of the sizing criteria.

Table 5.1 - Review of the UBC studies – reactor key specifications and performance indicators.

Reactor Section	Height, H_s (cm)	$Ø_s$ (cm)	Maximum P- removal efficiency (%)	Struvite recovery efficiency (%)	Reference
A	45.7	1.54	74.5	Not provided	(Dastur, 2001)
B	45.7	2.06			
C	45.7	2.62			
D	45.7	7.81			
A	101	4	97.5	Not provided	(Adnan, 2002) reactor A
B	108	5.20			
C	250	7.70			
D	45.7	20.20			
A	106	4	97.8	80	(Adnan, 2002) reactor B
B	275	5.20			
C	93	7.70			
D	45.7	20.20			
A	96	4	90	87	(Britton, 2002)
B	177	5.20			
C	94	7.70			
D	38	20.20			
A	106	4	98.4	86	(Huang, 2003) reactor A
B	108	5.20			
C	250	7.70			
D	45.7	20.20			
A	106	4	97.3	81.7	(Huang, 2003) reactor B
B	276	5.20			
C	93	7.70			
D	45.7	20.20			
A	74.9	7.60	97.2	86	(Fattah, 2004)
B	154.9	10.20			
C	127	15.20			
D	45.7	38.10			

Before diving into the analysis of the reactors' dimensions presented in Table 5.1, one should firstly ensure that the reactors are indeed capable of removing phosphorus from wastewater capably. For that reason and to assess the ability of the different reactors in recovering P from wastewater, the review summed up in Table 5.1 also included two key performance indicators - the maximum value of phosphorus removed (max. P-removal efficiency) and the struvite recovery efficiency. These indicators will be defined below.

Except for the studies carried out by Huang (2003) and Britton (2002), all UBC studies defined P-removal efficiency as highlighted in equation (5.1). $P_{influent}$ is the PO_4-P concentration at the inlet of the reactor and $P_{effluent}$ is the concentration of the effluent collected from the external clarifier.

$$\text{P-removal efficiency (\%)} = \frac{P_{influent} - P_{effluent}}{P_{influent}} \times 100 = \frac{\frac{[P_i]*Q_i}{Q_{i_{total}}} - P_{effluent}}{\frac{[P_i]*Q_i}{Q_{i_{total}}}} \times 100 \qquad (5.1)$$

$P_{influent}$ is determined by multiplying the PO_4-P concentration of the influent used (centrate/ digester supernatant), $[P_i]$, with its feed flow into the reactor, Q_i, and then dividing that product by the total influent flow into the reactor $Q_{i_{total}}$. By calculating $P_{influent}$ this way, equation (5.1) considers the dilution of the influent in study at the inlet, occasioned by the addition of NaOH and $MgCl_2$.

Huang (2003) and Britton (2002) expressed the P-removal efficiency differently, as seen in equation (5.2). Likewise, here, $[P_i]$ is the PO_4-P concentration of the feed/influent and Q_i is the flow of the influent into the reactor. $[P_e]$ is the concentration of PO_4-P in the effluent collected from the external clarifier, and Q_e is the flow of the effluent.

$$\text{P-removal efficiency (\%)} = \frac{[P_i] * Q_i - [P_e] * Q_e}{P_i * Q_i} \times 100 \qquad (5.2)$$

Both equations - (5.1) and (5.2) - consist of valid methods to assess the phosphorus removal carried out by the reactor. Since $P_{effluent}$ and $Q_{i_{total}}$, as stated in (5.1), stand for the same as $[P_e]$ and Q_e, stated in (5.2), respectively, both equations are interchangeable. This renders the comparison between studies easier.

The reason for using the maximum value of P-removal efficiency as a key performance indicator will now be clarified. During the operation of the reactor, optimal operational conditions and parameters are usually not known from the beginning or are unfeasible to reproduce immediately or to maintain throughout the study. As a result, the phosphorus removal efficiencies in these phases are significantly lower than the efficiencies achieved during optimal operation conditions. Thus, using other metric, rather than the maximum value of the phosphorus removal efficiency (e.g. the average) would incorporate the effect of these lower efficiencies and lead to the underestimation of the actually demonstrated ability of the reactor in removing P at optimal and controlled conditions.

At last, the struvite recovery efficiency was considered in the review to assess if and how much of the phosphate being removed was in fact being recovered in the form of struvite. For that purpose, the dry weight of each harvest of struvite was recorded, and the theoretical struvite that should have been formed was calculated based on the quantity of P removed from the influent. The struvite recovery efficiency was then calculated as represented in equation (5.3).

$$\text{Struvite recovery efficiency (\%)} = \frac{\text{Mass of struvite harvested}}{\text{Theoretical mass of struvite formed}} \times 100 \qquad (5.3)$$

Theoretically, all the removed phosphate should have been converted into struvite (Huang, 2003). Nonetheless, efficiencies were lower than 100% since the fine particles that arose inside the reactor could not be completely harvested due to their small size. Also, there was mass loss in the process of harvesting, drying, transferring and sieving the formed struvite. Some fine struvite also escaped the reactor and accumulated at the bottom of the clarifier or even exited with the effluent.

To perceive the order of magnitude of the P concentration present in the influent that relates to the maximum phosphorus removal efficiencies presented in Table 5.1, Table 5.2 is useful. Table 5.2 indicates, for the maximum observed phosphorus removal efficiency of each UBC study, the related concentration of soluble orthophosphate of the influent used.

Table 5.2 - Maximum P-removal efficiencies and influent P concentrations of the UBC studies.

Reference of the UBC study	Maximum P-removal efficiency (%)	Soluble [PO_4-P] of the influent at maximum removal efficiency (mg/L)	Range of soluble [PO_4-P] of the influent (mg/L)	Average of soluble [PO_4-P] of the influent (mg/L)	Origin of the influent
(Dastur, 2001)	74.5	61.60	23.6 - 171	81.7	Synthetic feedwater
(Adnan, 2002) reactor A	97.5	68.00	54.6 - 255	113.40	Synthetic feedwater
(Adnan, 2002) reactor B	97.8	74.90		111.60	
(Britton, 2002)	91	59.80	8-71	55.10	Anaerobic digester supernatant
(Huang, 2003) reactor A	98.4	136.20	72.21-141	108.41	Anaerobic digester supernatant
(Huang, 2003) reactor B	97.3	136.20			
(Fattah, 2004)	97.2	54.44	38.8 - 88.4	59.15	Centrate

The data showed in Table 5.2 do not mean that high efficiencies were only achievable when the influent used had the related concentrations of soluble PO_4-P. It solely means that the maximum efficiencies were obtained in such conditions. As a matter of fact, similar efficiencies were obtained for a vast range of concentrations, independently of them being higher or lower, for all different studies. The range and the average of the concentration of soluble PO_4-P of the influents used are therefore also indicated in Table 5.2. These data show a vast range of influent concentrations tested. This was encouraging, since, at the time being, the composition of the influent intended to be studied in this dissertation (Chelas WWTP centrate) was unknown.

The origin of the influent used – natural or synthetic – was taken into account in Table 5.2 since the two earlier UBC studies, carried out by Dastur (2001) and Adnan (2002), used synthetic wastewater rather than centrate or supernatant collected from a WWTP. The synthetic feedwater, containing the constituent ions of struvite, was used as influent mainly because large volumes of digester supernatant were not available for continuous operation of the reactor

(Adnan, 2002; Dastur, 2001). Also, full control over feed characteristics was imperative at these earlier stages (Dastur, 2001).

At this point, some remarks about the present review should be made. Table 5.1 summarizes the studies, which are in the form of thesis, carried out by the UBC research P- recovery group, available in literature until 2004. After 2004, more UBC studies can be found in literature. However, from the perspective of sizing a pilot-reactor, the information provided there is either redundant, or the dimensions of the reactor are not provided. Some cases of redundant information consist on a few papers published based on the UBC studies. The information contained in these papers is the one contained in the UBC studies which originated them, and for this reason, these papers were not included in Table 5.1. The papers have, however, the advantage of providing a less extensive read, and for that reason, Table 5.3 specifies its references, so they can be easily consulted.

Table 5.3 - References of the UBC studies reviewed and associated published papers.

Reference of the UBC study	Reference of the associated paper
(Adnan, 2002)	(Adnan, Mavinic, et al., 2003)
(Britton, 2002)	(Britton et al., 2005)
(Huang, 2003)	(Mavinic et al., 2007)

As for the shortage of new data concerning the reactor sizing after 2004, this may be explained by the fact that Ostara was founded in 2005 (Lee, 2017). After that, full-scale demonstrations took place before the implementation of commercial facilities (Lee, 2017).

5.1.2 Data validation

Thus far, every aspect reviewed in Table 5.1 has been described. Before proceeding to the analysis of the collected data, the reactors' ability in removing P in the form of struvite will be firstly examined. This preliminary analysis intends to restrain the collected data so that the only reactors to be further analysed in terms of their dimensions are the ones that showed the highest ability in recovering P.

As it can be seen from Table 5.1, all reactors, except the reactor designed by Dastur (2001), were capable of removing more than 90% of the phosphorus present in the influent. Also, regarding the studies whose reactors were able to remove more than 90%, apart from the study carried out by Britton (2002), all studies were able to achieve maximum values of efficiency above 97%. The lowest maximum P-removal efficiency of 74.5%, observed in the study carried out by Dastur (2001), was attributed in part to some design problems that limited the success of the reactor operation (Dastur, 2001). As for the struvite recovery efficiency, the reactors for which this data was provided, were able to recover 80% or more of the P removed in the form of harvestable struvite.

To conclude, except for the reactor designed by Dastur (2001), all reactors proved to be considerably successful in removing P from its respective influent and can, therefore, be considered in the further analysis that will follow – the analysis of the dimensions of the reactors. Furthermore, in what concerns these studies, 80% or more of the phosphorus removed was indeed recovered in the form of struvite. The only exception is reactor A designed by Adnan (2002), for which the information about its respective struvite recovery efficiency was not provided. Thus, this reactor will also be discarded from further analysis. Table 5.4 indicates the heights and diameters of the sections of the reactors that will be analysed below.

Table 5.4 - Reactor key specifications of the reviewed and validated UBC studies.

Reactor Section	Height, H (cm)	$Ø_s$ (cm)	Reference of the UBC study
A	106	4	(Adnan, 2002) reactor B
B	275	5.20	
C	93	7.70	
D	45.7	20.20	
A	96	4	(Britton, 2002)
B	177	5.20	
C	94	7.70	
D	38	20.20	
A	106	4	(Huang, 2003) reactor A
B	108	5.20	
C	250	7.70	
D	45.7	20.20	
A	106	4	(Huang, 2003) reactor B
B	276	5.20	
C	93	7.70	
D	45.7	20.20	
A	74.9	7.60	(Fattah, 2004)
B	154.9	10.20	
C	127	15.20	
D	45.7	38.10	

5.1.3 Analysis of the sections' heights of the reactors

From Table 5.4, it can be seen that all reactors, except the reactor A designed by Huang (2003), share the following tendency: there is an increase in height from section A to section B and then the height decreases from section B to C, and from section C to D. As for reactor A designed by Huang (2003), there is an increase in height from section A to section B, and from section B to C, followed by a decrease in height from section C to D.

In order to assess if the height of each section of the reactor related somehow to the remaining sections in the same way along all studies, for each reactor, the ratios between the possible combinations of different sections' heights were calculated. Thus, $\frac{H_B}{H_A}$, $\frac{H_C}{H_B}$, $\frac{H_D}{H_C}$, $\frac{H_A}{H_D}$, $\frac{H_B}{H_D}$ and $\frac{H_A}{H_C}$, are plotted in Figure 5.2 to Figure 5.7, respectively. By doing so, if the different sections' heights relate to each other in a fixed proportion, this may be easily identified.

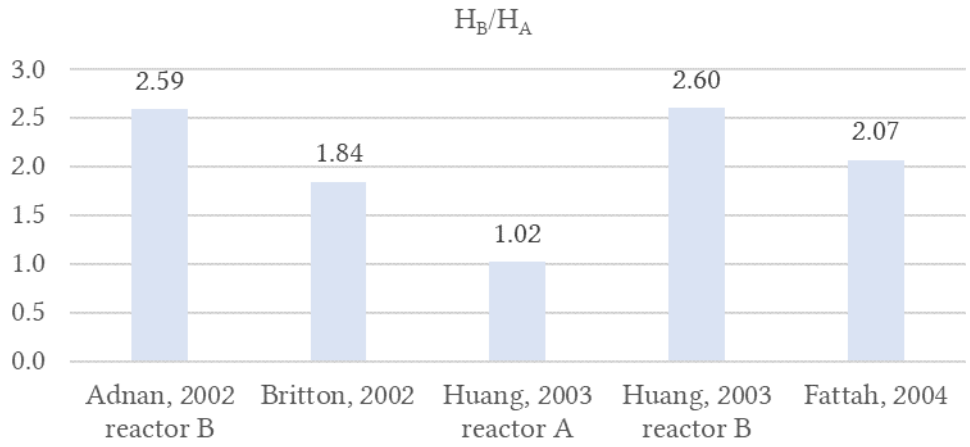

Figure 5.2 - Ratio between the reactor sections' heights H_B and H_A, of the reviewed and validated UBC studies.

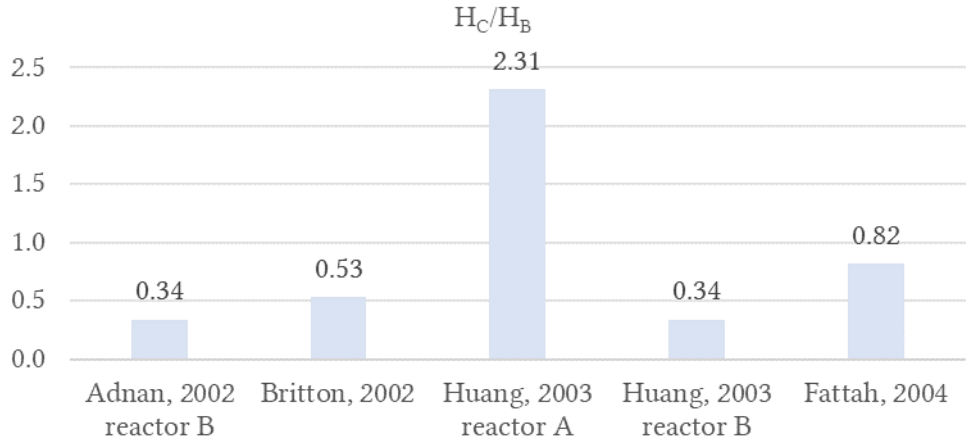

Figure 5.3 - Ratio between the reactor sections' heights H_C and H_B, of the reviewed and validated UBC studies.

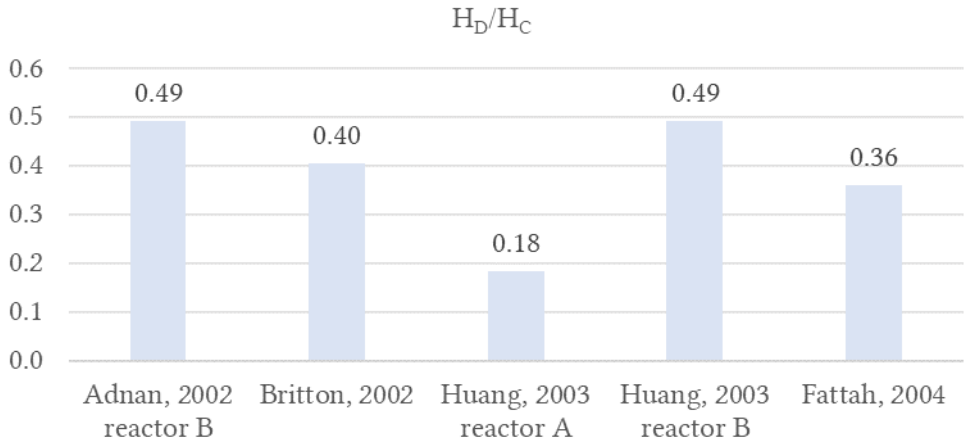

Figure 5.4 - Ratio between the reactor sections' heights H_D and H_C, of the reviewed and validated UBC studies.

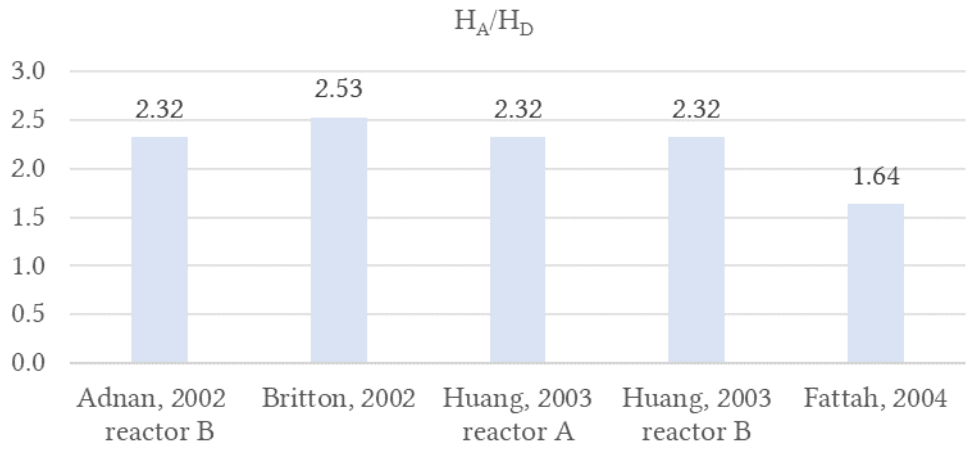

Figure 5.5 - Ratio between the reactor sections' heights H_A and H_D, of the reviewed and validated UBC studies.

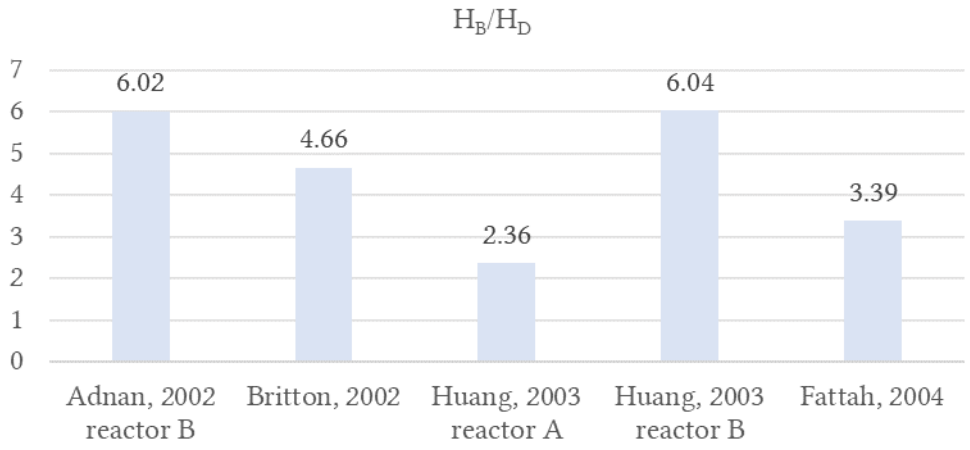

Figure 5.6 - Ratio between the reactor sections' heights H_B and H_D, of the reviewed and validated UBC studies.

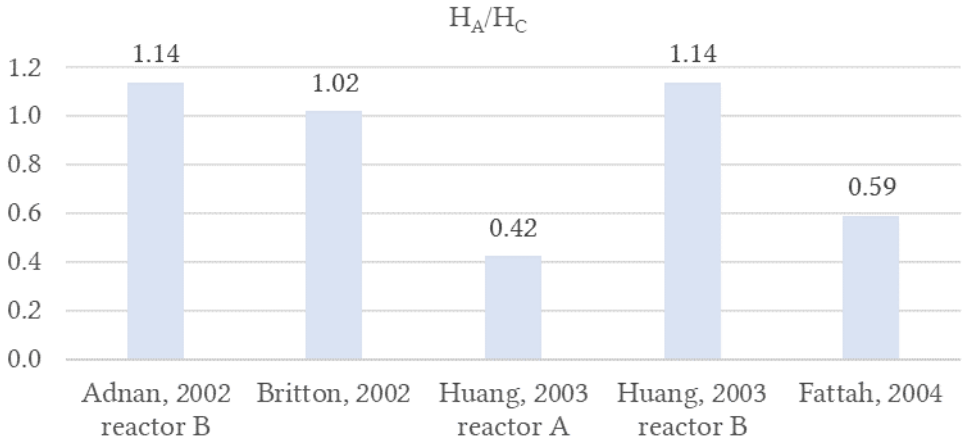

Figure 5.7 - Ratio between the reactor sections' heights H_A and H_C, of the reviewed and validated UBC studies.

From the analysis of Figure 5.2 to Figure 5.7 the following can be observed:

- The only reactors whose ratios are identical for all possible combinations of sections' heights are the following two reactors: reactor B designed by Adnan (2002) and reactor B designed by Huang (2003). Quotients $\frac{H_B}{H_A}$ and $\frac{H_B}{H_D}$, are the only quotients for which these two reactors do not exhibit the exact same value. However, the differences between these quotients, $\frac{H_B}{H_A}$ and $\frac{H_B}{H_D}$, are 0.01 and 0.02, respectively. This was expected and is justified by the fact that these two reactors have the exact same sections' heights, except for section B. Furthermore, section B of the reactor B designed by Adnan (2002) has a height of 275 cm whereas for reactor B designed by Huang (2003) this section height is 276 cm, ensuing a difference of 1 cm between these reactors' heights.
- When examining quotient $\frac{H_A}{H_D}$, it is also noticeable, that this quotient is the same not only for reactor B designed by Adnan (2002) and reactor B designed by Huang (2003), but also for the reactor A, also designed by Huang (2003). The three reactors exhibit a value of 2.32 for quotient $\frac{H_A}{H_D}$.
- Except for the just aforementioned cases, no quotient exhibits the same value for different reactors. The least difference amongst the reactors for a certain quotient is 0.04 and it relates to quotient $\frac{H_D}{H_C}$ and to the reactors designed by Britton (2002) and Fattah (2004). As to the largest difference between two reactors for a certain quotient, the difference is 3.65 and it relates to quotient $\frac{H_B}{H_D}$ of reactor B designed by Adnan (2002) and reactor A designed by Huang (2003).

Even though Table 5.5 does not add new information, it conveniently indicates, for each quotient, the calculated difference between the distinct quotients of each possible pair of reactors. This way, the information regarding all possible combinations of quotients and reactors is condensed. To ease the data visualization, the quotients' differences less than 0.1 were coloured green, between 0.1 and 1 were coloured from light yellow to dark yellow, and above 1 were coloured as red. It can be seen that for each one of the following ratios, $\frac{H_D}{H_C}$, $\frac{H_A}{H_D}$ and $\frac{H_A}{H_C}$, the differences amongst the different reactors are always inferior to 1. Unfortunately, Table 5.5 also allows to further sustain that there are no consistent and strict patterns in terms of the proportions between the different sections' heights of the analysed reactors.

Table 5.5 - Difference between each distinct sections' heights ratio related to each possible pair of reactors.

	Reference of the UBC study	**Britton, 2002**	**Huang, 2003 reactor A**	**Huang, 2003 reactor B**	**Fattah, 2004**
$\frac{H_B}{H_A}$	**Adnan, 2002 reactor B**	0.75	1.58	0.01	0.53
	Britton, 2002	-	0.82	0.76	0.22
	Huang, 2003 reactor A	-	-	1.58	1.05
	Huang, 2003 reactor B	-	-	-	0.54
$\frac{H_C}{H_B}$	**Adnan, 2002 reactor B**	0.19	1.98	0.00	0.48
	Britton, 2002	-	1.78	0.19	0.29
	Huang, 2003 reactor A	-	-	1.98	1.49
	Huang, 2003 reactor B	-	-	-	0.48
$\frac{H_D}{H_C}$	**Adnan, 2002 reactor B**	0.09	0.31	0.00	0.13
	Britton, 2002	-	0.22	0.09	0.04
	Huang, 2003 reactor A	-	-	0.31	0.18
	Huang, 2003 reactor B	-	-	-	0.13
$\frac{H_A}{H_D}$	**Adnan, 2002 reactor B**	0.12	0.72	0.00	0.55
	Britton, 2002	-	0.60	0.12	0.43
	Huang, 2003 reactor A	-	-	0.72	0.17
	Huang, 2003 reactor B	-	-	-	0.55
	Fattah, 2004	-	-	-	-
$\frac{H_A}{H_C}$	**Adnan, 2002 reactor B**	0.12	0.72	0.00	0.55
	Britton, 2002	-	0.60	0.12	0.43
	Huang, 2003 reactor A	-	-	0.72	0.17
	Huang, 2003 reactor B	-	-	-	0.55
$\frac{H_B}{H_D}$	**Adnan, 2002 reactor B**	1.36	3.65	0.02	2.63
	Britton, 2002	-	2.29	1.38	1.27
	Huang, 2003 reactor A	-	-	0.42	0.42
	Huang, 2003 reactor B	-	-	-	0.55

5.1.4 Analysis of the sections' diameters of the reactors

In what concerns the proportion between the diameters of the different reactors' sections, its analysis becomes rather simple. Except for the reactor designed by Fattah (2004), all reactors share, for each distinct section, the same respective diameter. These diameters are 4 cm, 5.2 cm, 7.7 cm and 20.2 cm regarding sections A, B C and D, respectively, as depicted in Table 5.6. The proportion amongst these different sections' diameters is always the same for these reactors.

Table 5.6 - Sections' diameters of the reactors whose related UBC reactors were reviewed and validated.

Reactor Section	$Ø_s$ (cm)	Reference of the UBC study
A	4	(Adnan, 2002) -reactor B; (Britton, 2002) ;(Huang, 2003) -reactors A and B;
B	5.20	
C	7.70	
D	20.20	
A	7.60	(Fattah, 2004)
B	10.20	
C	15.20	
D	38.10	

The worthwhile analysis is, thus, between these reactors and the reactor designed by Fattah (2004). For that purpose, Table 5.6 also presents the sections' diameter of the reactor designed by Fattah (2004).

From Table 5.6, it can be seen that the diameters of the different constituent sections of the reactor designed by Fattah (2004) seem to be a rough 2x scale-up of the ones used by the remaining UBC studies. Table 5.7 corroborates this by indicating, for each reactor section, the ratio between the diameter of the reactor designed by Fattah (2004) and the respective diameter of the remaining reactors.

Table 5.7 – Ratio between the distinct diameters' sections of the reactor designed by Fattah (2004) and the respective ones designed by the remaining UBC studies' authors.

$\frac{Ø_{A\,Fattah}}{Ø_{A\,remaining\ reactors}}$	1.90
$\frac{Ø_{B\,Fattah}}{Ø_{B\,remaining\ reactors}}$	1.96
$\frac{Ø_{C\,Fattah}}{Ø_{C\,remaining\ reactors}}$	1.97
$\frac{Ø_{D\,Fattah}}{Ø_{D\,remaining\ reactors}}$	1.89

Consequently, in what concerns the proportion between the diameters of the reactors' sections, all reactors exhibit the same patterns. The proportions between the reactors' distinct constituent sections can be seen in Figure 5.8.

As Figure 5.8 depicts, the differences between the distinct quotients obtained for the study carried out by Fattah (2004) and the ones obtained by the remaining studies range from 0.01 to 0.12. These differences are explained by the fact that the scale up factor used by Fattah for the diameters' sections is not exactly 2 as it ranges from 1.89 to 1.97 amongst the different sections (recall Table 5.7).

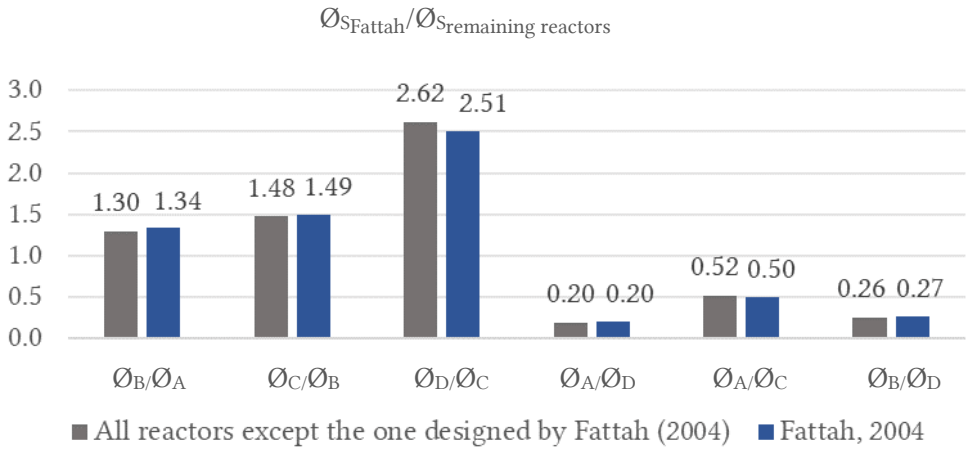

Figure 5.8 – Observed proportions between the diameters of the constituent sections of all UBC reactors reviewed and validated.

5.1.5 Outcome of the analysis of the sections' dimensions of the reactors

Even though it was observed to exist fixed proportions between the distinct sections' diameters of the reactors, no pattern was possible to identify in terms of the arrangement of the sections' heights. Also, besides the two practically identical reactors, each reactor had different sections' heights compared to the correspondent sections heights of the remaining reactors, for most of the sections. Bearing in mind that all reactors except the one designed by Fattah (2004) have the same sections' diameters, a further attempt to identify any proportion between the height and the diameter of each section would be effortless and was not done.

Thus, the jointly analysis of the diameters and heights of the reactors' sections undertaken here did not allow to recognize any pattern in terms of their arrangements in such way that this pattern could be replicated in the design of a new reactor. The effort to identify such a pattern was thus not at all unreasonable as, at first sight, the reactors seemed to correlate somehow between them.

As a matter of the fact, it seems that the heights of the reactors' sections were varied across the different UBC studies so that different heights were tested, by maintaining the same sections' diameters for all reactors. The reactor designed by Fattah (2004) was the only reactor with different diameters, but these were a 2x scale-up of the diameters of the remaining reactors.

For each reactor section, the height differs, however, slightly between the studies. This is supported by Table 5.8, which depicts the correlation between the respective sections' heights, for each possible pair of the studies, through the Pearson correlation coefficient. As Table 5.8 illustrates, the heights of the different reactors' sections show a strong correlation between them, as the correlation coefficient is more than 0.8 in most cases. Correlation values inferior to 0.8 were coloured blue. These values (<0.8) relate to the correlations where reactor A designed

by Huang (2003) is implied. This was expected and is explained by the fact that this reactor is the only one where there is an increase in height from section A to section B, and from section B to C, followed by a decrease in height from section C to D, whereas the remaining reactors increase in height from section A to section B and then the height decreases from section B to C, and from section C to D.

Table 5.8 - Correlation between the sections' heights of the reactors - Pearson correlation coefficient.

Reference of the UBC study	Adnan, 2002 reactor B	Britton, 2002	Huang, 2003 reactor A	Huang, 2003 reactor B	Fattah, 2004
Adnan, 2002 reactor B	-	0.97	0.00	1.00	0.82
Britton, 2002	-	-	0.20	0.97	0.89
Huang, 2003 reactor A	-	-	-	0.00	0.56
Huang, 2003 reactor B				-	0.82

Both the lack of information in the literature about the reactors' sizing criterion and the absence of a consistent replicable pattern between the reactor's dimensions led to the need of choosing one of the UBC reactors to replicate its dimensions.

Sizing a reactor from scratch, even if following the general outline of the UBC reactors, would neglect the expertise gained through the years by the UBC phosphorus recovery project. Mistakes or drawbacks that were previously met and overcome by the UBC phosphorus recovery project could be repeated unnecessarily. For this reason, the path chosen to design the new reactor was the replication of a given UBC reactor. The choice of such UBC reactor and the reasons behind that choice will be discussed next in subsection 5.1.6.

5.1.6 Choosing a UBC reactor to replicate

Concerning the studies carried out by the UBC phosphorus recovery project, presented in this dissertation in Table 5.1, some were initially discarded from further analysis, either because they showed relatively low performance, or because there was data missing with regards the ability of the reactors in recovering P in the form of struvite – recall subsection 5.1.2. For these same reasons, these reactors were also not considered in the process of choosing a UBC reactor to be replicated.

The validated reactors are depicted in Table 5.9, where the reactors' dimensions are indicated, as well as the following performance indicators: maximum value of phosphorus removed (max. P-removal efficiency) and the struvite recovery efficiency (both already described in subsection 5.1.1).

From Table 5.9, one reactor was chosen to be replicated. This choice was based on the following two criteria:

. The influent used had to be real wastewater (anaerobic digester supernatant or centrate), in lieu of synthetic wastewater containing the constituent ions of struvite. This provides more guarantees of the ability of the reactor in dealing with the composition of real wastewater and its variations through time.

. The chosen reactor had to have demonstrated the highest ability in recovering P in the form of struvite. Thus, the multiplication of both indicators, max. P- removal efficiency and the struvite recovery efficiency, had to be the highest.

Table 5.9 - Reactor key specifications, performance indicators, and origin of the influent used of the reviewed and validated UBC studies.

Reactor Section	Height, H_s (cm)	$Ø_s$ (cm)	Maximum P-removal efficiency (%)	Struvite recovery efficiency (%)	Origin of the influent used	Reference
A	106	4	97.8	80	Synthetic feedwater	(Adnan, 2002) reactor B
B	275	5.20				
C	93	7.70				
D	45.7	20.20				
A	96	4	90	87	Anaerobic digester supernatant	(Britton, 2002)
B	177	5.20				
C	94	7.70				
D	38	20.20				
A	106	4	98.4	86	Anaerobic digester supernatant	(Huang, 2003) reactor A
B	108	5.20				
C	250	7.70				
D	45.7	20.20				
A	106	4	97.3	81.7		(Huang, 2003) reactor B
B	276	5.20				
C	93	7.70				
D	45.7	20.20				
A	74.9	7.60	97.2	86	Centrate	(Fattah, 2004)
B	154.9	10.20				
C	127	15.20				
D	45.7	38.10				

Before proceeding to the reactor selection, the following caveat must be addressed: the efficiencies related to the studies indicated in Table 5.9 are not strictly comparable since the influent differs from study to study. As aforementioned in section 2.4, the composition of the wastewater greatly influences the formation of struvite. For example, the presence of foreign ions such as calcium inhibit the formation of struvite. Furthermore, each study used its own operational parameters. Thus, the optimal operational parameters also differ among studies.

The present caveat intends to clarify that comparisons between the reactors ability in recovering P from wastewater cannot be done so straightforwardly. Indeed, with so many other factors changing simultaneously (e.g. reactors dimensions, influent composition, operational parameters), this comparison becomes hard if not impossible. Nonetheless, and with the selection

of a reactor to be replicated in view, it is valid to select the reactor which attained the highest efficiency.

Naturally, at the time the reactor designed here is installed and operated, results different from the ones obtained in the UBC reactor that will be replicated are expected. Even though the composition of the wastewater to be studied was unknow by the time this reactor was outlined, one should bear in mind that each wastewater is unique, and, thus, different outcomes are expected.

From the above mentioned selection criteria, reactor B designed by Adnan (2002) is discarded for being the only reactor from Table 5.9 to have used synthetic wastewater as influent. As for the multiplication of the performance indicators (the max. P-removal efficiency and the struvite recovery efficiency), Table 5.10 indicates the product for each study.

Table 5.10 - Product of the two performance indicators - Struvite recovery efficiency and Maximum P-removal efficiency.

Maximum P- removal efficiency (%)	Struvite recovery efficiency (%)	Maximum P- removal efficiency (%) × Struvite recovery efficiency (%)	Reference
97.8	80	78.24	(Adnan, 2002) reactor B
90	87	78.3	(Britton, 2002)
98.4	86	84.62	(Huang, 2003) reactor A
97.3	81.7	79.49	(Huang, 2003) reactor B
97.2	86	83.59	(Fattah, 2004)

As it can be seen from Table 5.10, reactor A designed by Huang (2003) showed the highest product amongst the reactors - 84.62. According to the criteria defined for the reactor selection, this reactor should be the one chosen to be replicated.

Nevertheless, reactor A designed by Huang (2003) has a total height of more than 4 m which faces both logistical and economical constraints. Indeed, this is a constraint which is common to all the reactors in analysis – recall the sections' heights indicated in Table 5.9. All reactors are more than 4 m height. Apparently, this shortcoming could be simply overcome by scaling-down the heights of the constituent sections of reactor A designed by Huang (2003). Altering the heights without knowing the implications on struvite formation process may come with a great deal of uncertainty. Reached this point, this seems a bottleneck hard to solve. Fortunately, a study carried out by Rahaman et al. (2009), allowed to overcome this deadlock.

Rahaman et al. (2009) modelled the hydrodynamics of a UBC fluidized bed crystallizer using a commercial Computational Fluid Dynamics (CFD) software. CFD modelling allows the prediction of flow patterns, local solids concentration and local kinetic energy values, taking into account the reactor shape (Rahaman et al., 2009). The assumptions and the principles behind the model used are out of the scope of this thesis and can be consulted in the paper realized by Rahaman et al. (2009).

The configuration of the reactor used in the study of Rahaman et al. (2009) is the same of the reactor designed by Fattah (2004) – lets' call this reactor the pilot-scale reactor. Beyond this pilot-scale reactor, another one, with the same diameters but distinct sections' heights, was also used in that the study. Rahaman et al. (2009) named this reactor as the lab-scale reactor. The dimensions of both reactors and their respective aspect ratios for each one of the constituent sections can be observed in Table 5.11. The lab-scale reactor has a total height of 153.5 cm and lower aspect ratios compared to the ones of the pilot scale reactor.

Table 5.11 - Dimensions and aspect ratios of the reactors studied by Rahaman et al. (2009).

	Pilot-scale			**Lab-scale**		
Reactor Section	Height, H_s (cm)	$Ø_s$ (cm)	Aspect ratio (H_s/ $Ø_s$)	Height, H_s (cm)	$Ø_s$ (cm)	Aspect ratio (H_s/ $Ø_s$)
A	74.9	7.6	9.86	41	7.6	5.4
B	154.9	10.2	15.19	41	10.2	4.02
C	127	15.2	8.36	41	15.2	2.7
D	45.7	38.1	1.2	30.5	38.1	0.8

As Rahaman et al. (2009) stated:

> Both the lab and pilot scale configuration of the UBC fluidized-bed crystallizer were used for the hydrodynamics investigations. (…) A simulated two-dimensional (2-D) geometry of the UBC crystallizer was created (…) and meshed with the grid sizes of 2 mm by 2 mm. In order to specify the initial conditions, the grid is divided into upper and lower zone. At time t=0, the lower part is filled with solids at an appropriate volume fractions, while the upper portion doesn't contain any solids initially. (…). Since the crystallization process is a multi-particle system, for both the lab and pilot scale configurations, simulations were performed for a mixture of different sizes of struvite crystals (2, 1.5, 1 and 0.5 mm; volume ratio, 1:1:1:1), with initial bed height of 0.254 m, with a packed bed solids volume fraction of 0.65. A solution velocity of 0.065 m/s was selected to fluidize the mixture of particles. The simulations were performed for 120 s, with a time step of 0.001 s. The results were then analysed for the solids volume fractions and the overall bed expansion behavior of struvite crystals (…). (Rahaman et al., 2009, p. 135)

The snapshots of volume fraction of solid phases in both the pilot and lab scale crystallizer at three different time intervals (30, 60 and 120 s) were then plotted and analysed (Rahaman et al., 2009). According to Rahaman et al. (2009) one of the main findings of these simulations was the relative distribution of the different phases – the struvite crystals and the wastewater - within the reactor. This information is very important, in the sense that it helps to fix the size of the crystallizer (Rahaman et al., 2009).

By comparing the hydrodynamics of both the lab and pilot scale reactors, Rahaman et al. (2009) provided further findings which were essential for the selection of the reactor to replicate. Rahaman et al. (2009) found that after running the simulation for 60 s, the particles of sizes of 2, and 1.5 mm were completely segregated according to their sizes and confined in the bottom portion of the pilot scale reactor. As for the other two size ranges - 1 and 0.5 mm – these particles appeared to be reasonably well mixed, sparsely dispersed above that bottom portion of the reactor. After running the simulation for 120 s, all four different particle sizes clearly segregated

according to their sizes along the pilot scale reactor. The largest particles were found to settle at the bottom of the reactor whereas the smallest ones floated on the top of crystals bed.

On the contrary, the lab scale reactor exhibited both the mixing and segregation within the crystals bed at 60 s. Even though the bigger particles (2 and 1.5 mm) segregated reasonably well in the bottom of the reactor, some small fractions of these size ranges were observed to be mixed with the remaining sizes of particles (1 and 0.5 mm) in the upper zone of the reactor (above the bottom). At the same time, particles of sizes of 1 and 0.5 mm were also found to be considerably mixed in the upper zones of the reactor. One implication of such particle size distribution is that, if this reactor is intended to be used as a simultaneous particle classifier through the harvest of crystals of different sizes from different zones of the reactor, the reactor is poorly designed for that purpose. On the other hand, another outcome that turns out to be advantageous is that the crystals are not only confined in the bottom zone, but they also make their way up to the higher zones of the reactor. This means that a major portion of the reactor is used for the fluidization system. According to Rahaman et al. (2009), a very important point is that, if this configuration provides significant reduction in the soluble phosphorus and the reactor is only being used for harvesting single size struvite crystals from the bottom of the reactor, this configuration may provide the optimal design for the case. Rahaman et al. (2009) further stated that:

> Another interesting point is that the total expanded bed height for this particular case is 0.85 m which is only 3.35 times of the initial static bed height. So, by lowering the aspect ratios, a considerable reduction in bed expansion can also be achieved. With the same amount of in-reactor struvite particles, the expanded bed height in the reactor, with lower aspect ratios, is found to be lowered by almost 50% from that of the higher aspect ratios' reactor. As the total height of the reactor depends on the expansion characteristics of the crystal bed and the overall cost of the reactor significantly depends on the height of the reactor, an accurate knowledge of bed expansion can provide not only optimal design information, but also can reduce the construction cost considerably by selecting an appropriate height of the reactor.

To conclude, the study carried out by Rahaman et al. (2009) was used as an essential support tool for the decision-making process of selecting a UBC reactor to replicate. The UBC reactor chosen to replicate is the lab-scale reactor indicate in Table 5.11. This lab-scale reactor is the same as the reactor designed by Fattah (2004), with shortened sections' heights. There are two major conveniences of selecting this reactor to replicate:

- The study carried out by Rahaman et al. (2009) allowed to shorten the total height of the reactor designed by Fattah (2004), with a few reported predictions of its implications on the formation of struvite within the reactor. Indeed, according to Rahaman et al. (2009) if the reactor is only being used for harvesting single size struvite crystals from the bottom of the reactor, this configuration may provide the optimal design since a major portion of the reactor is used for the fluidization system. The major drawback is the loss of the possibility of harvesting crystals of different sizes from different zones of the reactor. For the present dissertation, harvesting crystals of different sizes from different zones of the reactor is not a priority.

- The reactor designed by Fattah (2004) showed the second highest product of the maximum P-removal efficiency by the struvite recovery efficiency, specifically, 83.59. This value differs only in 1.03 from the product related to reactor A designed by Huang (2003), which showed the highest product amongst the reactors. Thus, the reactor to be replicated is based on a reactor which showed a relatively high ability in removing P from the wastewater. Furthermore, the optimal operational parameters used by Fattah (2004) can be consulted in his dissertation and used as a guideline for the future reactor operation.

Using the same influent flows of the ones used by Fattah (2004) for the lab-scale reactor will result in the same cross-sectional up flow velocities along the distinct sections of the reactor. For the same operational influent flow, the hydraulic retention time will, however, be shorter in the case of the lab-scale reactor, as a consequence of the volume reduction from one reactor to the other. Since the reactor designed by Fattah (2004) has a total volume of about 91.2 L and the lab-scale reactor has a total volume of about 47.4 L, this translates in a difference of almost 2 times between the hydraulic retention times of the reactors. Hydraulic retention times from 5 to 10 minutes were studied by Fattah (2004). For the same influent flows, these retention times will vary from 2.6 to 5.2 minutes, respectively, for the lab scale reactor. Since there is a minimum hydraulic retention time required for the complete reaction of the influent in the reactor, this reduction may come out as a concern.

Nevertheless, another study, carried out by Crutchik et. al (2017) was successful in removing P from centrate obtained from the sludge anaerobic digester in a municipal wastewater treatment plant, through a similar FBR, using hydraulic retention times between 1.3 and 2.6 minutes. As stated by Crutchik et. al (2017), a high amount of phosphate that entered the FBR was converted to struvite in less than 3 min. Thus, the shorter hydraulic retention times obtained for the lab-scale reactor may not constitute a problem.

At last, an additional aspect related to the configuration of the reactor intended to be replicated shall be considered. In his dissertation, Fattah (2004) mentioned that the reactor diameter changes were accomplished using standard PVC expansion couplings with rounded transitions. As this rounded transitions were only mentioned in the reactor designed by Fattah (2004), they were not mentioned earlier and were not illustrated in the previous drawings of the UBC reactors.

Further information regarding specifications about these rounded transitions was, however, not provided. To tackle this issue, the study carried out by Guadie et. al (2014) was significant. Guadie et. al (2014) studied the feasibility of struvite recovery from wastewater by constructing a novel fluidized bed reactor. The reactor layout was identical to the UBC studies, except for the following: the reactor had three distinct sections instead of four and the transitions between distinct sections were conical. Inserting cone-shape structures at an angle of 45◦ between the reactor constituent sections parts was aimed to reduce unwanted crystal loss at each junction (due to crystal breakage). A fluidized bed reactor without cones was used as a control. Results showed that inserting the cones offered a special advantage in reducing unwanted crystal loss up to 67.5% and that P removal efficiencies were more than 90% under the optimal operating conditions (Guadie et al., 2014). This said, the insertion of cone-shape structures at an angle of 45◦ between the reactor constituent sections of the reactor to replicate seemed valuable and were adopted. These and other specifications of the reactor will be represented in section 5.2.

5.2 Dimensions of the constituents of the crystallization system

5.2.1 The reactor

The reactor and the complementary constituents of the crystallization system were sized to attend to the maximum flows used by Fattah (2004). Figure 5.9 is a cross-sectional representation (to scale) of the replicated reactor and indicates its dimensions (in centimetres), including the length of the inserted cone-shape structures at an angle of 45◦ between the constituent sections

of the reactor. The chosen material of the reactor, including the conical transitions, was transparent PVC in order to ease the observation of the struvite formation within the reactor or eventual scaling problems in its internal surface.

By comparing the dimensions specified in Table 5.11 (lab-scale reactor) and the ones depicted in Figure 5.9, it is evident that they do not exactly match. In what concerns the diameters specified in Table 5.11, there was the need to slight adjust them so they would match the available commercial diameters. Also, the conical transitions between sections were inserted without increasing the total height of the reactor, i.e., the original height of the lab-scale reactor was divided into the height of the conical transition and the cylindrical section, for each one of the sections A to C.

Two orifices were placed at the upmost section of the reactor (section D). One orifice was placed 10.5 cm below the top of section D. This orifice allows to transport the centrate within the reactor to the external clarifier, to be further recirculated through a tubing. The other orifice was located 6.5 cm from the top to avoid the reactor unwanted overflow, in the case something clogs or impedes the water passage through the first orifice. In case this occurs, this upper located orifice is connected to a tube that will lead the overflow to the sewer drain or to the reactor. For simplification purposes, the first orifice, placed 10.5 cm below the top of section D, will be called the overflow outlet and the orifice located 6.5 cm from it will be called the back-up outlet.

As it can be seen from Figure 5.9, the reagents ($MgCl_2$ and NaOH), the centrate (influent) and the recirculated centrate are pumped into the reactor through an injection port, located at the bottom of the reactor. Details of the injection port will be described in 5.2.2. Check-valves were installed to prevent any reactor backflow into the respective pumps in the event of an accidental reactor stoppage.

Two gate valves, one located immediately above the injection port and other located immediately above the conical transition from section A to B were also installed within the reactor. These gate valves were not draw in Figure 5.9 for simplification purposes. These valves will allow to continue to operate the reactor without having to shut it down during the harvesting of crystals or during the cleaning of the injection port.

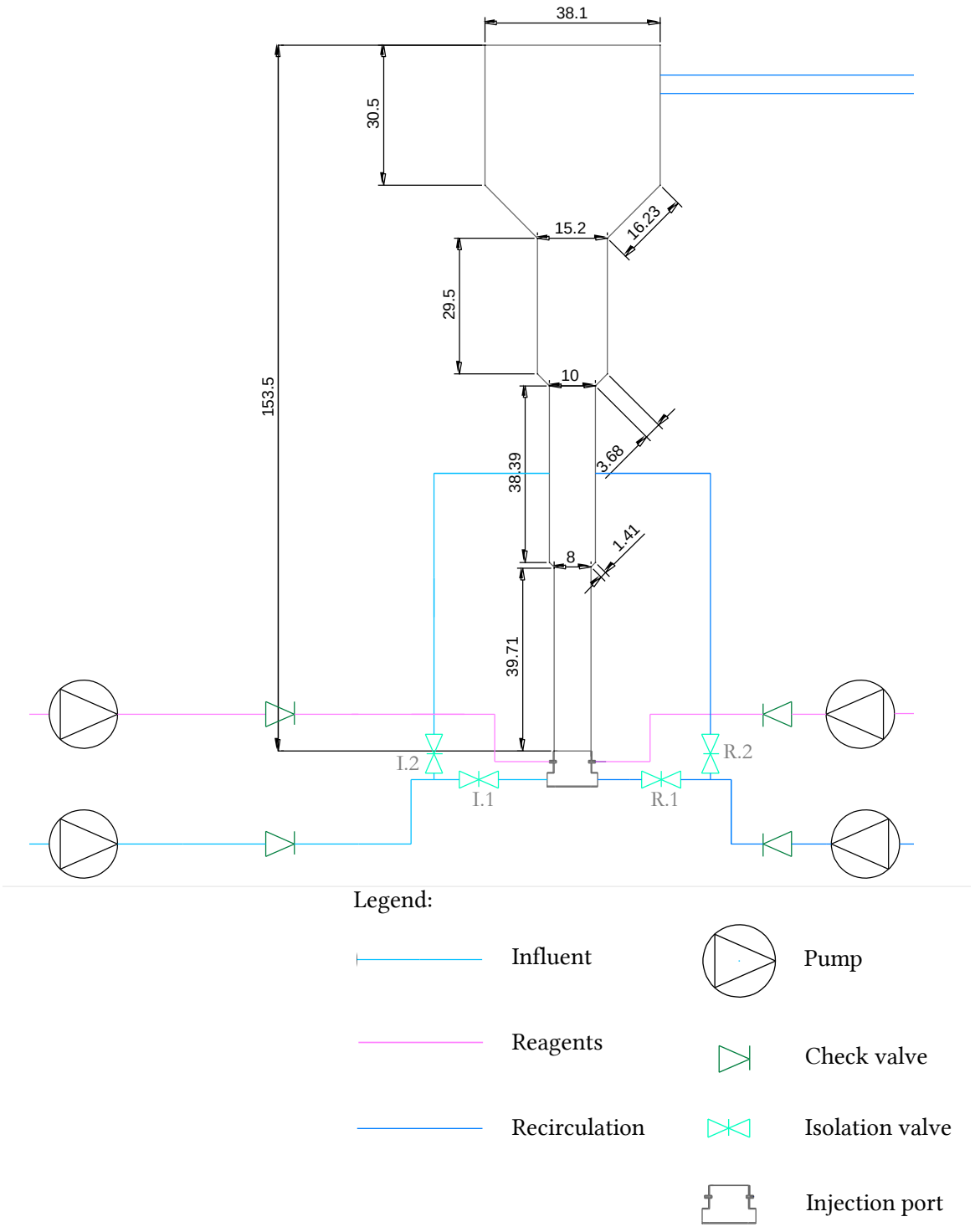

Figure 5.9 - Cross-sectional drawing (to scale) of the replicated reactor, in cm.

During the normal operation of the reactor, valves I.1 and R.1 should be open and I.2 and R.2 should be closed. The gate valves inside the reactor should be open. When one wants to harvest the crystals from the bottom of the reactor, the gate valve located immediately above the conical transition from section A to B should be closed. Simultaneously, the isolating valves identified as I.1 and R.1, which were previously open during the normal operation of the reactor should be closed, and valves I.2 and R.2 should be opened. Opening valves I.2 and R.2 will allow to continue to transport the centrate (both the influent and recirculation lines) into section B of

the reactor. Thus, section B should have two orifices for this purpose, which are in the middle of this section. As for the reagents feed, its pumps should also be stopped during the harvesting.

At last, every time harvesting is needed, the injection port needs to be detached from the reactor. The crystals can then be harvested as they will fall gravitationally.

As for cleaning the injection port, the gate valve located immediately above it should be closed during this procedure, simultaneously as valves I.1 and R.1 are also closed. Opening valves I.2 and R.2 will allow to continue to feed the reactor through section B.

Even though it was not draw in Figure 5.9, a pH meter was also installed near the transition from section A to B to aid in the control of the pH inside the reactor.

5.2.2 The injection port

The injection port, depicted in Figure 5.10 (cross-section, to scale) is intended to accomplish the best possible mixing of the feed - reagents, centrate and recirculated centrate - before it enters the reactor (Adnan, 2002). The injection port comprises four injection points, one for each distinct feed. Dimensions are depicted in centimetres.

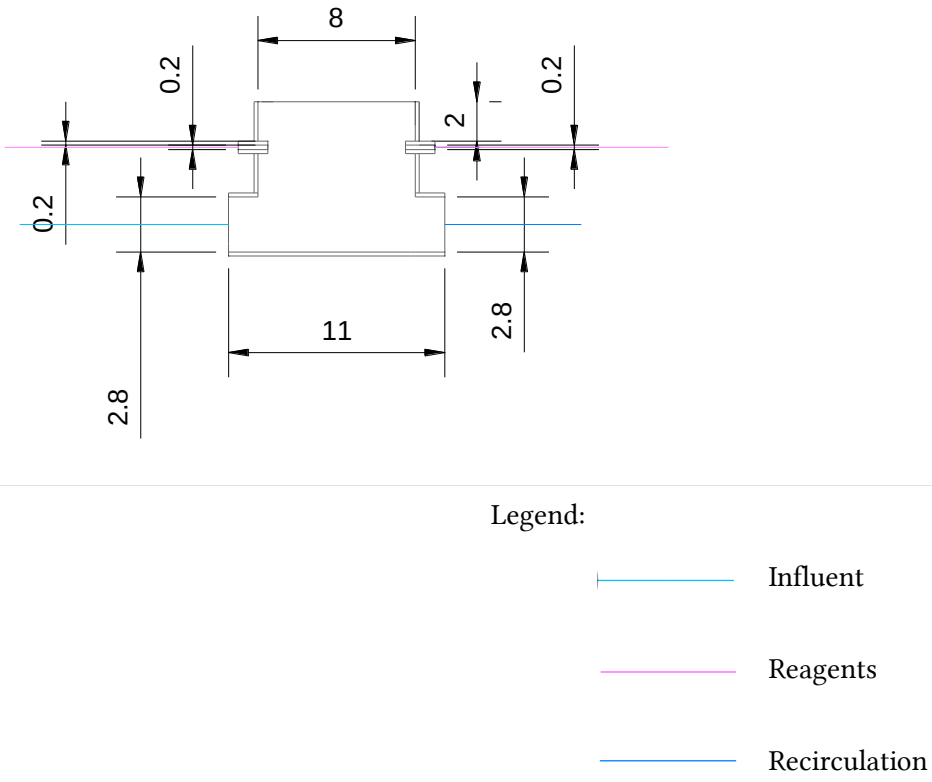

Figure 5.10 - Cross-sectional drawing (to scale) of the injection port of the reactor, in cm.

The magnesium chloride and sodium hydroxide injection points should be coincident so that a high local supersaturation ratio exists in this zone (Fattah, 2004). Due to these high local supersaturation ratios, encrustation due to struvite formation and accumulation of the chemical feed ports is expected during the reactor operation. To tackle this issue, the inflow points should be easily disconnected by means of quick release connectors to ease its later cleaning (Britton, 2002). The chosen material for the injection port was stainless steel, in order to prevent corrosion and to withstand regular scouring from cleaning (Britton, 2002).

The layout of the injection port presented in Figure 5.10 is identical to the injection ports used in all the UBC studies. There exist, however, differences in the dimensions of the injection ports amongst the studies. Since the study carried out by Fattah (2004) is to be used as a guideline for the reactor operation, it would make sense to use its injection port dimensions. Unfortunately, these dimensions were not provided in his dissertation. Information regarding the velocities of the distinct feeds through the respective cross-sectional areas of the port inlets were also not provided. To overcome this lack of information, the dimensions presented in Figure 5.10 were determined based on the information provided in the remaining UBC studies and on the distinct feed flows used by Fattah (2004).

The UBC studies presented in Table 5.9 were analysed in terms of the diameters of the cross-sectional areas of each distinct injection point. Once these diameters were identified, the cross-sectional areas of the injection points were calculated, for each study. The maximum feed velocities at each injection point were then determined based on these cross-sectional areas and on the maximum respective flows through the equation of continuity. From these maximum velocities, the highest velocity was chosen amongst the different studies for each injection point. Based on this velocity and on the respective feed flows used by Fattah (2004), the cross sectional areas were then determined, once more, by using the equation of continuity. Determining the cross-sectional area of the injection points as stated allows to assure that the highest velocity amongst the studies would be possible to arise in each distinct injection point. From the cross-sectional area, the diameters were at last calculated. Table 5.12 indicates, for each injection point, the maximum and minimum flows used by Fattah (2004), the maximum velocity recorded among the UBC studies, and the calculated cross sectional area and diameter. A verification of the resulting minimum velocities was also done.

Table 5.12 - Calculation of the diameters of the injection points of the reactor injection port.

Injection Point	Q_{max} (mL/min)	v_{max} (cm/min)	Cross-sectional area (cm^2)	Section diameter (cm)	Q_{min} (mL/min)	v_{min} (cm/min)
Recycle	21000	3394.5	6.2	2.81	11460	1852.4
Influent	2880	487.9	5.9	2.74	840	142.3
NaOH	75	1856.8	0.040	0.23	56	1386.4
$MgCl_2$	75	1856.8	0.040	0.23	56	1386.4

In the case of the NaOH injection point, as information regarding it was lacking in all studies, it was assumed that it would have the same dimensions of the injection point of the $MgCl_2$ injection point.

5.2.3 External clarifier

The external clarifier, which receives the reactor overflow, should serve two purposes (Britton, 2002; Fattah, 2004):

1. The recycling of fine crystals that may be washed out from the reactor back into it.
2. The settling of the suspended solids that may be present in the centrate. This way, any remaining fine-suspended solids will not return to the reactor.

Figure 5.11 is a cross-sectional (to-scale) drawing of the clarifier and its dimensions are in centimetres. All the clarifiers used in the UBC studies demonstrated good results in terms of

obtaining a relatively clear effluent and accumulated sludge in the bottom. Thus, the decision of designing a square pyramidal shaped clarifier was taken bearing in mind that this was a common characteristic to all the UBC clarifiers. The layout of the clarifier, including the inlets and outlets, also follows the layout of the clarifiers used in the UBC studies.

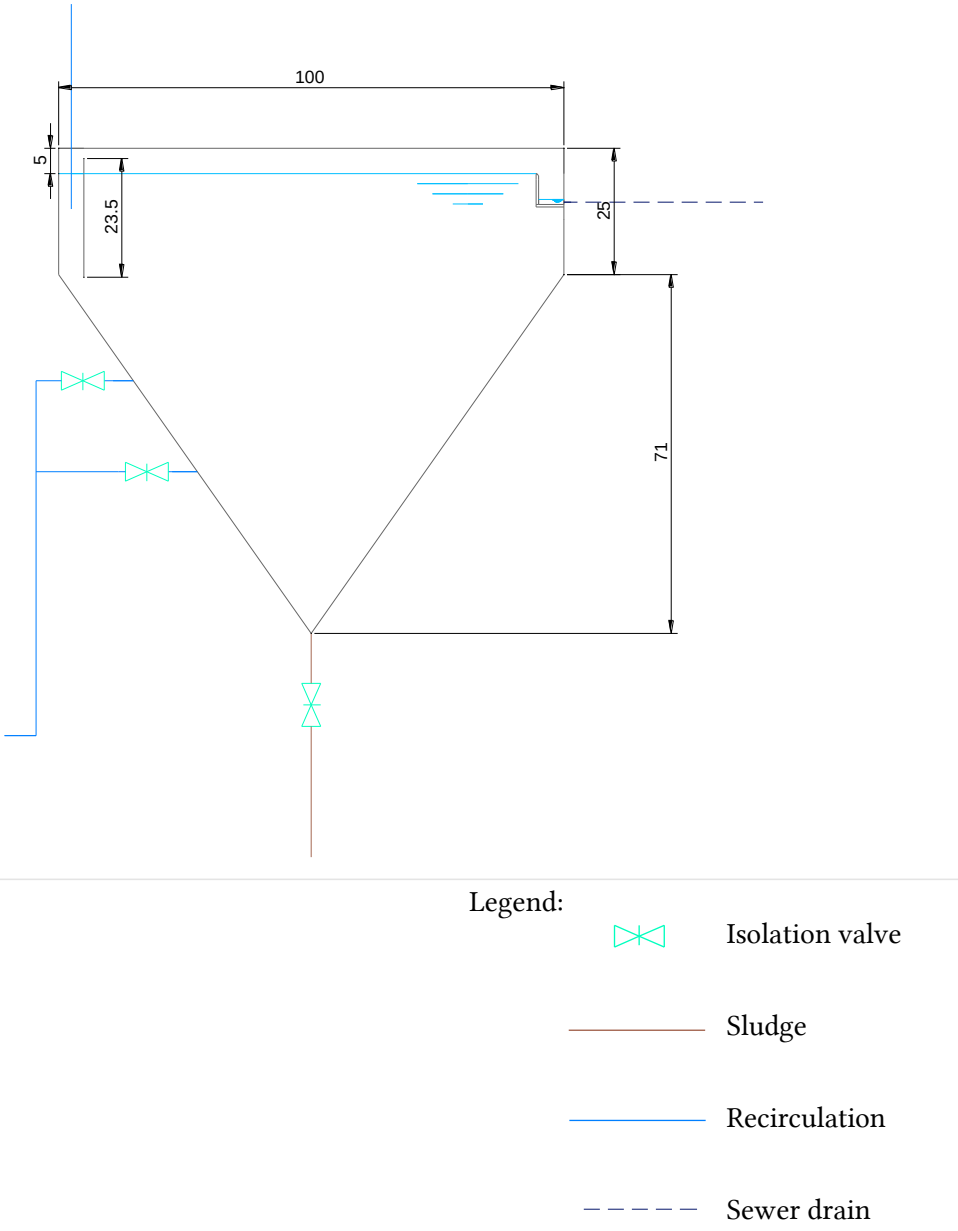

Figure 5.11 - Cross-sectional drawing (to scale) of the external clarifier, in cm.

The external clarifier should be fed from the top of the reactor (section D), gravitationally, through a tubing that serves that purpose. The tubing should be immersed in the clarifier, before the 23.5 cm width inlet baffle, as depicted in Figure 5.11. The baffle has two objectives: the dissipation of the incoming energy and the uniformization of the flow conditions. The water level in the clarifier should be 91 cm. A free board of 5 cm was considered.

The clarifier was provided with four outlets: one that allows the final effluent to flow to the sewer drain (back to the head of the WWTP), one that allows removing the accumulated sludge from the bottom of the clarifier, and, at last, two side outlets that will allow the clarified centrate to be pumped back (recirculated) into the reactor, trough the injection port.

The final effluent should be discharged to the sewer drain, firstly by passing through a weir and then to a launder in the external clarifier. The outlet that allows the final effluent to flow to the sewer drain should be placed in the final of the launder and connected to a tubing that will lead the effluent to the sewer drain at last.

As for the two side-outlets, they were positioned 32 cm and 50 cm from the bottom of the clarifier. The rationale behind placing two side-outlets, located at different heights, was to test which outlet performs better in recirculating the small crystals back into the reactor. Two isolation valves placed after these side-outlets will allow to alternate between them. Another isolation valve placed at the bottom of the reactor will allow to control the removal of the accumulated sludge.

In his dissertation, Fattah (2004) did not provide detailed information about the dimensions of the external clarifier. For example, information regarding the volumes occupied by the square prism and by the square pyramid were not indicated. Also, there was no agreement in terms of the surface loading rate (SLR) of the external clarifiers amongst the distinct UBC studies. The SLR ranged from 1.28 to 3.70 $m^3/m^2.h$ for the clarifier used by Fattah (2004), according to the flow, whereas, in the case of Huang (2003), the SLR ranged from 0.99 to 1.85 $m^3/m^2.h$, in the case of Britton (2002), the SLR ranged from 0.16 to 0.49 $m^3/m^2.h$, and, at last, for Adnan (2002), the SLR varied from 1.11 to 1.64 $m^3/m^2.h$. Thus, there was the need to size a new external clarifier. This would further allow to size a clarifier which would be tested in terms of its adaptability to the reactor intended to replicate.

As depicted in Figure 5.11, the volume of the clarifier is divided in a square prism with a height of 25 cm, and in an adjacent square pyramid, with a height of 71 cm. The square surface has a length of 100 cm. The reasons behind these dimensions will be explained throughout this section.

The external clarifier presented here was sized using a maximum SLR of around 1.5 $m^3/m^2.h$ as a sizing criterion. According to Latifian et al. (2014), struvite particles of different morphologies and with a diameter of 0.045 mm showed settling velocities between 3.96 and 5.04 $m^3/m^2.h$. These settling velocities were also later corroborated by Shaddel et al. (2019). It is, thus, expected that the external clarifier will be able to retain particles as small as the ones with 0.045 mm diameter, when the flow entering the clarifier is maximum, namely, 1.38 m^3/h (23 L/min). For particles with a higher diameter and consequently higher settling velocities associated (assuming the same particle density), a 100% retention in the reactor is also expected.

The surface area related to such SLR (1.5 $m^3/m^2.h$) is 0.95 m^2. For simplification purposes regarding the construction of the clarifier, it was determined that the total surface area of the clarifier would be a 1 m^2 square. The additional 0.5 m^2 comprise the inlet zone before the baffle, near the left border of the clarifier, as depicted in Figure 5.12, which represents the top view of the clarifier (to scale).

The total surface area of the clarifier can be divided in three distinct sections from left to right: (i) the area between the clarifier left border and the inlet baffle, comprising an area of 0.5 m^2; (ii) the area between the baffle and the weir; and (iii) the area between the weir and the right border of the clarifier, where the launder is located. Sections (ii) and (iii) totalize an area of 0.95 m^2, to which the SLR (1.5 $m^3/m^2.h$) relates.

The inlet baffle has 100 cm of length and is located 5 cm from the left border of the clarifier. In the middle of the area between the clarifier left border and the inlet baffle, a 4.5 cm diameter tubing is also depicted. This tubing arises from the overflow outlet of the reactor and should be immersed in the clarifier as aforementioned. The rationale behind the diameter of the tubing will be explained in subsection 5.2.4.

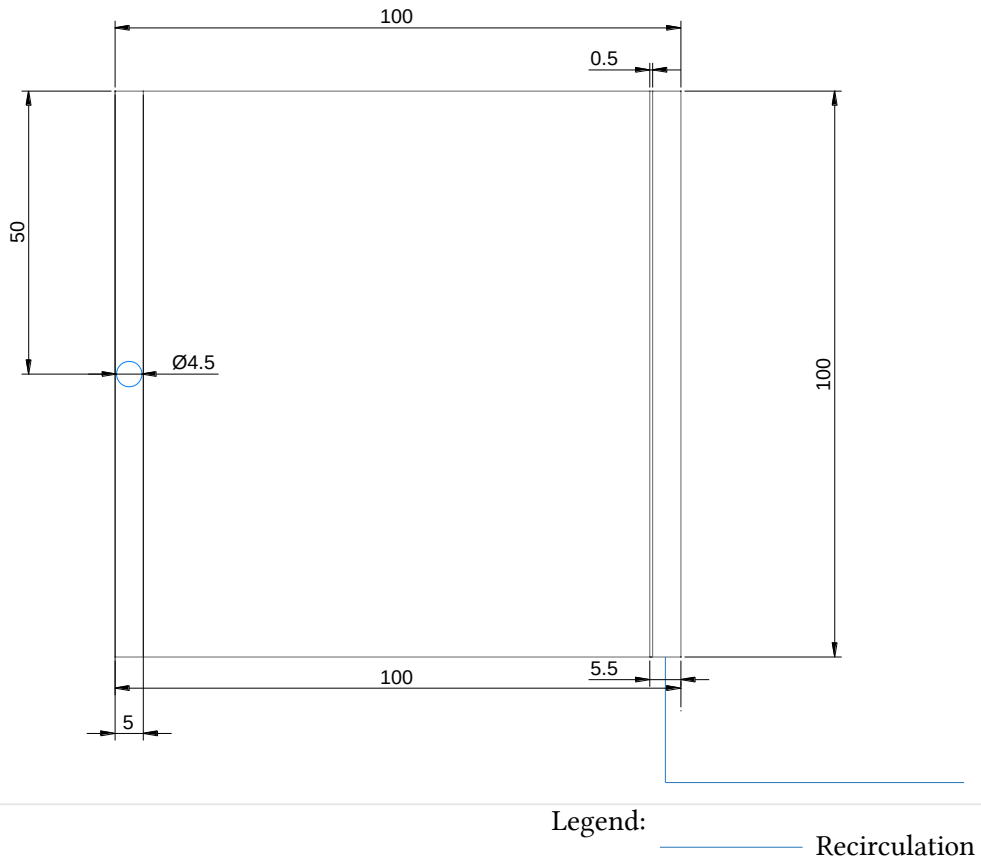

Figure 5.12 - Top-view drawing (to scale) of the external clarifier, in cm.

The effluent weir was placed 5.5 cm from the right border of the clarifier and has a total width of 0.5 cm. Both the weir and launder extend through the clarifier length and are, thus, also 1 m length. An orifice was placed in the bottom right corner, so that a tubing connects to it in order to transport the effluent to the sewer drain.

Figure 5.13 is a cross-sectional drawing (to scale) of the left corner of the reactor which allows to look at further details of the weir and launder. The surface of the weir was divided in a 0.2 cm width rectangular surface which is adjacent to a leaning one, of 0.4 cm width. The slope between these two surfaces is 45º. The base of both the weir and launder was placed 11.6 cm below the top of the clarifier and the weir has a total height of 6.5 cm (considering the thickness of its base of 0.5 cm). The thickness of the launder was assumed to be also 0.5 cm.

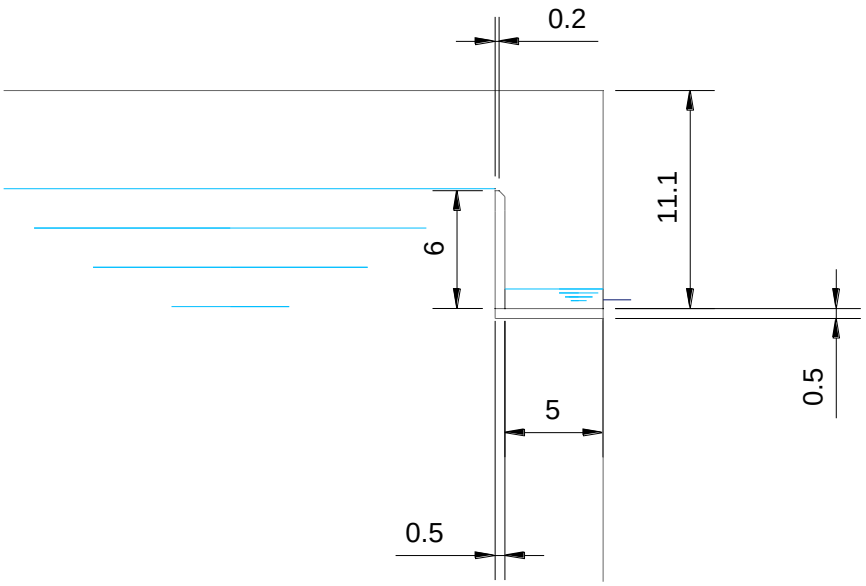

Figure 5.13 - Cross sectional drawing (to scale) of the weir and launder of the external clarifier, in cm.

The weir head, h, was calculated according to Bazin's formula for a rectangular weir, which is indicated in equation (5.4).

$$Q=\frac{2}{3}\times\mu\times l\times\sqrt{2g}\times h^{\frac{3}{2}} \quad (5.4)$$

Q is the flow discharged over the weir, μ is the coefficient of discharge, l is the length of the weir and g is the gravitational acceleration. For the maximum effluent flow used by Fattah (2004) - 2.94 L/min - the resulting water level above the weir is 0.1 cm. The respective calculation is presented in Table 5.13.

Table 5.13 - Calculation of the weir head of the external clarifier.

Q_{max} (L/min)	Q_{max} (m^3/s)	μ	l (m)	Gravitational acceleration (m/s^2)	h (cm)
2.94	0.000049	0.55	1	9.8	0.1

The critical depth of the launder, h_c, was calculated according to equation (5.5).

$$h_c=\left(\frac{Q^2}{g\times L^2}\right)^{1/3} \quad (5.5)$$

G is again the gravitational acceleration, Q the flow and L is the width of the launder. For the maximum effluent flow used by Fattah (2004) - 2.94 L/min - the critical depth is 0.46 cm. The respective calculation is represented in Table 5.14.

Table 5.14 - Calculation of critical depth of the launder of the external clarifier.

Gravitational acceleration (m/s^2)	Q_{max} (m^3/s)	Launder width (cm)	h_c (cm)	$h_c \times 1.73$ (cm)	$h_c \times 1.73 \times 1.2$ (cm)
9.8	0.000049	5	0.46	0.80	0.96

Finally, in what concerns the volume of the clarifier, once the surface area of the clarifier was calculated, it was determined that the height of the square prism would be 0.2 m, resulting in the volume of 0.238 m^3 for this section of the clarifier. The height of the square prism was determined excluding the height of the free board. The height of the square pyramid was then calculated attending to the fact that the slope between the triangular face of pyramid and the square base had to be 55º, through Pythagorean theorem. The calculated pyramid height was 0.71 m, resulting in a volume of 0.239 m^3 for the pyramidal section of the clarifier. The volume of the square prism and the square pyramid comprehend together a total volume of 0.438 m^3 (excluding the volume occupied by the free board). For the maximum and minimum flows utilised by Fattah, 23 L/min and 9.6 L/min, these translates into a hydraulic retention time (hrt) of around 19 and 46 min, respectively.

5.2.4 Tubes

The several tubes needed to complement the crystallization system are presented in Table 5.15. For each tube, Table 5.15. indicates the connecting points in the system by specifying the origin and the destination of the tube, according to the flow direction.

Since the diameters of the tubes used by Fattah (2004) were not provided in his dissertation, neither the associated cross-sectional flow velocities, there was the need to size the tubes resorting to the information available in the remaining UBC studies and the maximum flows used by Fattah (2004). To this end, the remaining UBC studies were once more reconsidered and surveyed in terms of the maximum flow and diameter of each tube. Gathering these data – the maximum flow and tube diameter - had the intent of subsequently using the continuity equation to calculate the respective maximum cross-sectional flow velocity. Once these maximum cross-sectional flow velocities were calculated for each tube, it was possible to size the tubing diameter by using the maximum flows observed in the study carried out by Fattah (2004), and by taking advantage, once more, of the continuity equation.

Information regarding both the flow and the diameter of the tubing found on the UBC studies was provided by Britton (2002) and by Huang (2003). Namely, Britton (2002) specified the diameter of the tubing connecting the two reactor's outlets and the external clarifier, as well as the respective flows, whereas the same information regarding the remaining tubes was provided by Huang (2003). Based on each tube diameter and its respective maximum observed flow, the corresponding cross-sectional area was firstly calculated and the maximum cross-sectional velocity, v_{max}, was then determined. The calculated maximum cross-sectional velocities are indicated in Table 5.15. Based on these velocities and on the maximum flows used in the study carried out by Fattah (2004), Q_{max}, also represented in Table 5.15, the cross-sectional area of each tube was determined. It was then possible to determine the inside diameter of the tubing, Ø, indicated in Table 5.15. At last, the minimum flow velocity in the tube, v_{min}, was verified based on the minimum flow rate operated by Fattah (2004).

Table 5.15 - Calculation of the tubing diameters of the crystallization system.

Origin	Destination	v_{max} (cm/min)	Q_{max} (cm/min)	Cross-sectional area of the tube (cm^2)	Ø (cm)	Q_{min} (L/min)	v_{min} (cm/min)
Overflow outlet of the reactor	External clarifier	1800	23.1	12.8	4.0	13.5	1051.9
Back-up outlet of the reactor							
External clarifier	Injection port -recirculation port	4790	21	4.4	2.4	8.4	1916.2
	Sewer drain - final effluent	5142	2.94	0.6	0.9	0.0	17.5
	Sludge container – accumulated sludge	-	-	0.6	0.9	-	-
$MgCl_2$ and NaOH storage tanks	Injection port (inlet port of each reagent)	9437	0.075	0.01	0.1	0.056	7047
Centrate storage tank	Injection port	2169.8	2.88	1.3	1.3	0.8	632.9

In the case of the tubing connecting the sludge outlet of the external clarifier to the sludge container there was no information at all that would allow to size the tubing. The corresponding diameter presented in Table 5.15 was assumed to be the same as the tubing transporting the final effluent which connects the external clarifier to the sewer drain. Also, in what concerns the tubing connecting the $MgCl_2$ and NaOH storage tanks to the injection port respective inlets, due to lack of information regarding the NaOH flow, it was assumed that the tubing would be identical to the one sized for the $MgCl_2$ reagent.

On the other hand, the diameter of the tube connecting the centrate storage tank to the injection port was specified by Fattah (2004). The respective cross-sectional flow velocities were then calculated.

At last, it should be also noted that the tubing connecting the external clarifier to the recirculation inlet of the injection port has an inside diameter of 2.4 cm. Since this diameter differs in around 4 cm to the diameter of the respective injection point of the injection port (sized in subsection 5.2.2), a proper tube adapter should be included.

5.2.5 Pumps

The crystallization system requires four pumps that suit the purpose of introducing the $MgCl_2$, the NaOH, the influent centrate, and the recirculated centrate into the respective inlets of the injection port of the reactor. Table 5.16 indicates the origin and the destination of the flow that each pump should drive, as well as the type of pump, according to Fattah (2004). The minimum and maximum flows operated and provided by Fattah (2004) are also presented here as a guideline and the pumps should be able to achieve these flows.

Table 5.16 - Pumps needed for the crystallization system.

Origin	Destination	Pump type	Q_{min} (mL/min)	Q_{max} (mL/min)
Centrate storage tank	Injection Port	Progressive cavity pump with digital speed controller	840	2880
NaOH storage tank	Injection Port	Dosing pump	-	-
$MgCl_2$ storage tank	Injection Port	Dosing pump	56	75
External clarifier - recirculation	Injection Port	Progressive cavity pump and a digital speed controlling panel	11460	21000

The pumps operation is controlled by a programmable logic controller connected to the them.

5.2.6 Storage Tanks

Before being pumped into the injection port, the $MgCl_2$, the NaOH and the influent centrate must be stored in its respective storage tanks. These storage tanks were not dimensioned here because, by the time the present dissertation was done, some logistical aspects concerning the storage tanks were not clear. This led to the postponement of this sizing.

5.3 Summary

In this chapter, to size a reactor, the studies carried out by the UBC research P-recovery group were firstly reviewed. Each one of these studies is in the form of a dissertation and comprehends the design and operation of a pilot-scale reactor to remove P from wastewater in the form of struvite. The reactors investigated in these studies followed the same layout and schematic process.

Indeed, the UBC studies were chosen as the basis to design a reactor because they are in the form of dissertations which provide systematic and detailed information regarding the early phases of the Ostara technology. Such a large amount of information was not found about any other P-recover technology in the literature. Furthermore, Ostara is the leading company in recovering P, being a spin-off company of the UBC P-Recovery Project, which accomplished consistently good results in recovering P from wastewater.

As there was no information regarding how the UBC reactors were sized – no explanation or mention of the sizing criteria – proportions and patterns amongst the diameters and heights of the reactor's constituent sections were sought. If these patterns existed, they could then be applied in the construction of a new reactor. Determining the sizing criteria was considered non-viable since various aspects studied in the dissertations varied considerably amongst them, e.g., composition of the influent used and operating flows into the reactor. Furthermore, the physical and chemical nature of the formation requirements of the struvite pellets added extra complexity.

The reactors had similar dimensions amongst them. Indeed, it seemed that the heights of the reactors' sections were slightly altered amongst the different UBC studies so that different heights were tested, by maintaining the same sections' diameters for all reactors. Unfortunately, no patterns or proportions, that could be reproduced in the design of a new reactor, were consistently identified in the literature. This led to the need of replicating an already existing UBC reactor.

At first, it seemed obvious that the UBC reactor which should be replicated would be the one that demonstrated the best ability in removing P from wastewater. However, this reactor, as well as all the UBC reactors, were more than 4 m height. The building of a new reactor, with such total height, faced both economical and logistical constraints. To tackle this issue, a study carried out by Rahaman et al. (2009) was of major importance. This study was used as a support tool for the decision-making process of selecting a reactor to replicate.

The reactor chosen to replicate was one of the reactors studied by Rahaman et al. (2009), which had the same dimensions as the reactor designed by Fattah (2004), with shortened sections' heights. It is important to notice that the reactor designed by Fattah (2004) showed the second highest product of the maximum P-removal efficiency by the struvite recovery efficiency.

For the sake of reader's convenience, Table 5.17 summarizes again the dimensions of the constructed reactor. According to Rahaman et al. (2009), if this reactor configuration provides significant reduction in the soluble phosphorus and the reactor is only being used for harvesting single size struvite crystals from the bottom of the reactor, this configuration may provide the optimal design. Indeed, at this point, it was intended to harvest only single size crystals from the bottom of the reactor.

Table 5.17 - Dimensions of the constructed reactor, in cm.

Reactor Section, s	Height, H_s (cm)	$Ø_s$ (cm)
A	39.71	8
B	38. 39	10
C	29.5	15.2
D	30.5	38.1

The diameters indicated by Rahaman et al. (2009) had to be slightly altered so that available commercial diameters could be used. The height of each section was also modified in order to include conical transitions between the sections. This was done to avoid the breaking of crystals between the sections. These modifications are already included in the dimensions presented in Table 5.17.

The complementary constituents of the crystallization system - the injection port, external clarifier, tubing and pumps - were then sized and specified. This was done based on the UBC studies to guarantee that the crystallization system would be able to attend the maximum flows used in these studies.

CHAPTER 6

STRUVITE'S SOLUBILITY CURVE DETERMINATION

Plotting the equilibrium conditional solubility product, $P_{s_{eq}}$, vs. pH establishes a struvite solubility limit curve, for a certain temperature and solution composition (Bhuiyan et al., 2007). Such curve is of great use since it can be harnessed to predict struvite crystallization. It can be easily used to determine the struvite saturation condition of a wastewater by comparing the P_s value for that wastewater with the solubility limit value (Huang, 2003). If the P_s value is above the limit curve, then struvite might precipitate from this wastewater. Furthermore, it is simple to develop a $P_{s_{eq}}$ curve, for a given sample matrix, that should be used in the operation of a struvite crystallizing reactor.

Controlling the phosphorus removal efficiency is usually exerted either by setting the pH in the reactors or by setting the inlet SSR. Thus, since the SSR is the ratio between P_s and $P_{s_{eq}}$, determining $P_{s_{eq}}$ for a pH range is crucial for the reactor operation. The struvite solubility curve should be determined for different wastewaters due to the effect of their varying characteristics. Also, the process of P-recovery through struvite crystallization is very site-specific and it is, therefore, recommended that a conditional solubility curve is determined when the conditions change (Adnan, 2002).

The present chapter made use of an already existing methodology to obtain a struvite solubility limit curve, for a centrate sample, taken from the centrifuge of Chelas WWTP. At the time the curve was determined, the construction of the reactor sized here, as described in section 5.2, was in progress. By the time the construction is finished, the centrate will probably have other characteristics and a new curve should be obtained. Accordingly, the purpose of having determined the curve for Chelas' centrate was not to profit from its applicability to operate the reactor right away. The aim of having followed, as far as possible, an existing methodology was to test it with Chelas centrate. Another goal was to try to complete this methodology, since a few omissions were contained in it.

Section 6.1 describes the treatment line of Chelas WWTP, whereas section 6.2 details the centrate's characteristics. The methodology applied in the laboratory room of Chelas WWTP is described in section 6.3. The obtained solubility curve is, at last, presented and discussed in section 6.4. The major conclusions of Chapter 6 are presented in section 6.5.

6.1 Chelas WWTP

Chelas WWTP is a tertiary wastewater treatment plant operated by Águas do Tejo Atlântico. The plant serves a few parishes of Lisbon and it was sized to serve 210.698 residents, corresponding to an average daily flow of 52,500 m^3/day. The origin of the influent is mainly domestic. Figure 6.1 depicts the flow diagram of Chelas WWTP, namely the liquid and solid line.

The liquid line comprehends the pre-treatment and the primary, secondary and tertiary treatments. The wastewater reaches the reception basin of the plant both gravitationally and through pumping stations. After that, the wastewater is screened, firstly through a bar screen, and then through a screw screener. The influent then undergoes through the grit and grease removal unit operation. After this pre-treatment, the influent is clarified in the primary sedimentation tank. The secondary treatment then follows, namely, in the form of a traditional activated sludge process with nitrogen removal. Thus, the activated sludge tanks are constituted by sequential anoxic and aerobic compartments. This alternation of anoxic and aerobic conditions promotes nitrogen removal due to nitrification and denitrification processes. As for P, its targeted removal is not concerned in Chelas WWTP. The mixed liquor is then elevated to the second clarifiers. At last, the tertiary treatment follows. Before being discharged into the Tejo river, the effluent is subjected to sand filtration.

Even though the liquid line does not comprise targeted P-removal, struvite scaling has been observed in the plant, in the centrifuges involved in the solid phase (the solid phase will be explained below). This is in line with section 3.4, where it was mentioned that the phenomenon of struvite scaling also occurs in conventional WWTP. The removal of P, namely particulate P, is thus associated to solid-liquid separation processes. On the other hand, struvite appearance may be attributed to the accumulation of soluble P in the plant. This accumulation may relate to the dehydration sidestreams which may return soluble phosphorus to the headwork of the plant.

In what concerns the solid line, it involves, firstly, the thickening of the primary sludge and the flotation of biological sludge. Once the primary and secondary sludges are thickened and concentrated, they are mixed in a tank for that purpose. The mixed sludge then undergoes anaerobic digestion. The produced biogas is collected and stored in spherical gasometers to be further used in two co-generation motors. After undergoing anaerobic digestion, the sludge is dewatered in centrifuges and chemically stabilized with lime afterwards.

Some of the originated sidestreams are returned to the primary clarifiers. These sidestreams include the ones originated in sludge flotation, thickening and dehydration. The sidestream related to filtration is returned to the plant headworks.

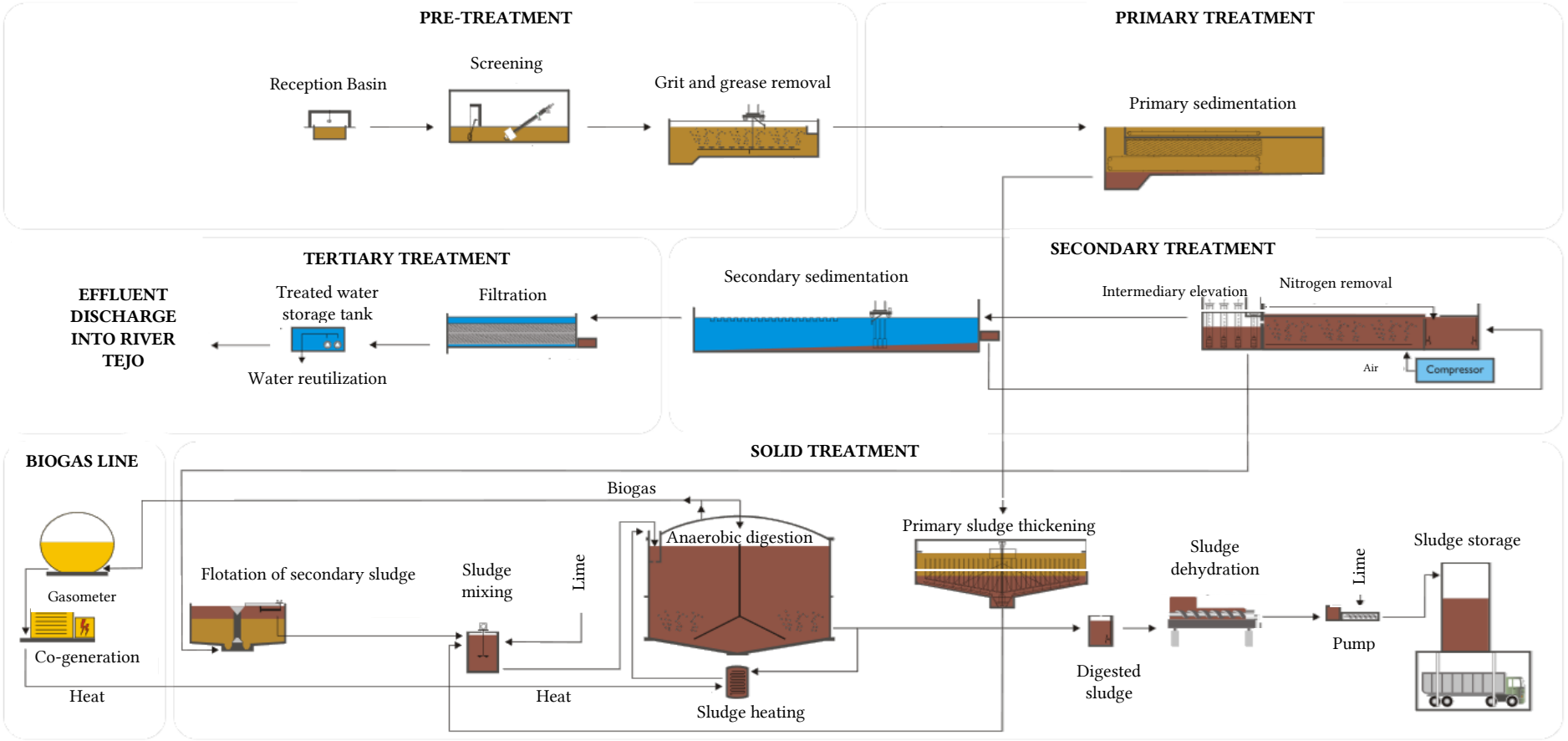

Figure 6.1 - Flow diagram of Chelas WWTP (adapted from SIMTEJO, n.d.)

6.2 Centrate

Available data concerning the characteristic of the centrifuge sidestream – the centrate - is concerned in this section. Figure 6.2 illustrates the phosphate concentration present in the centrate from the 10th of July to the 26th of July of 2018. Unfortunately, samples were not taken daily, as there is data available only for a few days of that period. On these days, samples were taken 3 times per day, namely at 10:00 h, 12:00 h and 15:00 h. An average of 577 mg/L of phosphate was observed for this period.

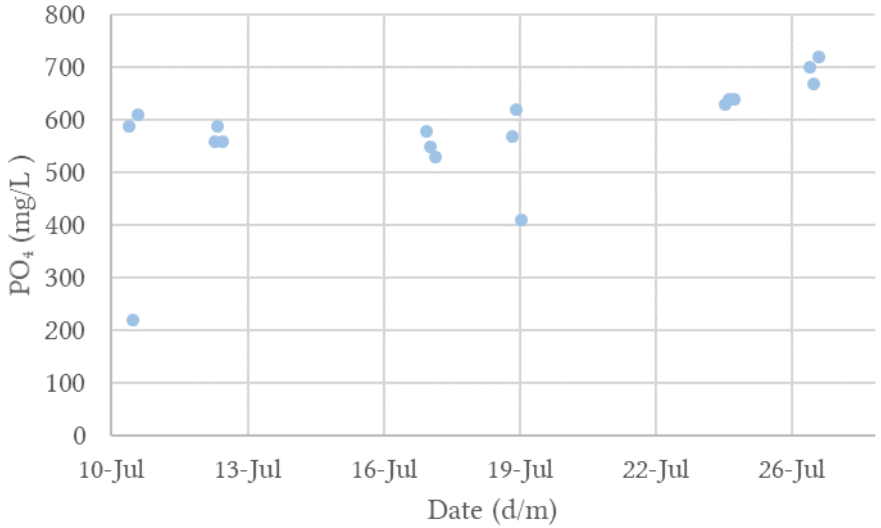

Figure 6.2 - Variation of the centrate phosphate concentration from 10th of July to the 26th of July of 2018.

Figure 6.3 depicts the centrate's pH, observed from the 9th of January 2018 until the 4th of February 2020. Samples were also not taken daily. For this period, the average pH was 7.3 and the pH varied from 5.8 to 8.

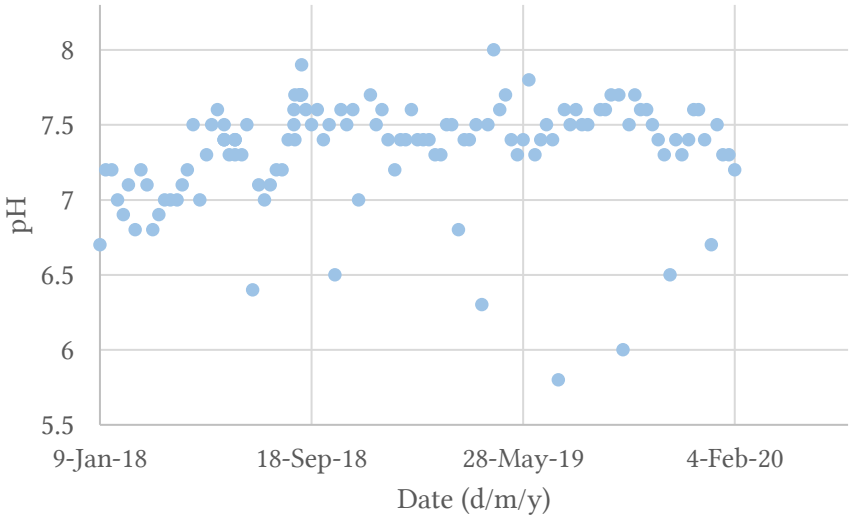

Figure 6.3 - Variation of the centrate's pH from the 9th of January 2018 until the 4th of February 2020.

The variation of the ammonium present in the centrate is not represented here because the data available regarding this parameter relates solely to the 18th of June of 2019. The ammonium concentration on this day was 1100 mg/L. More recently, two more centrate's samples where analysed in terms of the phosphates, ammonium, the dissolved fraction of calcium and magnesium, and pH – see Table 6.1.

Table 6.1 - Centrate's characteristics on the 19th and 26th February 2020– concentrations of phosphates, ammonium, dissolved fraction of calcium and magnesium, and pH.

Date	PO_4 (mg/L)	NH_4 (mg/L)	Dissolved Ca (mg/L)	Dissolved Mg (mg/L)	pH (Sörensen scale)
19 February 2020	230	940	40	11	7.3
26 February 2020	200	930	42	17	7.5

Unfortunately it was not possible to characterize the centrate in terms of the concentration of the struvites' constituents (i.e., the dissolved fractions of Mg^{2+}, NH_4^+, PO_4^{3-}), for a certain period of time, as this information was not available. Nonetheless, spontaneous struvite formation has been observed. In fact, struvite scaling is removed from the centrifuges periodically.

The reported occurrence of struvite formation in the centrifugues is in line with the dissolved fractions of Mg^{2+}, NH_4^+ and PO_4^{3-} present in a centrate's sample, which was later analysed for the purpose of the present thesis. Table 6.2 depicts the results of the analysis of this centrate sample, which was taken on the 14th of July 2020.

Table 6.2 - Centrate's characteristics on the 14th July 2020– concentrations of the dissolved fraction of phosphates, ammonium, magnesium, and pH.

Date	Dissolved PO_4 (mg/L)	Dissolved NH_4 (mg/L)	Dissolved Mg (mg/L)	pH (Sörensen scale)
14th of July 2020	620	1100	5.5	7.55

The concentration of soluble PO_4 present in the centrate – 620 mg/L - is relatively high, compared to the one present in the various nfluents tested in the various UBC studies indicated in Table 5.4. The maximum PO_4 concentration present in an influent tested on an UBC reactor was of 255 mg/L (recall Table 5.2). As a matter of fact, even though it does not remove P biologically, Chelas WWTP was the chosen WWTP to test the reactor sized in this thesis due to the high concentration of soluble P present in its centrate.

6.3 Methods and materials

The methodology presented here is based on the one presented in the various UBC dissertations indicated in Table 5.4. These UBC dissertations share the same approach to determine the struvite's solubility curve related to a sidestream rich in P.

The theoretical foundations of using the equilibrium conditional solubility product, $P_{s_{eq}}$, to draw a solubility curve, related to a solution enriched in P, have been explained in subsection 2.2.6.

The drawing of this curve requires to experimentally determine the equilibrium total concentrations of the struvite's ions constituents (dissolved fraction), for a range of pH values.

Based on the curves obtained in the UBC dissertations, it was assumed that ten different pH values, resulting afterwards in ten distinct points (pH, -log P_s), would be sufficient to determine the curve. Table 6.3 indicates the desired distinct pH values. The rationale behind choosing these pH values was to obtain a pH range that would comprise the observed pH range of the centrate, illustrated in Figure 6.3. Since the observed centrate's pH was inferior to 6.5 only four times, these pH values were considered outliers and the minimum desired pH was chosen to be 6.5. It was determined that the pH values should be equidistant between them. A maximum pH of 9.2 was chosen so that the curve could also be determined over the potential expected operating range of the struvite crystallization equipment.

Table 6.3 - Desired ten pH values to obtain the struvite's solubility curve of the centrate.

pH (Sörensen scale)									
6.5	6.8	7.1	7.4	7.7	8.0	8.3	8.6	8.9	9.2

In order to obtain the equilibrium total concentrations for the desired pH values, a sample of 11 L of centrate was taken initially from the centrifuge of Chelas WWTP. Five glass beakers of 1 L were then filled with the centrate's sample. The rationale behind delivering centrate in five distinct beakers, of 1 L each, was to later adjust the pH of the centrate contained in each one of them. Each beaker would then have a distinct pH value, equal to one of the desired pH values of Table 6.3. The reason for fulfilling each one of the five beakers with the centrate, rather than ten (the number of desired points for the curve), will be explained later in this section.

A 250 mL plastic beaker was also filled with the centrate sample to serve as a control. This 250 mL plastic beaker will be henceforth called the control sample. This plastic beaker was then stored in a fridge, at 7ºC. The remaining volume of the centrate's sample was also stored in a fridge at 7ºC, so that its characteristics would be better preserved than at room temperature, until it would be used again.

Before proceeding to the adjustment of the pH solution in each beaker, there was the need to ensure that some solid-phase struvite would remain at equilibrium. For that purpose, around 10 g of struvite were introduced in each beaker.

The introduced struvite was originally removed from the centrifuge of Chelas WWTP in one of the periodically cleansings of the centrifuge. For logistical reasons, it was impossible to coincide the day of the struvite removal with the day it was introduced in the beakers. In order to obtain better preserving conditions, the removed struvite was stored in a cold room for 23 days, since the day the cleansing took place until the day the struvite was introduced in the beakers.

The removed struvite was in the form of large blocks that had to be broken down into smaller ones. The blocks were broken down by hand (wearing gloves), and afterwards measured in a scale. After obtaining the small blocks of 10 g, a lot of larger struvite blocks remained. This excess of struvite was stored in the fridge at 7ºC, until it was used again.

Figure 6.4 illustrates the small struvite blocks (each one weighting around 10 g) in front of the respective beaker (before the beakers were filled with centrate), in the laboratory of Chelas WWTP. After each glass beaker was filled with centrate, a 10 g struvite block was delivered into it.

Figure 6.4 - Small blocks of struvite (removed from the centrifuge) placed in front of the respective beaker, each block weighting around 10g (run 1).

The pH adjustment then followed. The pH of the centrate was primarily measured with a portable digital pH meter. The measured pH of the centrate sample was of 7.55. A few drops of NaOH and HCl solutions were then added to each one of the five beakers, depending whether the desired pH value was higher or lower than 7.55, respectively.

Unfortunately, the previous methodologies consulted in the literature did not specify the concentrations of these reagents (HCl and NaOH). This led to the need of firstly determining the most convenient concentrations that should be used to adjust the pH of the centrate of Chelas WWTP. With this in view, a former centrate's sample was taken from the centrifuge a few weeks before determining the struvite's solubility curve. Several reagents' concentrations were then tested at a time, by adding a few drops of the reagent with a dropper (Pasteur pipette) into 1 L of this earlier centrate sample. Each time a drop was added, the solutions' pH was afterwards measured with a digital pH meter. The concentration that better suited the intended pH adjustment was of 1N, both for the case of the NaOH and HCl. This concentration enabled to precisely change the pH of the solution, in the order of magnitude of 0.1 pH, by adding a few reagents drops. Other concentrations (0.1 N and 10N), either took too many reagents drops to change the pH or would change it in a higher order of magnitude compared to the desired.

Table 6.4 indicates the pH values desired - each distinct pH relates to one of the five beakers. Adding drops of NaOH or HCl into the beaker, with a dropper, at a concentration of 1N, allowed to adjust the pH.

Table 6.4 - pH values desired to obtain the struvite's solubility curve of the centrate - run 1.

pH (Sörensen scale)				
7.1	7.4	8.0	8.6	8.9

While the reagent drops were being introduced in the beaker, one by one, the pH was being continuously measured, by immersing a portable digital pH meter in the solution. This enabled to control the addition of reagent drops according to the desired pH value. Also, to enhance the homogeneity of the centrate during the addition of reagents, the beakers were being continuously mixed throughout this pH adjustment process. To assure the continuous mixing, a jar test apparatus was used. This jar test apparatus is the one also depicted in Figure 6.4. The paddle stirrers of the apparatus were immersed in each one of the five beakers and were set to operate at 70 RPM. Caution had to be taken with the handling of the pH meter so it wouldn't hit the paddle stirrer.

Immediately after the pH adjustment was concluded, the jar test apparatus was not stopped, and it was left to operate for the consecutive 24 h, at 70 RPM. According to the previous methodologies provided in the UBC studies, under continuously mixing conditions and after 24 h, it was expected that the equilibrium would be attained in each one of the five beakers.

The solution in each glass beaker, at equilibrium, was then analysed for pH, again with a portable pH meter. The measured equilibrium pH values were registered and written on the respective glass beakers. A volume of 250 mL of centrate was then transferred from each glass beaker, to a respective plastic sample beaker, labelled with the corresponding measured pH value at equilibrium.

After this step, the plastic sample beakers were immediately transported to an external laboratory - EDP Labelec – to be analysed in terms of the total analytical concentrations of the constituents of struvite, Mg, NH_4, and PO_4, denoting $C_{T_{Mg}}$, $C_{T_{NH_4}}$, $C_{T_{PO_4}}$ (recall the nomenclature in subsection 2.2.6). At the same time, the control sample that was being stored meanwhile in a fridge, at 7ºC, was also transported to the external laboratory to undergo these analytical methods. The six solutions (each contained in a plastic beaker of 250 mL) were filtered using Polyether Sulfone (PES) filter membranes, with a pore size of 0.45 microns. The analytical methods used for the determination of these analytical concentrations are present in Table 6.5.

Table 6.5 - Analytical methods used to determine the analytical concentrations of the constituent ions of struvite in the solution.

Analytical concentrations of struvite's constituent ions	Analytical methods
$C_{T_{NH_4}}$	Distillation, retention in absorbing solution, and titration
$C_{T_{PO_4}}$	Molecular absorption spectrophotometry (Segmented continuous flow) (Molybdenum blue)
$C_{T_{Mg}}$	Acidification and inductively coupled plasma-optical emission spectrometry

After the analytical concentrations were determined, it was possible to calculate the distinct $P_{s_{eq}}$, each one relating to its respective equilibrium pH. $P_{s_{eq}}$ was calculated according to equation (2.23), by multiplying the analytical concentrations of the struvite's constituent ions. Even though it was not indicated in the consulted methodology, the units of the analytical concentrations must be in mol/L in order to obtain the intended solubility curve.

Plotting $P_{s_{eq}}$ vs. pH would then result in five distinct points that could be adjusted to a 2nd order polynomial curve. The goal was, however, to obtain a curve with 10 distinct points, not 5. Unfortunately, it was only possible to obtain 5 points at a time. This limitation was due to the

fact that there was only one jar test apparatus, with six paddle stirrers, available. Since the equilibrium takes 24 h to complete, the jar test could only be used one time per day, to mix, at most, the solution contained in five beakers (one paddle stirrer was not working properly). Furthermore, the external laboratory realized the intended analysis only one day per week. Thus, the processes of taking the centrate sample from the centrifuge, distributing it into five beakers with a solid phase of struvite, adjusting the pH in each beaker, and initiating the mixing of each solution for the consecutive 24 h, had to be done, in this order, in one single day, antecedent to the day the laboratory would realize the intended analyses. This was done to minimize the degradation/modification of the centrate sample associated to its storage.

Preferably, it would have been ideal to have two jar test apparatus operating simultaneously so that ten solutions, rather than five, could be analysed in the same day. As this was not possible, the determination of the solubility curve had to be divided into two consecutive weeks - the first week, entitled run 1, and the second week, named run 2. Run 1 comprised the aforementioned processes, since the 11 L of centrate was sampled from the centrifuge, until the six plastic sample beakers – comprising the control sample and the five adjusted pH solutions – were analysed in terms of $C_{T_{Mg}}$, $C_{T_{NH_4}}$ and $C_{T_{PO_4}}$.

It was decided that the two runs would use the same centrate sample and, for this reason, the centrate sample initially taken was of 11 L so that a sufficient volume would be available for the two runs. The reason behind this decision was to avoid using two centrate samples, collected in different weeks, that could be significantly different from each other. This concern was related to the fact that the composition of the wastewater changes on an hourly, daily and seasonal basis.

Run 2 begun, thus, one week after run 1 had been initiated. The remaining volume of the 11 L of centrate sample, which was not used in run 1, was stored in the fridge (7ºC) for one week, until run 2 was initiated. A few hours before initiating run 2, the remaining centrate sample was taken out from the fridge, so it would achieve the room's temperature. The remaining volume of the centrate sample was of around 6 L and its pH was identical to the one measured one week before, in run 1, with a value of 7.6.

Five glass beakers, of 1 L each, were then filled with the centrate sample, as well as a 250 mL plastic beaker - the control sample of run 2. This control sample (run 2) was stored in the fridge, at 7ºC, for 24 h. Meanwhile, and analogously to run 1, small struvite blocks of 10 g were added in each one of the five beakers. The small blocks of struvite used in run 2 were broken down from the previously stored excess struvite of run 1. The pH adjustment of the solution contained in each glass beaker then followed, similarly as occurred in run 1. The desired pH values for run 2 were the ones depicted in Table 6.6. These values were obtained by the addition of drops of either HCl (1N) or NaOH (1N) in the glass beakers.

Table 6.6 - pH values desired to obtain the struvite's solubility curve of the centrate - run 2.

pH (Sörensen scale)				
6.5	6.8	7.7	**7.3**	9.2

The pH values indicated in Table 6.6 are the ones depicted in Table 6.3, which had not been yet attained in the pH adjustment of run 1 (Table 6.4). The exception is the pH of 7.3, pointed out in blue and bold – this value was supposed to be 8.3 rather than 7.3. The reason for choosing 7.3 over 8.3 will be explained right away.

When the equilibrium pH of the solutions was measured in run 1 (after the 24 h continuous mixing in the jar test had been concluded), the measured pH varied from 8.19 to 8.74. Reasons for this will be discussed in section 6.4, but at first, it was thought that these behavior could be partly explained by the temperature influence on the pH. When the centrate was taken from the centrifuge in run 1, its temperature was higher than the temperature of the laboratory room (in Chelas WWTP). Due to time shortage, the centrate was immediately used for the determination of the curve, rather than allowed to rest until attaining the room temperature firstly.

Nonetheless, the point here is that run 1 did not achieve the pH values desired (depicted in Table 6.4) since all of the five solutions' pH at equilibrium were superior to 8. This also prevented the points of the solubility curve from being equidistant from each other (regarding the x-axis) as initially wanted. In an attempt to obtain equilibrium pH values inferior to 8 in run 2, it was decided that the initially desired point of 8.3 had to be replaced by a value inferior to 8, namely 7.3.

Once the pH adjustment was concluded, run 2 proceeded identically to run 1: the solutions contained in the glass beakers were left to mix for the consecutive 24 h, and after that, the solution (the centrate) in each glass beaker, at equilibrium, was then analysed for pH. The measured equilibrium pH values were registered and written on the respective glass beakers. A volume of 250 mL of centrate was then transferred from each glass beaker to a respective plastic sample beaker. The five plastic sample beakers and the control sample of run 2 were then transported to the external laboratory, where the analytical concentrations - $C_{T_{Mg}}$, $C_{T_{NH_4}}$ and $C_{T_{PO_4}}$ - were determined.

After the analytical concentrations of all the ten solutions at equilibrium, in mol/L, had been determined, it was possible to finally calculate the respective $P_{s_{eq}}$ and adjust the ten points to a 2^{nd} order polynomial curve. The control samples of runs 1 and 2 were analysed to verify in which way storing the centrate sample during one week in the fridge affected the concentrations the struvite's constituent ions present in it.

The materials and reagents used to determine the struvite's solubility curve are listed in Table 6.7. This list does not include the materials and reagents used to determine the analytical concentrations, as that was done in the external laboratory.

Table 6.7 - List of materials and reagents used to determine the struvite's solubility curve.

Material/Reagent	Number of units (if appliable)	Volume (if appliable)
Centrate		11 L
Plastic container	1	5.5 L
Glass beaker	6	1 L
Struvite (large blocks)		
Gloves (pair)	1	
Scale	1	
HCl (1N)		100 mL
NaOH (1N)		100 mL
Pasteur pipette	2 (one for the HCl and other to the NaOH)	
Portable pH meter with incorporated thermometer	1	
Jar test apparatus with six paddle stirrers	1	
Plastic sample beaker	12	250 mL

Only six glass beakers were used since they were emptied and washed after run 1 was completed and re-used for run 2. A container of 5.5 L was used to obtain the sample of 11 L of centrate from the centrifuge (the 2nd volume of centrate sample was taken in the same day, a few moments after the first sample was taken).

At last, some differences between the methodology followed here, to determine the solubility curve, and the one indicated in the UBC dissertations are worth mentioning:

- Unfortunately, and contrary to what was indicated in the UBC methodology, it was not possible to control the temperature during the determination of the curve. The laboratory at Chelas WWTP had no temperature control systems and the experiments carried there (both run 1 and run 2) were performed at room temperature, which would change throughout the day. The variation of the room temperature was therefore measured and registered, with a periodicity of 2 h, for 24 h, when the jar test apparatus was being used to provide mixing conditions in the beakers.

- Information provided in the UBC studies indicated that filled glass beakers had 1.5 L of capacity rather than 1 L. The present methodology used 1 L beakers because beakers of 1.5 L of capacity were too large to fit in the jar test apparatus of Figure 6.4, five at a time.

- Some differences regarding the introduction of struvite in the beakers also occurred. The UBC methodology used struvite pellets, previously formed through the operation of already existing UBC reactors. The construction of the reactor designed and sized in the present thesis was not completed at the time that the determination of the solubility curve took place. For that reason, blocks of involuntary formed struvite, removed from the centrifuge, had to be used.

- There was no indication provided in the UBC dissertations that the jar-test apparatus was used to mix the solution in the glass beaker at the same time the pH was being adjusted through the addition of drops of HCl or NaOH into it.

- The unavailability of more than 1 jar test apparatus led to the need of realizing two identical runs to determine the solubility curve in the present thesis. Lack of information regarding this logistical aspect in the UBC dissertations may suggest that two apparatus were available at the same time for the curve determination.

- Two final aspects were not specified in the UBC methodologies: the concentrations of the NaOH and HCl, and the indication that the analytical concentrations must be in mol/L before the calculation of $P_{s_{eq}}$ takes place. The concentration of the NaOH and HCl, specified in the present methodology, applies, naturally, only to the centrate in study.

- Analytical methods used in the present methodology, indicated in Table 6.5, also differed from the ones of the UBC dissertations. Ammonia and orthophosphate samples were analysed at the UBC laboratory by flow injection analysis and magnesium analysis was performed by flame atomic absorption spectrophotometry.

6.4 Results and Discussion

6.4.1 pH at Equilibrium

Table 6.8 depicts the adjusted pH values considered for the determination of the solubility curve, obtained by adding HCl or NaOH into the centrate contained in each glass beaker. Unfortunately, it was not always possible to obtain the exact pH value initially desired (these desired values are depicted in Table 6.4 and Table 6.6). Nonetheless, approximate values were obtained, which can be verified by comparing Table 6.4 and Table 6.6 with Table 6.8.

After 24 h, and in continuously mixing conditions, the pH at equilibrium in each beaker was again measured. The respective value is indicated in the rightmost column of Table 6.8. Each beaker was labelled from 1 to 10, and according to the run where the pH measurement took place (run 1 or run 2). The need of determining the solubility curve into 2 runs was due to logistical issues that have been explained in section 6.3.

Table 6.8 - pH values measured during the determination of the solubility curve: adjusted pH and pH at equilibrium (measured after 24 h of continuous mixing)

	ID	Adjusted pH	pH at equilibrium
run 1	1	7.40	8.29
	2	8.00	8.30
	3	8.60	8.53
	4	8.90	8.74
	5	7.10	8.19
run 2	6	9.28	8.97
	7	7.63	8.25
	8	7.25	8.21
	9	6.83	8.12
	10	6.53	8.03

As it can be seen from Table 6.8, the adjusted pH values and the corresponding pH values at equilibrium differ from each other. Differences between the adjusted pH and the corresponding equilibrium pH varied from 0.07 to 1.5. The variation between the adjusted pH and the equilibrium pH was in fact expected. In other words, the pH of the centrate in each beaker was adjusted to an ideally desired value, with the awareness that the pH wouldn't remain exactly the same after the equilibrium was reached. The reasons why this variation was expected will be explained right away.

The pH of a solution is defined as the negative logarithm of the hydrogen ion concentration (in mol/L) – see equation (6.1) (Chang & Goldsby, 2012). It is a measure of the free hydrogen ions, H^+, in the solution.

$$pH = - \log [H^+] \tag{6.1}$$

HCl was used to lower the pH of the solution because it is highly acidic and completely dissociates into hydrogen and chloride ions, raising the concentration of H^+ in the solution. As for NaOH, it was used because it is highly basic and gives up OH^- rapidly when placed in water.

The OH^- ions then react with H^+ in solution, creating new water molecules and lowering the amount of free H^+ in the system, thereby raising the overall pH.

During the process of adjusting each solution's pH with either NaOH or HCl, the pH was being simultaneously measured, with a pH probe. The pH probe measured the free ions in the solution, either increased by the addition of HCl or decreased by the addition of NaOH drops into the solution. Adding NaOH or HCl in the solution seemed to have a quite rapid effect in its pH. The solution's pH changed after a few seconds after the reagent's drops were added, and then the pH stabilized (until new drops would be introduced). However, 24 h after this pH adjustment, the solutions' pH values were no longer the same. 24 h was the minimum period to attain a new equilibrium, stipulated by literature.

Introducing reagents into the centrate to obtain a desired pH disturbed the initial equilibrium (when the centrate was at 7.55 for run 1 and 7.6 at run 2). According to Le Chatelier's Principle, if a dynamic equilibrium is disturbed by changing the conditions, the position of equilibrium moves to counteract the change. Thus, the equilibrium pH values, measured 24 h after the pH adjustment, are a reflection of this counteraction. In the case where HCl drops were added to the solution during the pH adjustment, the position of equilibrium of reactions involving H^+ moved so that a decrease in the concentration of H^+ in the solution would occur. As for the case where NaOH drops were added, the position of equilibrium moved so that an increase in the concentration of H^+ in the solution would occur. Table 2.1 depicts some of the chemical reactions that may have taken place during this process. Nonetheless, many other reactions may have taken place due to the rich composition that characterizes wastewater.

Furthermore, the unfeasibility of controlling temperature also contributed to the pH values measured after 24 h being different from the adjusted ones. Not only the position of equilibrium changes if one changes the temperature, as the equilibrium constants also change with temperature. This significantly affects the chemical reactions taking place in the achievement of a new equilibrium, and therefore in the pH of the solution. This effect (of temperature variation) was aggravated in run 1 because the centrate sample was taken from the centrifuge at 34.7ºC, and used right away to determine the solubility curve, at a room temperature which varied from 27.4 to 30.7ºC. Unfortunately, it was not logistically possible to wait for the temperature of the centrate to attain the room temperature. The variation of temperature in the room, and during the transportation of the centrate to the external laboratory, may cast doubt on if a stationary equilibrium was indeed attained.

At last, the glass beakers where not covered, which means that they were exposed to the atmosphere of the laboratory room. This may also have affected the pH of the solutions contained in the beakers. If absorbed by a liquid, the CO_2 contained in the atmosphere will produce carbonic acid (H_2CO_3). Carbonic acid may then change the pH value of the solution.

To sum-up, the combination of the solutions' exposition to the air, and the temperature variation in the room, during the 24 h mixing, along with the initial equilibrium disruption caused by the addition of NaOH or HCl drops, resulted in the equilibrium pH values presented in Table 6.8. Even though, a variation between the adjusted pH values and the equilibrium pH values (indicated in Table 6.8) was expected, this variation was larger than desirable, in the sense that the solubility curve was obtained for a pH range of 8.03 to 8.97, rather than from 6.5 to 9.2.

To prevent such large variation from happening in the determination of a forthcoming solubility curve (related to a new sample of centrate), it is thus suggested that one of two measures are taken. One option is to adjust the pH of the centrate so that a wider range of pH equilibrium can be obtained afterwards. That is, one should adjust the pH of the centrate to a pH value higher than the maximum actually desired for the curve. Proceeding analogously to the

minimum pH desired value for the curve is advised. Also, it is desirable to obtain more than ten points for the curve's determination. This will be useful when dealing with the hardly predictable pH values at equilibrium. The other, more graceful, measure is to use models. Modeling can be used to predict the pH value at equilibrium, based on the centrate's initial pH and on the added volume of the reagent used to adjust the pH. Naturally, the model will work better with more complete information about the centrate. More than solely the $C_{T_{Mg}}$, $C_{T_{NH_4}}$ and $C_{T_{PO_4}}$, the concentration of foreign ions and of H+ and OH^- would be helpful. Fixing the temperature is also required.

6.4.2 Struvite's solubility curve

In order to obtain the solubility curve, the analytical concentrations of Mg, NH_4 and PO_4, determined in the external laboratory, in mg/L, were expressed in mol/L. The unit conversion was done by firstly converting mg/L to g/L, and then dividing the concentration (of Mg, NH_4 and PO_4,), in g/L, by the respective molar mass, in g/mol.

Table 6.9 indicates the analytical concentrations of Mg, NH_4 and PO_4, determined in the external laboratory expressed in mg/L and in mol/L. Each line of Table 6.9 corresponds to the centrate contained in one of the 10 beakers, each beaker identified from 1 to 10. The pH indicated in Table 6.9 refers to the one obtained after the 24 h of continuously mixing in the jar-test apparatus (the equilibrium pH).

Table 6.9 - Analytical concentrations of Mg, NH_4 and PO_4, determined in the external laboratory and calculation of the pP_s values.

	ID	pH	Mg (mg/L)	PO_4 (mg/L)	NH_4 (mg/L)	Mg (mol/L)	PO_4 (mol/L)	NH_4 (mol/L)	P_s	$pP_{s_{eq}}$
run 1	1	8.29	0.83	600	1000	3.41×10^{-5}	6.32×10^{-3}	5.55×10^{-2}	1.20×10^{-8}	7.92
	2	8.30	1.00	570	970	4.11×10^{-5}	6.00×10^{-3}	5.38×10^{-2}	1.33×10^{-8}	7.88
	3	8.53	0.74	560	900	3.04×10^{-5}	5.90×10^{-3}	4.99×10^{-2}	8.96×10^{-9}	8.05
	4	8.74	0.59	550	740	2.43×10^{-5}	5.79×10^{-3}	4.10×10^{-2}	5.77×10^{-9}	8.24
	5	8.19	1.10	580	1100	4.53×10^{-5}	6.11×10^{-3}	6.10×10^{-2}	1.69×10^{-8}	7.77
run 2	6	8.97	0.54	590	740	2.22×10^{-5}	6.21×10^{-3}	4.10×10^{-2}	5.66×10^{-9}	8.25
	7	8.25	0.90	640	1200	3.70×10^{-5}	6.74×10^{-3}	6.66×10^{-2}	1.66×10^{-8}	7.78
	8	8.21	1.00	620	1200	4.11×10^{-5}	6.53×10^{-3}	6.66×10^{-2}	1.79×10^{-8}	7.75
	9	8.12	1.00	630	1200	4.11×10^{-5}	6.63×10^{-3}	6.66×10^{-2}	1.82×10^{-8}	7.74
	10	8.03	1.90	620	1200	7.82×10^{-5}	6.53×10^{-3}	6.66×10^{-2}	3.40×10^{-8}	7.47

The $P_{s_{eq}}$ related to each beaker was then calculated by multiplying the respective concentrations of Mg, NH_4 and PO_4, in mol/L. The negative logarithm of $P_{s_{eq}}$, $pP_{s_{eq}}$ was then determined. Both the calculated $P_{s_{eq}}$ and $pP_{s_{eq}}$ are also indicated in Table 6.9. Ten points (pH, $pP_{s_{eq}}$) were, thus, obtained for the determination of the curve.

At last, a second order polynomial curve was fitted to the data using Microsoft Excel software, which resulted in the solubility curve depicted in Figure 6.5.

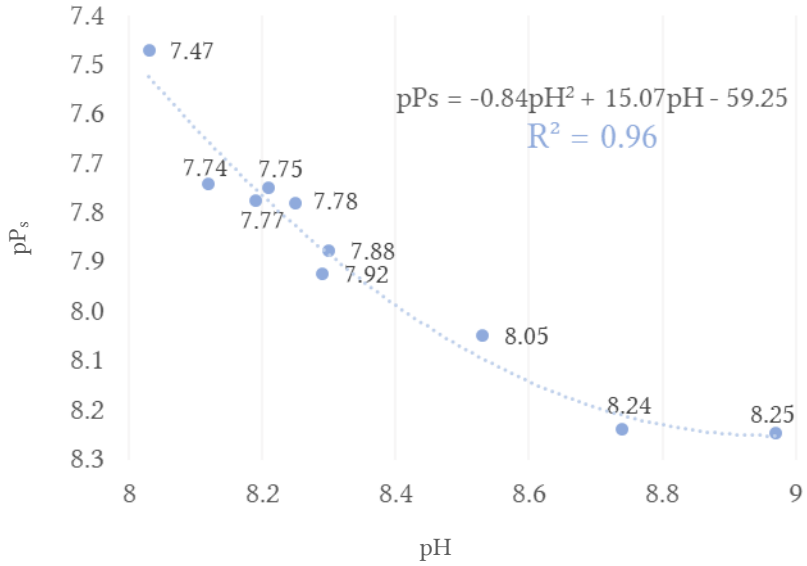

Figure 6.5 - Struvite $P_{s_{eq}}$ in a centrate sample taken from the centrifuge of Chelas WWTP, as function of pH.

Observing Figure 6.5, it is evident that the 2nd order polynomial curve fitted significantly well to the points obtained for the determination of the solubility curve, with a coefficient of determination of around 0.96. The obtained R^2 is in accordance with the ones obtained in several UBC dissertations, as Table 6.10 corroborates.

Table 6.10 - Equations of the curves obtained in some of the UBC dissertations consulted.

Equation	R^2	Temperature (°C)	Reference
$pPs = -0.203pH^2 + 4.09pH - 11.76$	0.99	20	Britton, 2002
$pPs = -0.13pH^2 + 3.04pH - 8.52$	0.99	10	Huang, 2003
$pPs = -0.14pH^2 + 3.21pH - 9.34$	0.98	15	
$pPs = -0.11pH^2 + 2.67pH - 7.72$	0.96	20	
$pPs = -0.1981pH^2 + 4.0555pH - 11.768$	1.00	20	Fattah, 2004
$pPs = 0.222pH^2 - 2.2628pH + 11.447$	1.00	25	

Thus, one of the most notable inferences that can be made is that, despite all the logistical constraints, which obliged the methodology followed in this present thesis to undergo changes related to the UBC methodology, similar results were obtained. The changes in the methodology seemed to have caused no significant effect on the curve determination.

For instance, the determination of the curve had to be done in two consecutive weeks, which forced the storage of the centrate sample for 7 days. Even though the storage raised concerns in terms of the preservation of the characteristics of the centrate sample, it seemed to have no significant influence on the determination of the curve. Table 6.11 indicates the characteristics of the centrate sample in the two runs, regarding the concentration of Mg, PO_4, NH_4, and the pH. From Table 6.11, it can be verified that the characteristics of the centrate changed from one week to the other.

Table 6.11 - Characteristics of the centrate sample used in run 1 and run 2 – concentration of Mg, PO_4, NH_4, and pH.

Sample identification	pH	Mg (mg/L)	PO_4 (mg/L)	NH_4 (mg/L)
Control sample - run 1	7.55	5.50	620	1100
Control sample - run 2	7.6	4.10	630	1300

Also, the variation of the temperature during the curve determination seemed to have had no significant effect on it. Contrarily to the curves obtained in the UBC dissertations (Table 6.10), the curve obtained here does not correspond to a fixed temperature. It relates to a temperature range.

It is worth highlighting that what is being concluded here is that both the variation of the temperature and of the centrate characteristics (from one week to another) did not produce a significant impact in the determination of the curve, in the magnitude they both occurred. Larger variations may have indeed a significant impact. If possible, fixing the temperature is preferable, as well as not storing the centrate sample.

The analytical methods used to determine the analytical concentrations of the constituent ions of struvite in the solution deserve further attention. The total analytical concentrations of the constituents of struvite, Mg, NH_4, and PO_4, denoting $C_{T_{Mg}}$, $C_{T_{NH_4}}$, $C_{T_{PO_4}}$, were defined in subsection 2.2.6 as the sum of the dissolved concentrations of their complexes and free ions, as expressed in equations (2.16) to (2.18), recalled below.

$$C_{T_{Mg}} = \left[Mg^{2+}\right]+[MgOH^{+}]+[MgH_2\,PO_4^{+}]+[MgHPO_4]+[MgPO_4^{-}] \tag{6.2}$$

$$C_{T_{NH_4}} = [NH_4^{+}] + [NH_3] \tag{6.3}$$

$$C_{T_{PO_4}} = [H_3PO_4] + [H_2PO_4^{-}] + \left[HPO_4^{2-}\right] + \left[PO_4^{3-}\right] + [MgH_2\,PO_4^{+}] + [MgHPO_4] + [MgPO_4^{-}] \tag{6.4}$$

However, the analytical methods used (Table 6.5) do not allow to strictly determine these concentrations, in the sense that they realize a more comprehensive determination. These analytical methods measure not only the dissolved concentrations of the complexes of Mg, NH_4, and PO_4 - indicated in equations (2.16) to (2.18) -, as any complex, whose constituent ions is magnesium, orthophosphate or ammonia. The diversity of foreign ions that characterizes the wastewater renders the formation of complexes, not included in equations (2.16) to (2.18), probable.

Thus, it might be the case that equations (2.16) to (2.18) are a simplification. In other words, even though there are foreign ions in the wastewater that may complex with the struvite's forming ions, the streams in study are enriched in orthophosphate and ammonia in such a way that the foreign ions are negligible.

6.5 Summary

Chelas WWTP does not remove P biologically. Nevertheless, this was the chosen plant to settle the reactor developed in this thesis. The reason behind this decision was the presence of a high concentration of phosphate in the centrate of the centrifuge.

Even though data regarding the dissolved fractions of the struvite's constituent ions in the centrate was initially not available, struvite scaling has been forming involuntarily in the centrifuge. Analysis of the dissolved fractions of PO_4, NH_4 and Mg present in the centrate were afterwards realized for the purpose of the present thesis, on the 14th of July of 2020. The results of these analysis showed high concentrations of both dissolved PO_4 and NH_4 – 620 mg/L and 1100 mg/L, respectively – that agree with the struvite formation in the centrifuge. As expected, the concentration of dissolved Mg was relatively lower – 5.5 mg/L.

A centrate sample was taken from the centrifuge of Chelas WWTP to be used in the determination of a struvite solubility limit curve for that solution composition. Such curve is of major importance to the reactor operation. Nonetheless, the curve here obtained was not intended to be used in the operation of the reactor, whose construction is in progress. By the time the reactor's construction is completed, the centrate's composition will be probably different from the one that the obtained curve relates to. Since the reactor is initially intended to be fed in batch mode, a struvite solubility curve should be determined for each new batch (assuming that the wastewater composition in each batch is different).

In order to determine the solubility curve, an already existing methodology, indicated in several UBC dissertations (coinciding with the same ones that were used to develop a new reactor) was applied, as far as it was possible. These UBC dissertations obtained curves that fitted reasonably well to the experimental points (pH, $pP_{s_{eq}}$), with $R^2 \geq 0.96$. The goal of this chapter was to apply this methodology to test if it would reproduce identical results when using Chelas WWTP centrate. Making explicit some omitted aspects in the already existing methodology was also necessary, to expedite the determination of further curves which will be needed throughout the future reactor operation.

Against several logistical difficulties, which did not permit to strictly follow the UBC methodology, identical results were nevertheless obtained for the centrate sample of Chelas WWTP. A 2nd order polynomial curve fitted well to the experimentally obtained data through an R^2 of 0.96. It is advised, however, that in the future, the solubility curve should be determined according to the UBC methodology, rigorously. Nonetheless, in what concerns the analytical methods used to determine the concentrations of PO_4, NH_4 and Mg present in the centrate, there is no apparent reason not to use them, even if they differ from the ones present in the UBC thesis.

Not having followed the UBC methodology stringently but having obtained the desired result does not necessarily mean that the introduced modifications will reproduce an identical outcome in the future. It solely means that the modifications - in the magnitude they occurred - did not seem to have had a significant impact on obtaining a curve that fitted well to the experimental data.

Unfortunately, contrarily to what was indicated in the UBC methodology, it was not possible to control the temperature room during the curve determination. Even though this did not seem to affect the curve fit, it prevented the obtained solubility curve to correspond to a fixed temperature.

The experimental data (pH, $pP_{s_{eq}}$) was obtained for a pH range of around 8 to 9 (pH at equilibrium). The initial desired range was, however, of 6.5 to 9. Thus, for the development of future curves, it is advised that more than ten points are used. Also, when adjusting the initial pH, it is advised that the range of the adjusted pH values is broader than the pH values desired at equilibrium. 24 h after the pH adjustment, the pH at equilibrium will be different and it is hard to predict the new equilibrium pH. Modeling can be used for this purpose but requires fixing the temperature and a more detailed knowledge on the composition of the wastewater.

At last, it was possible to verify that the reagents concentration that best suited the pH adjustment of the centrate under study was of 1N, for both HCl and NaOH. Also, to obtain the solubility curve, the analytical concentrations of PO_4, NH_4 and Mg, used to calculate $pP_{s_{eq}}$, must be expressed in mol/L. Both the concentration of reagents and the need of expressing the analytical concentrations in mol/L were not indicated in the already existing methodology. Thus, applying the UBC methodology allowed to complete it as intended.

CHAPTER 7

CONCLUSIONS AND FUTURE WORK

7.1 Conclusions

There is a lot of know-how in what concerns recovering P, from phosphate-rich wastewater, in the form of struvite. In fact, several technologies, focused in obtaining this phosphorus-containing by-product, have been established. Ostara is the market leader and stands out for the quality of its recovered struvite, a ready-to-use premium fertilizer.

The review of the fundamental principles of struvite crystallization was one of the main aims of this thesis, and of major importance to understand how these principles are used in struvite recovery technologies. This was achieved in the literature review carried out, in sections 2.1 to 2.4.

Another objective of the present thesis was to design and size a reactor to remove P from wastewater in the form of struvite. The reactor was designed and sized. The dimensions of the reactor and the remaining constituents of the crystallization system were depicted in section 5.2. The construction of the reactor was initiated during the realization of this thesis. When ready, it will then be installed and operated at Chelas WWTP. Therefore, the elaboration, in section 4.3, of a review of the struvite recovery technologies most commonly implemented at full-scale worldwide – another goal of this dissertation – provided the basis for the sizing of the crystallization reactor.

To benefit from the technological advances available in the literature, the reactor was based on an already existing technology, namely the early stages of Ostara's technology. The studies carried out by the research P-recovery group of the UBC were thus used as a foundation for the reactor development. These studies comprise the earlier development stages of the Ostara technology, as Ostara is a spin-off company of the research P-recovery group.

Not only these UBC studies were systematically structured in an identical form amongst them, as they also developed FBR which removed phosphorus efficiently (P-removal efficiencies over 90%), at the pilot scale. These reactors had a layout identical to the Ostara's reactor, i.e., a reactor's configuration constituted by cylindrical sections of increasing diameter from bottom to top.

Nonetheless, the sizing criteria to develop a crystallization reactor were not provided in the reviewed literature. Also, the fact that the wastewater composition differed amongst and

throughout the above studies, along with the variation of the operating conditions, rendered the determination of the sizing criteria very hard, if not impossible. Thus, rather than looking for the UBC reactors' sizing criteria, the focus was to inspect and learn from the proportions amongst their reported dimensions.

The following findings, obtained during the reactor's sizing process in this thesis, could be drawn:

- In general, the UBC reactors were very identical amongst them, and they even shared the same section's diameters. In fact, it seemed that they were sized to test the impact of the slightly altering of the heights of the cylindrical sections in the reactor performance. Such minor modifications did not cause any evident effect in the performance of the reactors.

- Even though the UBC reactors were similar amongst them, the proportions between the different dimensions of each reactor (sections' diameters and heights) did not consistently repeat for all reactors.

- The lack of patterns that could be used in the sizing of a new reactor prompted the need to replicate one of the UBC reactors, to be picked. Given that all UBC reactors reviewed were more than 4 m high, none of them could be used to be exactly replicated due to onsite logistical constraints. This was overcome by reducing the sections' heights of the reactor studied by Fattah (2004), as indicated by Rahaman et al. (2009).

- To base the reactor development in the UBC studies proved to be an appropriate choice in the sense that these studies were used complementarily to each other to size the new reactor. When information useful for the sizing of the constituents of the crystallization system lacked in a given study, that data could be usually found in one of the remaining UBC studies. Such detailed information was not provided elsewhere in the remaining literature consulted. Furthermore, guidelines for the reactor future operation can also be obtained from these UBC studies.

To expedite the future operation of the reactor, a struvite solubility limit curve, referring to a centrate sample of Chelas WWTP, was also determined here and reported in Chapter 6. The determination of the curve took place in the laboratory room of Chelas WWTP, according to the methodology proposed in the UBC studies. The results were encouraging: a 2^{nd} order polynomial curve fitted to the experimental data through an R^2 of 0.96. Therefore, the goal of testing an existing methodology to determine a solubility curve was achieved. This methodology can, thus, be applied to determine such type of curves referring to the centrate in the future. Moreover, having applied this methodology allowed to make explicit some important aspects that happen to be omitted in the literature.

The determination of the solubility curve allowed to conclude the following:

- The reagents concentration that best suit the pH adjustment of the centrate under study is of 1N, for both HCl and NaOH.

- To obtain the solubility curve, the analytical concentrations of PO_4, NH_4 and Mg, used to calculate $pP_{s_{eq}}$, must be expressed in mol/L.

. The adjusted pH values and the corresponding pH values at equilibrium will differ. This difference is expected and may be explained by the combination of the solutions' exposition to the air and to the temperature variation in the room (if not fixed), along with the initial equilibrium disruption caused by the addition of NaOH or HCl drops.

. The analytical methods described in Table 6.5 can be used to determine the analytical concentrations of the constituent ions of struvite in the solution.

To sum-up, all the objectives embraced in the present dissertation were accomplished.

7.2 Future Work

Additionally, the forthcoming operation of the reactor prompts a reasonable amount of future work, out of the scope of this dissertation. By the time the reactor is installed in the plant, it is advised that the storage tanks that will contain the centrate and reagents (NaOH and $MgCl_2$) are sized and constructed. It was not possible to size these storage tanks in this thesis because there was a lack of information concerning a few relevant logistical aspects.

Also, data regarding the dissolved fractions of the struvite's constituents for a period is missing. This information, along with the defined control parameters (pH and SSR), can be used to estimate the volume of reagents necessary to the reactor operation. In the case of $MgCl_2$, this is rather important since the introduction of this reagent into the reactor is necessary to control the SSR. Thus, a decision regarding the range of the desired control parameters should also be made. For instance, pH values between 7.5 and 8, and SSR values between 1 and 3 in the reactor, have been successfully used in the operation of some reactors.

At this earlier stage, and to avoid dealing with the variation of the wastewater composition along the time, feeding the reactor in batch-mode should be the first procedure. The monitoring of the crystallization system can be done by measuring the pH and the PO_4 concentrations, in the centrate storage tank, reactor and external clarifier. Comparing the PO_4 concentration present in the centrate (in the storage tank) to the one present in the final clarified effluent will determine the P-removal efficiency. Awaiting for the analytical concentrations, determined by an external laboratory, can be time consuming and constitute a significant time lag between changing conditions in the reactor and knowing their effect. To tackle this issue some phosphate chemical test kits can be used complementarily to realize a closer monitoring, even though precision of the results is lost.

The determination of more solubility curves, each one relating to the respective batch trial, will also be needed. It is important that they can be obtained for a fixed temperature. Suggestions to obtain these curves successfully have been made in section 6.4.

Furthermore, it is noteworthy that the sizing criteria of the reactor was not found in the literature. This hindered the sizing of a new reactor. In the future, research regarding the impact of the reactor dimensions on the P-removal efficiency should be pursued. Modelling can be useful for this purpose. As demonstrated by Rahaman et al. (2009), using CFD modelling to test the impact of different reactor configurations can be extremely helpful.

BIBLIOGRAPHY

Aage, H. K., Andersen, B. L., Blom, A., & Jensen, I. (1997). The solubility of struvite. *Journal of Radioanalytical and Nuclear Chemistry*, *223*(1–2), 213–215. https://doi.org/10.1007/BF02223387

Abbona, F., & Boistelle, R. (1979). Growth morphology and crystal habit of struvite crystals ($MgNH_4PO_4 \cdot 6\ H_2O$). *Journal of Crystal Growth*, *46*(3), 339–354. https://doi.org/10.1016/0022-0248(79)90082-4

Abbona, F., Madsen, H. E. L., & Boistelle, R. (1986). The initial phases of calcium and magnesium phosphates precipitated from solutions of high to medium concentrations. *Journal of Crystal Growth*, *74*(3), 581–590. https://doi.org/10.1016/0022-0248(86)90205-8

Adnan, A. (2002). *Pilot-scale study of phosphorus recovery through struvite crystallization* [Master Thesis, University of British Columbia]. https://open.library.ubc.ca/cIRcle/collections/ubctheses/831/items/1.0063520

Adnan, A., Koch, F. A., & Mavinic, D. (2003). Pilot-scale study of phosphorus recovery through struvite crystallization – II: Applying in-reactor supersaturation ratio as a process control parameter. *Journal of Environmental Engineering and Science*, *2*(6), 473–483. https://doi.org/10.1139/s03-048

Adnan, A., Mavinic, D., & Koch, F. A. (2003). Pilot-scale study of phosphorus recovery through struvite crystallization – examining the process feasibility. *Journal of Environmental Engineering and Science*, *2*(5), 315–324. https://doi.org/10.1139/s03-040

Ali, I., & Schneider, P. A. (2005). Crystallization of struvite from metastable region with different types of seed crystal. *Journal of Non-Equilibrium Thermodynamics*, *30*(2). https://doi.org/10.1515/JNETDY.2005.007

Ali, I., & Schneider, P. A. (2006). A fed-batch design approach of struvite system in controlled supersaturation. *Chemical Engineering Science*, *61*(12), 3951–3961. https://doi.org/10.1016/j.ces.2006.01.028

Ali, I., & Schneider, P. A. (2008). An approach of estimating struvite growth kinetic incorporating thermodynamic and solution chemistry, kinetic and process description. *Chemical Engineering Science*, *63*(13), 3514–3525. https://doi.org/10.1016/j.ces.2008.04.023

Ali, I., Schneider, P. A., & Hudson, N. (2005). Thermodynamics and solution chemistry of struvite. *Journal of the Indian Institute of Science*, *85*(3), 141–149.

Alvarez, J., Alvarez, J., & González, E. (1989). Global nonlinear control of a continuous stirred tank reactor. *Chemical Engineering Science*, *44*(5), 1147–1160. https://doi.org/10.1016/0009-2509(89)87014-9

Amann, A., Zoboli, O., Krampe, J., Rechberger, H., Zessner, M., & Egle, L. (2018). Environmental impacts of phosphorus recovery from municipal wastewater. *Resources, Conservation and Recycling*, *130*, 127–139. https://doi.org/10.1016/j.resconrec.2017.11.002

Anderson, G. M. (2005). *Thermodynamics of Natural Systems*. Cambridge University Press.

Andrade, A., & Schuiling, R. D. (2001). The chemistry of struvite crystallization. *Mineralogical Journal (Ukraine)*, *23*, 37–46. https://www.researchgate.net/publication/46690671_The_chemistry_of_struvite_crystallization

Antoniewicz, P. (2018, December 21). *Understanding And Coping With Struvite/Vivianite Formation In WWTPs*. Water Online. https://www.wateronline.com/doc/understanding-and-coping-with-struvite-vivianite-formation-in-wwtps-0001

Arend, H., & Hulliger, J. (Eds.). (1989). *Crystal Growth in Science and Technology* (Vol. 210). Springer.

Ariyanto, E., Ang, H. M., & Sen, T. K. (2014). Impact of various physico-chemical parameters on spontaneous nucleation of struvite ($MgNH_4PO_4$. $6H_2O$) formation in a wastewater treatment plant: Kinetic and nucleation mechanism. *Desalination and Water Treatment*, *52*(34–36), 6620–6631. https://doi.org/10.1080/19443994.2013.821042

Ashley, K., Cordell, D., & Mavinic, D. (2011). A brief history of phosphorus: From the philosopher's stone to nutrient recovery and reuse. *Chemosphere*, *84*(6), 737–746. https://doi.org/10.1016/j.chemosphere.2011.03.001

Asimov, I. (1974). *Asimov on chemistry*. Knopf Doubleday Publishing Group.

Babić-Ivančić, V., Kontrec, J., Kralj, D., & Brečević, L. (2002). Precipitation Diagrams of Struvite and Dissolution Kinetics of Different Struvite Morphologies. *Croatica Chemica Acta*, *75*(1), 89–106.

Baur, R. (2010). Operating North America's First Full Scale Nutrient Recovery Facility. *Proceedings of the Water Environment Federation*, *2010*, 497–506. https://doi.org/10.2175/193864710802767074

Baur, R., Britton, A., & Prasad, R. (2010). Full Scale Nutrient Recovery by Struvite Crystallization at Clean Water Services Durham AWWTP: Operational Data Analysis. *Proceedings of the Water Environment Federation*, *2010*(10), 5950–5957. https://doi.org/10.2175/193864710798194193

Bayuseno, A. P., Perwitasari, D. S., Muryanto, S., Tauviqirrahman, M., & Jamari, J. (2020). Kinetics and morphological characteristics of struvite ($MgNH_4PO_4.6H_2O$) under the influence of maleic acid. *Heliyon*, *6*(3), e03533. https://doi.org/10.1016/j.heliyon.2020.e03533

Belessiotis, V., Kalogirou, S., & Delyannis, E. (2016). Water, the Raw Material for Desalination. In *Thermal Solar Desalination* (pp. 21–102). Academic Press. https://doi.org/10.1016/B978-0-12-809656-7.00002-7

Benisch, M., Baur, R., Britton, A. T., Neethling, J., & Oleszkiewicz, J. A. (2009). Startup of the First Commercial Phosphorus Recycling Facility in the US at Durham AWWTP.

Proceedings of the Water Environment Federation, *2009*, 102–119. https://doi.org/10.2175/193864709793955456

Benjamin, M. M., & Lawler, D. F. (2013). *Water Quality Engineering: Physical / Chemical Treatment Processes*. John Wiley & Sons.

Bennett, E. M., Carpenter, S. R., & Caraco, N. F. (2001). Human Impact on Erodable Phosphorus and Eutrophication: A Global Perspective. *BioScience*, *51*(3), 227. https://doi.org/10.1641/0006-3568(2001)051[0227:HIOEPA]2.0.CO;2

Bhamidi, V., Kenis, P. J. A., & Zukoski, C. F. (2017). Probability of Nucleation in a Metastable Zone: Induction Supersaturation and Implications. *Crystal Growth & Design*, *17*(3), 1132–1145. https://doi.org/10.1021/acs.cgd.6b01529

Bhuiyan, M. I. H., Mavinic, D., & Koch, F. A. (2008). Phosphorus recovery from wastewater through struvite formation in fluidized bed reactors: A sustainable approach. *Water Science and Technology*, *57*(2), 175–181. https://doi.org/10.2166/wst.2008.002

Bhuiyan, M. I. H., Mavinic, D. S., & Beckie, R. D. (2007). A solubility and thermodynamic study of struvite. *Environmental Technology*, *28*(9), 1015–1026. https://doi.org/10.1080/09593332808618857

Blackall, L. L., Crocetti, G. R., Saunders, A. M., & Bond, P. L. (2002). A review and update of the microbiology of enhanced biological phosphorus removal in wastewater treatment plants. *Antonie van Leeuwenhoek*, *81*(1/4), 681–691. https://doi.org/10.1023/A:1020538429009

Booker, N. A., Priestley, A. J., & Fraser, I. H. (1999). Struvite Formation in Wastewater Treatment Plants: Opportunities for Nutrient Recovery. *Environmental Technology*, *20*(7), 777–782. https://doi.org/10.1080/09593332008616874

Borgerding, J. (1972). Phosphate Deposits in Digestion Systems. *Journal of Water Pollution Control Federation*, *44*, 813–819.

Bouropoulos, N. C., & Koutsoukos, P. G. (2000). Spontaneous precipitation of struvite from aqueous solutions. *Journal of Crystal Growth*, *213*(3–4), 381–388. https://doi.org/10.1016/S0022-0248(00)00351-1

Bowker, R. P. G., & Stensel, H. D. (1987). *Design Manual: Phosphorus Removal*. U.S. Environmental Protection Agency, Office of Research and Development, Center for Environmental Research Information.

Brett, S., Guy, J., Morse, G., & Lester, J. N. (1997). *Phosphorus removal and recovery technologies*. Selper Publications.

Britton, A. T. (2002). *Pilot Scale Struvite Recovery Trials from a Full-scale Anaerobic Digester Supernatant at the City of Penticton Advanced Wastewater Treatment Plant* [Master Thesis, University of British Columbia]. https://open.library.ubc.ca/cIRcle/collections/ubctheses/831/items/1.0063936

Britton, A. T., & Baur, R. (2010). Phosphorus: A Resource in Decline. *American Water Works Association, 102*(9), 117–118. https://doi.org/doi:10.1002/j.1551-8833.2010.tb10177.x

Britton, A. T., Koch, F. A., Mavinic, D., Ali, A., Oldham, W. K., & Udala, B. (2005). Pilot-scale struvite recovery from anaerobic digester supernatant at an enhanced biological phosphorus removal wastewater treatment plant. *Journal of Environmental Engineering and Science*, *4*(4), 265–277. https://doi.org/10.1139/s04-059

Britton, A. T., Prasad, R., Balzer, B., & Cubbage, L. (2009). *Pilot testing and economic evaluation of struvite recovery from dewatering centrate at HRSD's Nansemond WWTP* (K. I. Ashley, D. S. Mavinic, & F. A. Koch, Eds.; pp. 193–202). IWA Publishing.

Broecker, W. S. (1976). *Chemical Oceanography*. Harcourt Brace Jovanowich Inc.

Burgot, J.-L. (2017). Equilibrium Constant, Activities, and Reaction Gibbs Energy. In *The Notion of Activity in Chemistry* (pp. 205–219). Springer, Cham. https://doi.org/10.1007/978-3-319-46401-5_17

Capdevielle, A., Sýkorová, E., Biscans, B., Béline, F., & Daumer, M.-L. (2013). Optimization of struvite precipitation in synthetic biologically treated swine wastewater—Determination of the optimal process parameters. *Journal of Hazardous Materials*, *244–245*, 357–369. https://doi.org/10.1016/j.jhazmat.2012.11.054

Carliell-Marquet, C. M., & Wheatley, A. D. (2002). Measuring metal and phosphorus speciation in P-rich anaerobic digesters. *Water Science and Technology*, *45*(10), 305–312. https://doi.org/10.2166/wst.2002.0360

Centrisys Corporation. (2019). *PROCESS: AirPrex® Installations* [PDF]. Centrisys CNP. https://cdn2.hubspot.net/hubfs/4299619/6-1%20Literature/PROCESS%20AirPrex%20Installations%20CNP.pdf

Chang, R., & Goldsby, K. (2012). *Chemistry* (11th edition). McGraw-Hill.

Childs, C. W. (1970). Potentiometric study of equilibriums in aqueous divalent metal orthophosphate solutions. *Inorganic Chemistry*, *9*(11), 2465–2469. https://doi.org/10.1021/ic50093a017

Chirmuley, D. G. (1994). Struvite precipitation in WWTPs: Causes and solutions. *Water Journal, Australian Water and Wastewater Association*, *21*(6), 21–23. https://issuu.com/australianwater/docs/1994_-_6_-_dec

Cordell, D., Drangert, J.-O., & White, S. (2009). The story of phosphorus: Global food security and food for thought. *Global Environmental Change*, *19*(2), 292–305. https://doi.org/10.1016/j.gloenvcha.2008.10.009

Cordell, D., Rosemarin, A., Schröder, J. J., & Smit, A. L. (2011). Towards global phosphorus security: A systems framework for phosphorus recovery and reuse options. *Chemosphere*, *84*(6), 747–758. https://doi.org/10.1016/j.chemosphere.2011.02.032

Cordell, D., & White, S. (2014). Life's Bottleneck: Sustaining the World's Phosphorus for a Food Secure Future. *Annual Review of Environment and Resources*, *39*(1), 161–188. https://doi.org/10.1146/annurev-environ-010213-113300

Cornel, P., & Schaum, C. (2009). Phosphorus recovery from wastewater: Needs, technologies and costs. *Water Science and Technology*, *59*(6), 1069–1076. https://doi.org/10.2166/wst.2009.045

Crutchik, D., & Garrido, J. (2011). Struvite crystallization versus amorphous magnesium and calcium phosphate precipitation during the treatment of a saline industrial

wastewater. *Water Science and Technology: A Journal of the International Association on Water Pollution Research*, *64*(12), 2460–2467. https://doi.org/10.2166/wst.2011.836

Crutchik, D., & Garrido, J. (2016). Kinetics of the reversible reaction of struvite crystallisation. *Chemosphere*, *154*, 567–572. https://doi.org/10.1016/j.chemosphere.2016.03.134

Crutchik, D., Morales, N., Vázquez-Padín, J. R., & Garrido, J. (2017). Enhancement of struvite pellets crystallization in a full-scale plant using an industrial grade magnesium product. *Water Science and Technology*, *75*(3), 609–618. https://doi.org/10.2166/wst.2016.527

Cullen, N., Baur, R., & Schauer, P. (2013). Three years of operation of North America's first nutrient recovery facility. *Water Science and Technology*, *68*(4), 763–768. https://doi.org/10.2166/wst.2013.260

Daneshgar, S., Callegari, A., Capodaglio, A., & Vaccari, D. (2018). The Potential Phosphorus Crisis: Resource Conservation and Possible Escape Technologies: A Review. *Resources*, *7*(2), 37. https://doi.org/10.3390/resources7020037

Darwish, M., Aris, A., Puteh, M. H., Abideen, M. Z., & Othman, M. N. (2016). Ammonium-Nitrogen Recovery from Wastewater by Struvite Crystallization Technology. *Separation & Purification Reviews*, *45*(4), 261–274. https://doi.org/10.1080/15422119.2015.1119699

Dastur, M. B. (2001). *Investigation into the Factors Affecting Controlled Struvite Crystallization at the Bench-Scale* [Master Thesis, University of British Columbia]. https://open.library.ubc.ca/cIRcle/collections/ubctheses/831/items/1.0063895

Davis, M. L., & Masten, S. J. (2016). *Princípios de Engenharia Ambiental* (3rd ed.). McGraw Hill.

de-Bashan, L. E., & Bashan, Y. (2004). Recent advances in removing phosphorus from wastewater and its future use as fertilizer (1997–2003). *Water Research*, *38*(19), 4222–4246. https://doi.org/10.1016/j.watres.2004.07.014

Delegard, C. H., & Peterson, R. (2019). Precipitation and Crystallization Processes in Reprocessing, Plutonium Separation, Purification and Finishing, Chemical Recovery, and Waste Treatment. In R. Peterson (Ed.), *Engineering Separations Unit Operations for*

Nuclear Processing. CRC Press. https://www.crcpress.com/Engineering-Separations-Unit-Operations-for-Nuclear-Processing/Peterson/p/book/9781138605824

Demeestere, K., Smet, E., Van Langenhove, H., & Galbacs, Z. (2001). Optimalisation of Magnesium Ammonium Phosphate Precipitation and its Applicability to the Removal of Ammonium. *Environmental Technology*, *22*(12), 1419–1428. https://doi.org/10.1080/09593330.2001.11090876

Desmidt, E., Ghyselbrecht, K., Zhang, Y., Pinoy, L., Van der Bruggen, B., Verstraete, W., Rabaey, K., & Meesschaert, B. (2015). Global Phosphorus Scarcity and Full-Scale P-Recovery Techniques: A Review. *Critical Reviews in Environmental Science and Technology*, *45*(4), 336–384. https://doi.org/10.1080/10643389.2013.866531

Doran, P. M. (2013). Unit Operations. In P. M. Doran, *Bioprocess engineering principles* (2nd ed.). Academic Press.

Doyle, J. D., & Parsons, S. (2002). Struvite formation, control and recovery. *Water Research*, *36*(16), 3925–3940. https://doi.org/10.1016/s0043-1354(02)00126-4

Driessen, W., Hendrickx, T., Maxime, R., & Haarhuis, R. (2018). The PHOSPAQ^{TM} process. In C. Schaum (Ed.), *Phosphorus: Polluter and Resource of the Future – Removal and Recovery from Wastewater* (pp. 351–357). International Water Association. https://doi.org/10.2166/9781780408361_351

Drizo, A. (2019). *Phosphorus pollution control: Policies and strategies*. Wiley.

Durrant, A. E., Scrimshaw, M. D., Stratful, I., & Lester, J. N. (1999). Review of the Feasibility of Recovering Phosphate from Wastewater for Use as a Raw Material by the Phosphate Industry. *Environmental Technology*, *20*(7), 749–758. https://doi.org/10.1080/09593332008616870

Egle, L., Rechberger, H., Krampe, J., & Zessner, M. (2016). Phosphorus recovery from municipal wastewater: An integrated comparative technological, environmental and economic assessment of P recovery technologies. *Science of The Total Environment*, *571*, 522–542. https://doi.org/10.1016/j.scitotenv.2016.07.019

Ellis, K. J., & Morrison, J. F. (1982). Buffers of constant ionic strength for studying pH-dependent processes. In D. L. Purich (Ed.), *Methods in Enzymology* (Vol. 87, pp. 405–426). Academic Press. https://doi.org/10.1016/S0076-6879(82)87025-0

Elving, P. J., Markowitz, J. M., & Rosenthal, Isadore. (1956). Preparation of Buffer Systems of Constant Ionic Strength. *Analytical Chemistry*, *28*(7), 1179–1180. https://doi.org/10.1021/ac60115a034

Fang, C., Zhang, T., Jiang, R., & Ohtake, H. (2016). Phosphate enhance recovery from wastewater by mechanism analysis and optimization of struvite settleability in fluidized bed reactor. *Scientific Reports*, *6*(1), 32215. https://doi.org/10.1038/srep32215

Fattah, K. P. (2004). *Pilot scale struvite recovery potential from centrate at Lulu Island Wastewater Treatment Plant* [Master Thesis, University of British Columbia]. https://open.library.ubc.ca/cIRcle/collections/ubctheses/831/items/1.0063488

Fattah, K. P. (2012). Assessing Struvite Formation Potential at Wastewater Treatment Plants. *International Journal of Environmental Science and Development*, *3*(6), 548–552. https://doi.org/DOI: 10.7763/IJESD.2012.V3.284

Fattah, K. P. (2014). Phosphorus and Struvite – Rethinking Their Existence. *International Journal of Advances in Agricultural & Environmental Engineering*, *1*(1). https://doi.org/10.15242/IJCCIE.C0114044

Fattah, K. P., Mavinic, D., Rahaman, M. S., & Koch, F. A. (2009). Development of a Process Control System for Online Monitoring and Control of a Struvite Crystallization Process. In K. I. Ashley, D. S. Mavinic, & F. A. Koch (Eds.), *International Conference on Nutrient Recovery from Wastewater Streams* (pp. 257–268).

Fattah, K. P., Mavinic, D. S., Koch, F. A., & Jacob, C. (2008). Determining the feasibility of phosphorus recovery as struvite from filter press centrate in a secondary wastewater treatment plant. *Journal of Environmental Science and Health, Part A*, *43*(7), 756–764. https://doi.org/10.1080/10934520801960052

Févotte, G., Zhang, X., Qian, G., Zhou, X.-G., & Yuan, W.-K. (2011). Solubility prediction of weak electrolyte mixtures. *ISIC 18 18th International Symposium on Industrial Crystallization*, 145.

Filippelli, G. M. (2011). Phosphate rock formation and marine phosphorus geochemistry: The deep time perspective. *Chemosphere*, *84*(6), 759–766. https://doi.org/10.1016/j.chemosphere.2011.02.019

Flowers, P., Theopold, K., Langley, R., & Robinson, W. R. (2016). *Chemistry*. Openstax. https://opentextbc.ca/chemistry/

Forrest, A. L., Fattah, K. P., Mavinic, D., & Koch, F. A. (2008). Optimizing Struvite Production for Phosphate Recovery in WWTP. *Journal of Environmental Engineering*, *134*(5), 395–402. https://doi.org/10.1061/(ASCE)0733-9372(2008)134:5(395)

Forrest, A. L., Fattah, K. P., Mavinic, D., & Koch, F. A. (2009). Standardizing the struvite solubility product for field trial optimization. In K. Ashley, D. Mavinic, & F. Koch (Eds.), *International Conference on Nutrient Recovery from Wastewater Streams Vancouver, 2009* (pp. 203–213). IWA Publishing. https://doi.org/10.2166/9781780401805

Freiser, H., & Freiser, M. (1992). *Concepts & Calculations in Analytical Chemistry, Featuring the Use of Excel*. CRC Press.

Garrett, R. H., & Grisham, C. M. (2008). *Biochemistry*. Cengage Learning.

Garside, J., Mersmann, A., & Nývlt, J. (2002). *Measurement of crystal growth and nucleation rates*. Institution of Chemical Engineers (IChemE).

Gaterell, M. R., Gay, R., Wilson, R., Gochin, R. J., & Lester, J. N. (2000). An Economic and Environmental Evaluation of the Opportunities for Substituting Phosphorus Recovered from Wastewater Treatment Works in Existing UK Fertiliser Markets. *Environmental Technology*, *21*(9), 1067–1084. https://doi.org/10.1080/09593332108618050

Ghosh, S., Lobanov, S., & Lo, V. K. (2019). An overview of technologies to recover phosphorus as struvite from wastewater: Advantages and shortcomings. *Environmental Science*

and Pollution Research, *26*(19), 19063–19077. https://doi.org/10.1007/s11356-019-05378-6

Girard, J. E. (2005). *Principles of Environmental Chemistry*. Jones & Bartlett Publishers.

Grady, C. P. L., Daigger, G. T., & Lim, H. C. (1999). *Biological wastewater treatment* (2nd ed. rev. and expanded). Marcel Dekker.

Greenberg, A. E., Klein, G., & Kaufman, W. J. (1955). Effect of Phosphorus on the Activated Sludge Process. *Sewage and Industrial Wastes*, *27*(3), 277–282. https://www.jstor.org/stable/25032730

Guadie, A., Xia, S., Jiang, W., Zhou, L., Zhang, Z., Hermanowicz, S. W., Xu, X., & Shen, S. (2014). Enhanced struvite recovery from wastewater using a novel cone-inserted fluidized bed reactor. *Journal of Environmental Sciences*, *26*(4), 765–774. https://doi.org/10.1016/S1001-0742(13)60469-6

Günther, S., Grunert, M., & Müller, S. (2018). Overview of recent advances in phosphorus recovery for fertilizer production. *Engineering in Life Sciences*, *18*(7), 434–439. https://doi.org/10.1002/elsc.201700171

Gutierrez, F., Kinney, K. A., & Katz, L. E. (2020). Phosphorus Speciation in Municipal Wastewater Solids and Implications for Phosphorus Recovery. *Environmental Engineering Science*, ees.2019.0360. https://doi.org/10.1089/ees.2019.0360

Gysin, A., Lycke, D., & Wirtel, S. (2018). The Pearl® and WASSTRIP®processes (Canada). In C. Schaum (Ed.), *Phosphorus: Polluter and resource of the future: Removal and recovery from wastewater* (pp. 359–365). IWA Publishing.

Haandel, A. C. van, & Lubbe, J. G. M. van der. (2015). *Handbook of biological wastewater treatment: Design and optimisation of activated sludge systems.*

Hanhoun, M., Montastruc, L., Azzaro-Pantel, C., Biscans, B., Frèche, M., & Pibouleau, L. (2011). Temperature impact assessment on struvite solubility product: A thermodynamic modeling approach. *Chemical Engineering Journal*, *167*(1), 50–58. https://doi.org/10.1016/j.cej.2010.12.001

Hao, X.-D., & van Loosdrecht, M. C. M. (2003). A proposed sustainable BNR plant with the emphasis on recovery of COD and phosphate. *Water Science and Technology*, *48*(1), 77–85. https://doi.org/10.2166/wst.2003.0021

Hartman, P., & Perdok, W. G. (1955). On the relations between structure and morphology of crystals. I. *Acta Crystallographica*, *8*(1), 49–52. https://doi.org/10.1107/S0365110X55000121

Haynes, W. M. (2016). *CRC Handbook of Chemistry and Physics* (97th edition). CRC Press.

Hitachi Zosen Group Channel. (2019, September 24). *[Hitachi Zosen Group] Recovery Phosporus System—Phosnix® Process* [YouTube video]. https://www.youtube.com/watch?v=ZD7BxEdsDlE&feature=youtu.be

Hobbs, P. (2004). Phosphorus recovery fromunprocessed manure. In E. Valsami-Jones (Ed.), *Phosphorus in environmental technologies: Principles and applications* (pp. 507–520). IWA Publ.

Hruska, K. (2017). Overview of Phosphorus Homeostasis. In O. M. Gutiérrez, K. Kalantar-Zadeh, & R. Mehrotra (Eds.), *Clinical Aspects of Natural and Added Phosphorus in Foods* (pp. 11–28). Springer.

Huang, H. (2003). *Pilot Scale Phosphorus Recovery from Anaerobic Digester Supernatant* [Master Thesis, University of British Columbia]. https://open.library.ubc.ca/cIRcle/collections/ubctheses/831/items/1.0063536

Hutnik, N., Piotrowski, K., Wierzbowska, B., & Matynia, A. (2011). Continuous reaction crystallization of struvite from phosphate(V) solutions containing calcium ions. *Crystal Research and Technology*, *46*(5), 443–449. https://doi.org/10.1002/crat.201100049

Iqbal, M., Bhuiyan, H., & Mavinic, D. S. (2008). Assessing struvite precipitation in a pilot-scale fluidized bed crystallizer. *Environmental Technology*, *29*(11), 1157–1167. https://doi.org/10.1080/09593330802075452

IUPAC. (1997). *Compendium of Chemical Terminology, 'the Gold Book', compiled by A. D. McNaught and A. Wilkinson* (2nd ed.). Blackwell Scientific Publications, online version (2019-) created by S. J. Chalk. https://doi.org/10.1351/goldbook

Jaffer, Y., & Pearce, P. (2004). Phosphorus recovery via struvite production at Slough sewage treatment works, UK – a case study. In E. Valsami-Jones (Ed.), *Phosphorus in environmental technologies: Principles and applications* (pp. 402–427). IWA Publ.

Janssen, P. M. J. (2002). *Biological phosphorus removal: Manual for design and operation*. IWA.

Jeyanayagam, S. (2018). Phosphorus recovery—The North American perspective. In C. Schaum (Ed.), *Phosphorus: Polluter and resource of the future: Removal and recovery from wastewater*. IWA Publishing.

Jeyanayagam, S., Hahn, T., Fergen, R., & Boltz, J. (2012). Nutrient Recovery, an Emerging Component of a Sustainable Biosolids Management Program. *Proceedings of the Water Environment Federation*, *2012*(2), 1078–1088. https://doi.org/10.2175/193864712811693830

Jeyanayagam, S., Khunjar, W., & Mehta, C. (2016). Accelerating the Implementation of Extractive Nutrient Recovery as An Integral Component of Sustainable Nutrient Management. *Water E-Journal*, 1–8. https://doi.org/10.21139/wej.2016.010

Johnston, A. E. (2000). Soil and Plant Phosphate. *International Fertilizer Industry Association*, 46. https://repository.rothamsted.ac.uk/item/88q93/soil-and-plant-phosphate

Jones, A. (2002). *Crystallization Process Systems* (A. Jones, Ed.). Butterworth-Heinemann.

Jönsson, H., Stintzing, A. R., Vinnerås, B., & Salomon, E. (2004). *Guidelines on the Use of Urine and Faeces in Crop Production.* (EcoSanRes). Stockholm Environment Institute.

Kabbe, C. (2019). Circular Economy: Bridging The Gap Between Phosphorus Recovery and Recycling. In H. Ohtake & S. Tsuneda (Eds.), *Phosphorus Recovery and Recycling* (pp. 45–59). Springer, Singapore. https://doi.org/10.1007/978-981-10-8031-9

Kabbe, C., & Rinck-Pfieffer, S. (2019). *Global Compendium on Phosphorus Recovery from Sewage/Sludge/Ash.* Global Water Research Coalition.

Kang, S. J., Olmstead, K., Takacs, K., & Collins, J. (2008). *Municipal Nutrient Removal Technologies Reference Document* (Technical Report No. 832-R-08–006). U.S Environmental Protection Agency, Office of Wastewater Management, Municipal Support Division.

Kataki, S., & Baruah, D. C. (2018). Prospects and Issues of Phosphorus Recovery as Struvite from Waste Streams. In C. M. Hussain (Ed.), *Handbook of Environmental Materials Management* (pp. 1–50). Springer International Publishing. https://doi.org/10.1007/978-3-319-58538-3_19-1

Khopkar, A. R., & Ranade, V. V. (2019). Stirred Vessels: Computational modelling of multiphase flows and mixing. In David J. am Ende & Mary T. am Ende (Eds.), *Chemical Engineering in the Pharmaceutical Industry: Active Pharmaceutical Ingredients* (2nd ed., pp. 261–318). Wiley & Sons.

Kim, Daegi, Min, K. J., Lee, K., Yu, M. S., & Park, K. Y. (2016). Effects of pH, molar ratios and pre-treatment on phosphorus recovery through struvite crystallization from effluent of anaerobically digested swine wastewater. *Environmental Engineering Research*, *22*(1), 12–18. https://doi.org/10.4491/eer.2016.037

Kim, Daekeun, Kim, J., Ryu, H.-D., & Lee, S.-I. (2009). Effect of mixing on spontaneous struvite precipitation from semiconductor wastewater. *Bioresource Technology*, *100*(1), 74–78. https://doi.org/10.1016/j.biortech.2008.05.024

Koch, F. A., Mavinic, D. S., Yonemitsu, N., & Britton, A. T. (2009). *Fluidized Bed Wastewater Treatment* (US Patent and Trademark Office Patent No. US 7,622,047).

Koga, D. (2019). Struvite Recovery from Digested Sewage Sludge. In H. Ohtake & S. Tsuneda (Eds.), *Phosphorus Recovery and Recycling* (pp. 255–264). Springer, Singapore. https://doi.org/10.1007/978-981-10-8031-9

Koga, D., & Hagino, T. (2016). Technology for high efficiency phosphorus removal and recovery from digested sewage sludge. *Environ. Sol. Technol.*, *15*(3).

Korchef, A., Saidou, H., & Amor, M. B. (2011). Phosphate recovery through struvite precipitation by CO2 removal: Effect of magnesium, phosphate and ammonium concentrations. *Journal of Hazardous Materials*, *186*(1), 602–613. https://doi.org/10.1016/j.jhazmat.2010.11.045

Korving, L., Loosdrecht, M. V., & Philipp Wilfert. (2019). Effect of Iron on Phosphate Recovery from Sewage Sludge. In H. Ohtake & S. Tsuneda (Eds.), *Phosphorus Recovery and Recycling* (pp. 303–326). Springer, Singapore. https://doi.org/10.1007/978-981-10-8031-9

Kuba, T., Smolders, G., van Loosdrecht, M. C. M., & Heijnen, J. J. (1993). Biological Phosphorus Removal from Wastewater by Anaerobic-Anoxic Sequencing Batch Reactor. *Water Science and Technology*, *27*(5–6), 241–252. https://doi.org/10.2166/wst.1993.0504

Kulaev, I. S. (1979). *The biochemistry of inorganic polyphosphates*. Wiley.

Kumar, R., & Pal, P. (2015). Assessing the feasibility of N and P recovery by struvite precipitation from nutrient-rich wastewater: A review. *Environmental Science and Pollution Research*, *22*(22), 17453–17464. https://doi.org/10.1007/s11356-015-5450-2

Kunii, D., & Levenspiel, O. (2012). *Fluidization engineering*. Elsevier;

Latifian, M., Liu, J., & Mattiasson, B. (2012). Struvite-based fertilizer and its physical and chemical properties. *Environmental Technology*, *33*(24), 2691–2697. https://doi.org/10.1080/09593330.2012.676073

Latifian, M., Liu, J., & Mattiasson, B. (2014). Recovery of struvite via coagulation and flocculation using natural compounds. *Environmental Technology*, *35*(18), 2289–2295. https://doi.org/10.1080/09593330.2014.902110

Lavelle, P., Dugdale, R., Scholes, R., Berhe, A. A., Carpenter, E., & et al. (2005). Nutrient cycling. In R. Hassan, R. Scholes, & N. Ash (Eds.), *Ecosystemsand Human Well-being: Current State and Trends* (Millenn. Ecosyst. Assess. Ser, Vol. 1, pp. 331–353). Island Press. http://www.millenniumassessment.org/documents/document.281.aspx.pdf

Le Corre, K., Valsami-Jones, E., Hobbs, P., & Parsons, S. (2009). Phosphorus Recovery from Wastewater by Struvite Crystallization: A Review. *Critical Reviews in Environmental Science and Technology*, *39*(6), 433–477. https://doi.org/10.1080/10643380701640573

Le Corre, K., Valsami-Jones, E., Hobbs, P., & Parsons, S. A. (2005). Impact of calcium on struvite crystal size, shape and purity. *Journal of Crystal Growth*, *283*(3–4), 514–522. https://doi.org/10.1016/j.jcrysgro.2005.06.012

Lee, P. E. R. M. (2017). *Nutrient Recovery Solutions* [PDF]. Ohio Water Environment Association. https://ohiowea.org/docs/180926_NRS_OhioNutrients.pdf

Lehninger, A. L. (1973). *Short Course in Biochemistry*. Worth Publishers.

Li, B., Boiarkina, I., Yu, W., Huang, H. M., Munir, T., Wang, G. Q., & Young, B. R. (2019). Phosphorous recovery through struvite crystallization: Challenges for future design. *Science of The Total Environment*, *648*, 1244–1256. https://doi.org/10.1016/j.scitotenv.2018.07.166

Li, B., Huang, H. M., Boiarkina, I., Yu, W., Huang, Y. F., Wang, G. Q., & Young, B. R. (2019). Phosphorus recovery through struvite crystallisation: Recent developments in the understanding of operational factors. *Journal of Environmental Management*, *248*, 109254. https://doi.org/10.1016/j.jenvman.2019.07.025

Liu, Y., Kumar, S., Kwag, J.-H., & Ra, C. (2012). Magnesium ammonium phosphate formation, recovery and its application as valuable resources: A review. *Journal of Chemical Technology & Biotechnology*, *88*(2), 181–189. https://doi.org/10.1002/jctb.3936

Lodish, H., Berk, A., Zipursky, S. L., Matsudaira, P., Baltimore, D., & Darnell, J. (2000). Chemical Equilibrium. In *Molecular Cell Biology. 4th edition.* https://www.ncbi.nlm.nih.gov/books/NBK21503/

Lötter, G., Wentzel, M. C., Loewenthal, R. E., Ekama, G. A., & Marais, G. v. R. (1986). A study of selected characteristics of Acinetobacter ssp. Isolated from activated sludge in anaerobic/anoxic/aerobic and aerobic systems. *Water SA*, *12*, 203–208.

MacIntyre, F. (1976). Concentration scales: A plea for physico-chemical data. *Marine Chemistry*, *4*, 205–224.

Martell, A. E., & Smith, R. M. (1989). *Critical Stability Constants*. Plenum Press.

Martí, N., Bouzas, A., Seco, A., & Ferrer, J. (2008). Struvite precipitation assessment in anaerobic digestion processes. *Chemical Engineering Journal*, *141*(1–3), 67–74. https://doi.org/10.1016/j.cej.2007.10.023

Martí, N., Pastor, L., Bouzas, A., Ferrer, J., & Seco, A. (2010). Phosphorus recovery by struvite crystallization in WWTPs: Influence of the sludge treatment line operation. *Water Research*, *44*(7), 2371–2379. https://doi.org/10.1016/j.watres.2009.12.043

Mavinic, D., Koch, F. A., Huang, H., & Lo, K. V. (2007). Phosphorus recovery from anaerobic digester supernatants using a pilot-scale struvite crystallization process. *Journal of Environmental Engineering and Science*, *6*(5), 561–571. https://doi.org/10.1139/S07-007

McGrath, J. W., & Quinn, J. P. (2004). Biological phosphorus removal. In E. Valsami-Jones (Ed.), *Phosphorus in environmental technologies: Principles and applications* (pp. 272–290). IWA Publ.

McTigue, N. E., Symons, J. M., & American Water Works Association (Eds.). (2010). *The water dictionary: A comprehensive reference of water terminology* (2nd ed.). American Water Works Association.

Mehta, C. M., & Batstone, D. J. (2013). Nucleation and growth kinetics of struvite crystallization. *Water Research*, *47*(8), 2890–2900. https://doi.org/10.1016/j.watres.2013.03.007

Michałowska-Kaczmarczyk, A. M., & Michałowski, T. (2015). Solubility product challenge. *Analytical and Bioanalytical Chemistry*, *407*(7), 1789–1791. https://doi.org/10.1007/s00216-014-8407-2

Min, K. J., Kim, D., Lee, J., Lee, K., & Park, K. Y. (2019). Characteristics of vegetable crop cultivation and nutrient releasing with struvite as a slow-release fertilizer. *Environmental Science and Pollution Research*, *26*(33), 34332–34344. https://doi.org/10.1007/s11356-019-05522-2

Mines Jr, R. O. (2014). *Environmental Engineering: Principles and Practice* (1st edition). Wiley-Blackwell.

Minnesota Pollution Control Agency. (2006). *Phosphorus Treatment and Removal Technologies.*

Misselhorn, A., Challinor, A., Thornton, P., Jones, J., Schaldach, R., & Plocq-Fichelet, V. (2010). Surprises and Possibilities. In J. Ingram, P. Ericksen, & D. Liverman (Eds.), *Food Security and Global Environmental Change*. Taylor & Francis.

Moore, J. W., Stanitski, C. L., & Jurs, P. C. (2010). *Chemistry: The Molecular Science*. Cengage Learning.

Morel, F. M. M. (1983). *Principles of Aquatic Chemistry*. John Wiley & Sons.

Morse, G., Brett, S., Guy, J., & Lester, J. (1998). Review: Phosphorus removal and recovery technologies. *The Science of The Total Environment*, *212*(1), 69–81. https://doi.org/10.1016/S0048-9697(97)00332-X

Motlagh, A. M., & Goel, R. K. (2014). Sustainability of Activated Sludge Processes. In *Water Reclamation and Sustainability* (pp. 391–414). Elsevier. https://doi.org/10.1016/B978-0-12-411645-0.00016-X

Mousa, K. M., & Dawood, Z. E. (2015). Study on Dynamics of Saponification Process Using State Space Model. *American Journal of Chemical Engineering*, *3*(4), 52. https://doi.org/10.11648/j.ajche.20150304.11

Muhmood, A., Lu, J., Dong, R., & Wu, S. (2019). Formation of struvite from agricultural wastewaters and its reuse on farmlands: Status and hindrances to closing the nutrient loop. *Journal of Environmental Management*, *230*, 1–13. https://doi.org/10.1016/j.jenvman.2018.09.030

Mulkerrins, D., Dobson, A. D. W., & Colleran, E. (2004). Parameters affecting biological phosphate removal from wastewaters. *Environment International*, *30*(2), 249–259. https://doi.org/10.1016/S0160-4120(03)00177-6

Mullin, J. (2001). *Crystallization* (4th ed.). Butterworth-Heinemann.

Mullin, J. (2003). Crystallization and Precipitation. In F. Ullmann, *Ullmann's Encyclopedia of Industrial Chemistry*. Wiley-VCH. 10.1002/14356007.b02_03

Münch, E. V., & Barr, K. (2001). Controlled struvite crystallisation for removing phosphorus from anaerobic digester sidestreams. *Water Research*, *35*(1), 151–159. https://doi.org/10.1016/S0043-1354(00)00236-0

Muster, T. H., Douglas, G. B., Sherman, N., Seeber, A., Wright, N., & Güzükara, Y. (2013). Towards effective phosphorus recycling from wastewater: Quantity and quality. *Chemosphere*, *91*(5), 676–684. https://doi.org/10.1016/j.chemosphere.2013.01.057

Myerson, A., & Ginde, R. (2002). Crystals, Crystal Growth and Nucleation. In A. Myerson (Ed.), *Handbook of Industrial Crystallization* (2nd ed., pp. 33–65). Butterworth-Heinemann.

Myerson, A., & Schwartz, A. M. (2002). Solutions and solutions properties. In A. Myerson (Ed.), *Handbook of Industrial Crystallization* (2nd ed., pp. 1–30). Butterworth-Heinemann.

Nättorp, A., Kabbe, C., Matsubae, K., & Ohtake, H. (2019). Development of Phosphorus Recycling in Europe and Japan. In H. Ohtake & S. Tsuneda (Eds.), *Phosphorus Recovery and Recycling* (pp. 3–27). Springer, Singapore. https://doi.org/10.1007/978-981-10-8031-9

Nelson, N. O., Mikkelsen, R. L., & Hesterberg, D. L. (2003). Struvite precipitation in anaerobic swine lagoon liquid: Effect of pH and Mg:P ratio and determination of rate constant. *Bioresource Technology*, *89*(3), 229–236. https://doi.org/10.1016/s0960-8524(03)00076-2

Nenov, V., Jemendjiev, H., Peeva, G., Bonev, B., & Zerrouq, F. (2016). Struvite recovery options in conventional wastewater treatment plants (WWTPs). *J. Mater. Environ. Sci.*, *7*(1), 113–122. https://www.researchgate.net/publication/297047665_Struvite_recovery_options_in_conventional_wastewater_treatment_plants_WWTPs

Nienow, A. W., & Paul, E. L. (2016). Mixing Issues in Crystallization and Precipitation Operations. In S. M. Kresta, A. W. E. III, D. S. Dickey, V. A. Atiemo-Obeng, & N. A. M. Forum, *Advances in Industrial Mixing: A Companion to the Handbook of Industrial Mixing* (pp. 665–672). John Wiley & Sons.

OECD. (2015). *Material Resources, Productivity and the Environment*. OECD Publishing. https://doi.org/10.1787/9789264190504-en.

Oh, S. T., Kim, J. R., Premier, G. C., Lee, T. H., Kim, C., & Sloan, W. T. (2010). Sustainable wastewater treatment: How might microbial fuel cells contribute. *Biotechnology Advances*, *28*(6), 871–881. https://doi.org/10.1016/j.biotechadv.2010.07.008

Ohlinger, K. (1999). *Struvite Controls in Anaerobic Digestion and Post-digestion Wastewater Treatment Processes*. University of California, Davis.

Ohlinger, K., P.E., Young, T. M., & Schroeder, E. D. (1999). Kinetics Effects on Preferential Struvite Accumulation in Wastewater. *Journal of Environmental Engineering*, *125*(8), 730–737. https://doi.org/10.1061/(ASCE)0733-9372(1999)125:8(730)

Ohlinger, K., Young, T. M., & Schroeder, E. D. (1998). Predicting struvite formation in digestion. *Water Research*, *32*(12), 3607–3614. https://doi.org/10.1016/S0043-1354(98)00123-7

Ohlinger, K., Young, T. M., & Schroeder, E. D. (2000). Postdigestion Struvite Precipitation Using a Fluidized Bed Reactor. *Journal of Environmental Engineering*, *126*(4), 361–368. https://doi.org/10.1061/(ASCE)0733-9372(2000)126:4(361)

Ojha, N., & Prabhakar, B. (2013). Advances in solubility enhancement techniques. *Int J Pharm Sci Rev Res*, *21(2)*, 351–358.

Omar, B., Entrena, M., González-Muñoz, M. T., Arias, J. M., & Huertas, F. (1994). Effects of pH and phosphate on the production of struvite by Myxococcus xanthus. *Geomicrobiology Journal*, *12*(2), 81–90. https://doi.org/10.1080/01490459409377974

Omar, W., & Ulrich, J. (1999). Ultrasonic methods for the control and study of batch crystallization processes. *14th International Symposium on Industrial Crystallization.*

Ortwein, B. (2018). AirPrex® sludge optimization and struvite recovery from digested sludge. In C. Schaum (Ed.), *Phosphorus: Polluter and Resource of the Future – Removal and Recovery from Wastewater* (pp. 343–350). International Water Association. https://doi.org/10.2166/9781780408361_343

Ostara. (2017). *Water Resource Recovery Facility Employing Ostara Nutrient Recovery Technologies* [PDF]. Ostara. http://ostara.com/wp-content/uploads/2017/04/EU_Ostara_ProcessFlowDiagram_Handout_170411.pdf

Ostara. (2020a). *Ostara Nutrient Management Solutions.* https://ostara.com/

Ostara. (2020b). *OSTARA Pearl®* [PDF]. http://ostara.com/wp-content/uploads/2018/08/EU_Ostara_Pearl-Handout-180424.pdf

Ostwald, W. (1897). Studien über die Bildung und Umwandlung fester Körper. *Zeitschrift Für Physikalische Chemie*, *22*, 289-330. https://doi.org/10.1515/zpch-1897-2233

Ovivo. (n.d.-a). *Phospaq Process—Operating Principle* [PDF]. Phospaq Process. Retrieved 3 April 2020, from https://d15l97oqcgwsnl.cloudfront.net/wp-content/uploads/2017/09/Ovivo-PhosPAQ-Brochure-0927_WEB.pdf?x38011

Ovivo. (n.d.-b). *Phospaq—Applications* [HTML]. Ovivo. Retrieved 4 April 2020, from https://www.ovivowater.com/product/municipal/municipal-wastewater/aerobic-treatment-nutrient-removal/sidestream-treatment/phospaq/

Özkaya, B., Kaksonen, A. H., Sahinkaya, E., & Puhakka, J. A. (2019). Fluidized bed bioreactor for multiple environmental engineering solutions. *Water Research*, *150*, 452–465. https://doi.org/10.1016/j.watres.2018.11.061

Pahren, H., & Jakubowski, W. (1980). *Wastewater Aerosols and Disease, Proceedings of a Symposium Held at Cincinnati, Ohio on September 19-21, 1979* (Report 600/9-80–028). U.S Environmental Protection Agency.

Parsons, S., & Berry, T.-A. (2004). Chemical phosphorus removal. In E. Valsami-Jones (Ed.), *Phosphorus in environmental technologies: Principles and applications* (pp. 260–271). IWA Publ.

Parsons, S., & Smith, J. A. (2008). Phosphorus Removal and Recovery from Municipal Wastewaters. *Elements*, *4*(2), 109–112. https://doi.org/10.2113/GSELEMENTS.4.2.109

Pastor, L., Mangin, D., Barat, R., & Seco, A. (2008). A pilot-scale study of struvite precipitation in a stirred tank reactor: Conditions influencing the process. *Bioresource Technology*, *99*(14), 6285–6291. https://doi.org/10.1016/j.biortech.2007.12.003

Petzet, S., & Cornel, P. (2012). Prevention of Struvite Scaling in Digesters Combined With Phosphorus Removal and Recovery—The FIX-Phos Process. *Water Environment Research*, *84*(3), 220–226. https://doi.org/10.2175/106143012X13347678384125

Pierrou, U. (1976). The Global Phosphorus Cycle. *Ecological Bulletins. Nitrogen Phosphorus Sulphur Glob. Cycles Scope Rep*, *22*, 75–88. JSTOR. https://www.jstor.org/stable/20112522

Prabesh, K. C. (2018). *New opportunities of nutrient recycling in water services*. Häme University of Applied Sciences.

Puchongkawarin, C., Gomez-Mont, C., Stuckey, D. C., & Chachuat, B. (2015). Optimization-based methodology for the development of wastewater facilities for energy and nutrient recovery. *Chemosphere*, *140*, 150–158. https://doi.org/10.1016/j.chemosphere.2014.08.061

Rahaman, S., Ellis, N., & Mavinic, D. S. (2008). Effects of various process parameters on struvite precipitation kinetics and subsequent determination of rate constants. *Water Science and Technology*, *57*(5), 647–654. https://doi.org/10.2166/wst.2008.022

Rahaman, S., Mavinic, D., Bhuiyan, M. I. H., & Koch, F. A. (2006). Exploring the Determination of Struvite Solubility Product from Analytical Results. *Environmental Technology*, *27*(9), 951–961. https://doi.org/10.1080/09593332708618707

Rahaman, S., Mavinic, D. S., A. T. Briton, Zhang, M., Fattah, K. P., & Koch, F. A. (2009). *Numerical investigations of the hydrodynamics of the UBC MAP fluidized bed crystallizer* (K. I. Ashley, D. S. Mavinic, F. A. Koch, & International Water Association, Eds.; pp. 131–143). IWA Publishing.

Rahman, M., Liu, Y., Kwag, J.-H., & Ra, C. (2011). Recovery of struvite from animal wastewater and its nutrient leaching loss in soil. *Journal of Hazardous Materials*, *186*(2–3), 2026–2030. https://doi.org/10.1016/j.jhazmat.2010.12.103

Rahman, M., Salleh, M. A. Mohd., Rashid, U., Ahsan, A., Hossain, M. M., & Ra, C. S. (2014). Production of slow release crystal fertilizer from wastewaters through struvite crystallization – A review. *Arabian Journal of Chemistry*, *7*(1), 139–155. https://doi.org/10.1016/j.arabjc.2013.10.007

Randall, C. W., Barnard, J. L., & Stensel, H. D. (1992). Design of Activated Sludge Biological Nutrient Removal Plants. In C. W. Randall, J. L. Barnard, & H. D. Stensel (Eds.), *Design and retrofit of wastewater treatment plants for biological nutrient removal* (Vol. 5, pp. 97–184). Technomic Pub. Co.

Regy, S., Mangin, D., Klein, J. P., & Lieto, J. (2002). *Phosphate recovery by struvite precipitation in a stirred reactor* (pp. 1–65) [Lagep Report]. Lagep (laboratoire dautomatique et de genie des procedes)/CEEP(Centre Europe´en d'Etude des Polyphosphates.

http://www.nhm.ac.uk/research-curation/departments/mineralogy/researchgroups/phosphaterecovery/LagepReportS.

Ridder, M. de, Jon, S. de, Polcha, J., & Lingemann, S. (2012). *Risks and Opportunities in the Global Phosphate Rock Market* (No. No 17 , 12 , 12; Robust Strategies in Times of Uncertainty). The Hague Centre for Strategic Studies (HCSS).

Robinson, D. A., & Woollard, J. M. (1982). *Chemistry for Colleges and Schools.* Macmillan International Higher Education.

Ronteltap, M., Maurer, M., & Gujer, W. (2007). Struvite precipitation thermodynamics in source-separated urine. *Water Research*, *41*(5), 977–984. https://doi.org/10.1016/j.watres.2006.11.046

Rosemarin, A., Bruijne, G. D., & Caldwell, I. (2009). Peak phosphorus: The next inconvenient truth. *The Broker*, *15*, 6–9. https://www.researchgate.net/publication/286783173_Peak_phosphorus_the_next_inconvenient_truth

Rudolph, P. (2015). *Handbook of Crystal Growth. Bulk Crystal Growth: Basic Techniques* (Peter Rudolph, Ed.; 2nd ed., Vols 2, Part A). Elsevier.

Ruttenberg, K. C. (2003). The Global Phosphorus Cycle. In *Treatise on Geochemistry* (pp. 585–643). Elsevier. https://doi.org/10.1016/B0-08-043751-6/08153-6

Ryan, M. P., Boyce, A., & Walsh, G. (2016). *Identification and evaluation of phosphorus recovery technologies in an Irish context* (Research Report No. 189). EPA research. 978-1-84095-667-2

Saidou, H., Korchef, A., Ben Moussa, S., & Ben Amor, M. (2009). Struvite precipitation by the dissolved CO2 degasification technique: Impact of the airflow rate and pH. *Chemosphere*, *74*(2), 338–343. https://doi.org/10.1016/j.chemosphere.2008.09.081

Salmi, T., Mikkola, J.-P., & Warna, J. (2019). *Chemical Reaction Engineering and Reactor Technology* (Second edition). Taylor & Francis, a CRC title, part of the Taylor & Francis imprint, a member of the Taylor & Francis Group, the academic division of T&F Informa, plc.

Satyaprakash, M., Sadhana, E. U. B. R., & Vani, S. S. (2017). Phosphorous and Phosphate Solubilising Bacteria and their Role in Plant Nutrition. *International Journal of Current Microbiology and Applied Sciences*, *6*(4), 2133–2144. https://doi.org/10.20546/ijcmas.2017.604.251

Schauer, P. (2015). *Six Years of Nutrient Recovery at Clean Water Services* [PDF]. Metropolitan Water Reclamation District of Greater Chicago. https://mwrd.org/sites/default/files/documents/seminar_series-09-25-2015_Waste_Activated.pdf

Schauer, P., & Laney, B. (2015). Continued Evolution of the WASSTRIP Process. *Proceedings of the Water Environment Federation*, *2015*(19), 4978–4991. https://doi.org/10.2175/193864715819538822

Schipper, W. (2019). Success Factors for Implementing Phosphorus Recycling Technologies. In H. Ohtake & S. Tsuneda (Eds.), *Phosphorus Recovery and Recycling* (pp. 101–130). Springer, Singapore. https://doi.org/10.1007/978-981-10-8031-9

Scholz, R. W. (2019). Foreword: Phosphorus Recycling—Mending a Broken Biogeochemical Cycl. In H. Ohtake & S. Tsuneda (Eds.), *Phosphorus Recovery and Recycling* (pp. v–x). Springer, Singapore. https://doi.org/10.1007/978-981-10-8031-9

Scholz, R. W., Roy, A. H., & Hellums, D. T. (2014). Sustainable Phosphorus Management: A Transdisciplinary Challenge. In R. W. Scholz, A. H. Roy, F. S. Brand, D. T. Hellums, & A. Ulrich (Eds.), *Sustainable Phosphorus Management* (pp. 1–128). Springer Netherlands. https://doi.org/10.1007/978-94-007-7250-2_1

Scholz, R. W., Ulrich, A., Eilittä, M., & Roy, A. (2013). Sustainable use of phosphorus: A finite resource. *Science of The Total Environment*, *461–462*, 799–803. https://doi.org/10.1016/j.scitotenv.2013.05.043

Schoumans, O. F., Bouraoui, F., Kabbe, C., Oenema, O., & van Dijk, K. C. (2015). Phosphorus management in Europe in a changing world. *AMBIO*, *44*(S2), 180–192. https://doi.org/10.1007/s13280-014-0613-9

Schröder, J. J., Cordell, D., Smit, A. L., & Rosemarin, A. (2010). *Sustainable Use of Phosphorus* (No. 357). Plant Research International, Wageningen UR Business Unit Agrosystems.

Seckler, M. M., Bruinsma, O. S. L., & Van Rosmalen, G. M. (1996). Phosphate removal in a fluidized bed—I. Identification of physical processes. *Water Research*, *30*(7), 1585–1588. https://doi.org/10.1016/0043-1354(96)00018-8

Shaddel, S., Ucar, S., Andreassen, J.-P., & Østerhus, S. W. (2019). Engineering of struvite crystals by regulating supersaturation – Correlation with phosphorus recovery, crystal morphology and process efficiency. *Journal of Environmental Chemical Engineering*, *7*(1), 102918. https://doi.org/10.1016/j.jece.2019.102918

Shih, K., & Yan, H. (2016). The Crystallization of Struvite and Its Analog (K-Struvite) From Waste Streams for Nutrient Recycling. In *Environmental Materials and Waste* (pp. 665–686). Elsevier. https://doi.org/10.1016/B978-0-12-803837-6.00026-3

Shu, L., Schneider, P., Jegatheesan, V., & Johnson, J. (2006). An economic evaluation of phosphorus recovery as struvite from digester supernatant. *Bioresource Technology*, *97*(17), 2211–2216. https://doi.org/10.1016/j.biortech.2005.11.005

Smil, V. (2000). Phosphorus in the environment: Natural flows and human interferences. *Annual Review of Energy and the Environment*, *25*(1), 53–88. https://doi.org/10.1146/annurev.energy.25.1.53

Snoeyink, V. L., & Jenkins, D. (1980). *Water Chemistry*. John Wiley & Sons.

Stratful, I., Brett, S., Scrimshaw, M. B., & Lester, J. N. (1999). Biological Phosphorus Removal, Its Role in Phosphorus Recycling. *Environmental Technology*, *20*(7), 681–695. https://doi.org/10.1080/09593332008616863

Stratful, I., Scrimshaw, M. D., & Lester, J. N. (2001). Conditions influencing the precipitation of magnesium ammonium phosphate. *Water Research*, *35*(17), 4191–4199. https://doi.org/10.1016/S0043-1354(01)00143-9

Stumm, W., & Morgan, J. J. (1996). *Aquatic chemistry: Chemical equilibria and rates in natural waters*. Wiley & Sons.

Tai, C. Y.-D., Chen, P.-C., & Chien, W.-C. (2006). Particle Nucleation and Growth. In P. Somasundaran (Ed.), *Encyclopedia of Surface and Colloid Science* (2nd ed., Vol. 6, pp. 4452–4466). CRC Press.

Tailford, J. (n.d.). *Lulu Island Wastewater Treatment Plant* [PDF]. Environmental Operators Certification Program. Retrieved 8 April 2020, from https://eocp.ca/wp-content/uploads/2012/10/plants-Lulu-Island.pdf

Tansel, B., Lunn, G., & Monje, O. (2018). Struvite formation and decomposition characteristics for ammonia and phosphorus recovery: A review of magnesium-ammonia-phosphate interactions. *Chemosphere*, *194*, 504–514. https://doi.org/10.1016/j.chemosphere.2017.12.004

Taylor, A. W., Frazier, A. W., Gurney, E. L., & Smith, J. P. (1963). Solubility products of di- and trimagnesium phosphates and the dissociation of magnesium phosphate solutions. *Transactions of the Faraday Society*, *59*(0), 1585–1589. https://doi.org/10.1039/TF9635901585

Tchobanoglous, G., & Burton, F. L. (1991). *Wastewater Engineering* (3rd ed.). McGraw-Hill.

ter Horst, J. H., Bedeaux, D., & Kjelstrup, S. (2011). The role of temperature in nucleation processes. *The Journal of Chemical Physics*, *134*(5), 054703. https://doi.org/10.1063/1.3544689

Thornton, C. (1998). *International Conference on Phosphorus Recovery from Sewage and Animal Wastes—Summary of conclusions and discussions.* https://phosphorusplatform.eu/images/download/Warwick-1998-1st-P-Recovery-and-Recycling-conference-summary--papers.pdf

Tomašić, V., & Zelić, B. (2018). *Environmental Engineering: Basic Principles* (B. Zelić & V. Tomašić, Eds.). De Gruyter.

Toyokura, K. (1993). Crystallization Concepts. In J. J. McKetta, *Unit Operations Handbook:* (1st ed., Vol. 1). CRC Press.

Tro, N. J. (2015). *Principles of Chemistry: A Molecular Approach.* Pearson Education.

Tsobanoglou, G., & Schroeder, E. D. (1985). *Water Quality: Characteristics, Modeling, Modification.* Addison-Wesley.

Türker, M., & Çelen, İ. (2010). Chemical equilibrium model of struvite precipitation from anaerobic digester effluents. *Turkish J. Eng. Env. Sci.*, *34*, 39 – 48. https://doi.org/10.3906/muh-1008-15

Turovskiy, I. S., & Mathai, P. K. (2006). *Wastewater Sludge Processing*. John Wiley & Sons, Inc. https://doi.org/10.1002/047179161X

Ueno, Y. (2004). Full scale struvite recovery in Japan. In E. Valsami-Jones (Ed.), *Phosphorus in environmental technologies: Principles and applications* (pp. 496–506). IWA Publ.

Ueno, Y., & Fujii, M. (2001). Three Years Experience of Operating and Selling Recovered Struvite from Full-Scale Plant. *Environmental Technology*, *22*(11), 1373–1381. https://doi.org/10.1080/09593332208618196

Ulrich, J., & Strege, C. (2002). Some aspects of the importance of metastable zone width and nucleation in industrial crystallizers. *Journal of Crystal Growth*, *237–239*, 2130–2135. https://doi.org/10.1016/S0022-0248(01)02284-9

Vedantam, S., & Ranade, V. V. (2013). Crystallization: Key thermodynamic, kinetic and hydrodynamic aspects. *Sadhana*, *38*(6), 1287–1337. https://doi.org/10.1007/s12046-013-0195-4

Vu, T. . T. . L., Hourigan, J. A., Sleigh, R. W., Ang, M. H., & Tade, M. O. (2003). Metastable control of cooling crystallisation. In *Computer Aided Chemical Engineering* (Vol. 14, pp. 527–532). Elsevier. https://doi.org/10.1016/S1570-7946(03)80169-4

Wagh, A., & Martini, S. (2017). Crystallization Behavior of Fats. In C. C. Akoh (Ed.), *Food lipids: Chemistry, nutrition, and biotechnology* (Fourth edition). CRC Press.

Wagner, M., & Loy, A. (2002). Bacterial community composition and function in sewage treatment systems. *Current Opinion in Biotechnology*, *13*(3), 218–227. https://doi.org/10.1016/S0958-1669(02)00315-4

Walker, C. (2017). Market Map—Beating the burn rate for resource and energy recovery from sludge. *Global Water Intelligence*, *1*, 40–47.

Wang, F., Fu, R., Lv, H., Zhu, G., Lu, B., Zhou, Z., Wu, X., & Chen, H. (2019). Phosphate Recovery from Swine Wastewater by a Struvite Precipitation Electrolyzer. *Scientific Reports*, *9*(1), 8893. https://doi.org/10.1038/s41598-019-45085-3

Wang, J., Burken, J. G., Zhang, X. (Jackie), & Surampalli, R. (2005). Engineered Struvite Precipitation: Impacts of Component-Ion Molar Ratios and pH. *Journal of Environmental Engineering*, *131*(10), 1433–1440. https://doi.org/10.1061/(ASCE)0733-9372(2005)131:10(1433)

Wang, L., Emmerling, P. P., Zachary J. Henneman, & Nancollas, G. H. (2016). New Models for Calcium Phosphate Scale Formation and Dissolution. In Z. Amjad, *The science and technology of industrial water treatment* (1st ed., pp. 105–111). CRC Press.

Wentzel, M. C., Comeaus, Y., Ekama, G. A., Loosdrecht, M. van, & Brdjanovic, D. (2008). Enhanced Biological Phosphorus Removal. In M. Henze, M. van Loosdrecht, G. Ekama, & D. Brdjanovic (Eds.), *Biological wastewater treatment: Principles, modelling and design* (pp. 155–220). IWA Pub.

Wertman, J., MKeown, R., Derdour, L., & Dell'Orco, P. (2019). Crystallization Design and Scale-Up. In D. J. am Ende & M. T. am Ende (Eds.), *Chemical Engineering in the Pharmaceutical Industry: Active Pharmaceutical Ingredients* (2nd ed.). Wiley & Sons.

Whitaker, A., & Jeffery, J. W. (1970). The crystal structure of struvite, $MgNH_4PO_4 \cdot 6\ H_2O$. *Acta Crystallographica Section B Structural Crystallography and Crystal Chemistry*, *26*(10), 1429–1440. https://doi.org/10.1107/S0567740870004284

Wiesmann, U., Choi, I. S., & Dombrowski, E.-M. (2007). *Fundamentals of biological wastewater treatment*. Wiley-VCH.

Yates, J. G., & Lettieri, P. (2016). *Fluidized-Bed Reactors: Processes and Operating Conditions* (Vol. 26). Springer International Publishing. https://doi.org/10.1007/978-3-319-39593-7

Yeoman, S., Stephenson, T., Lester, J. N., & Perry, R. (1988). The removal of phosphorus during wastewater treatment: A review. *Environmental Pollution*, *49*(3), 183–233. https://doi.org/10.1016/0269-7491(88)90209-6

Zamora, P., Georgieva, T., Salcedo, I., Elzinga, N., Kuntke, P., & Buisman, C. J. (2017). Long-term operation of a pilot-scale reactor for phosphorus recovery as struvite from source-separated urine: Long-term operation of a pilot-scale reactor for phosphorus. *Journal of Chemical Technology & Biotechnology*, *92*(5), 1035–1045. https://doi.org/10.1002/jctb.5079

Zhang, T., Ding, L., & Ren, H. (2009). Pretreatment of ammonium removal from landfill leachate by chemical precipitation. *Journal of Hazardous Materials*, *166*(2–3), 911–915. https://doi.org/10.1016/j.jhazmat.2008.11.101

Zhang, T., Jiang, R., & Deng, Y. (2017). Phosphorus Recovery by Struvite Crystallization from Livestock Wastewater and Reuse as Fertilizer: A Review. In R. Farooq & Z. Ahmad (Eds.), *Physico-Chemical Wastewater Treatment and Resource Recovery* (pp. 135–152). IntechOpen. DOI: 10.5772/65692

Zumdahl, S. (2007). *Chemical Principles*. Cengage Learning.

Appendix A

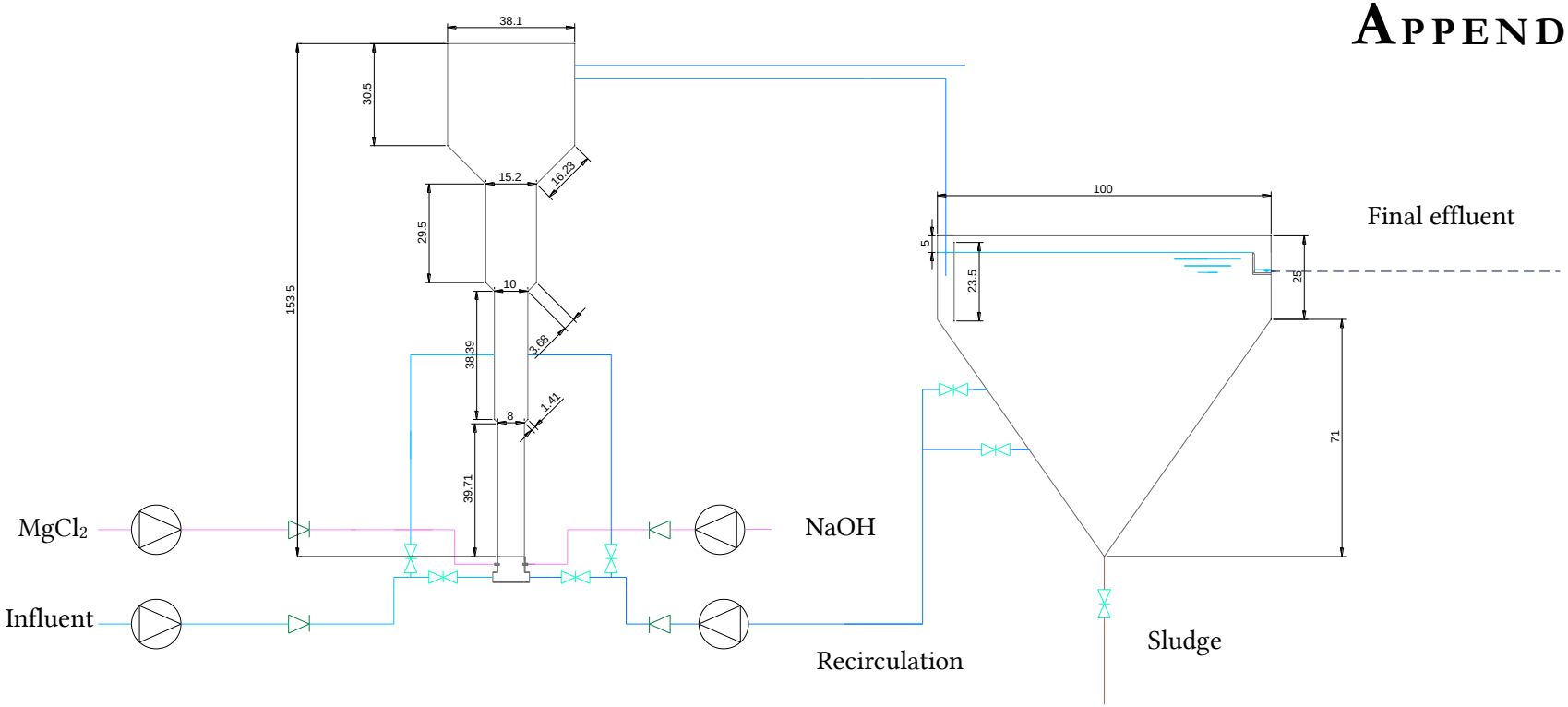

Legend:

- Influent
- Reagents
- Recirculation
- Sewer drain
- Pump
- Check valve
- Isolation valve
- Injection port

Appendix B

The reactor and the clarifier during construction.

Detail of the clarifier.

Appendix C

Finished reactor and the complementary constituents of the crystallization system at Chelas WWTP.

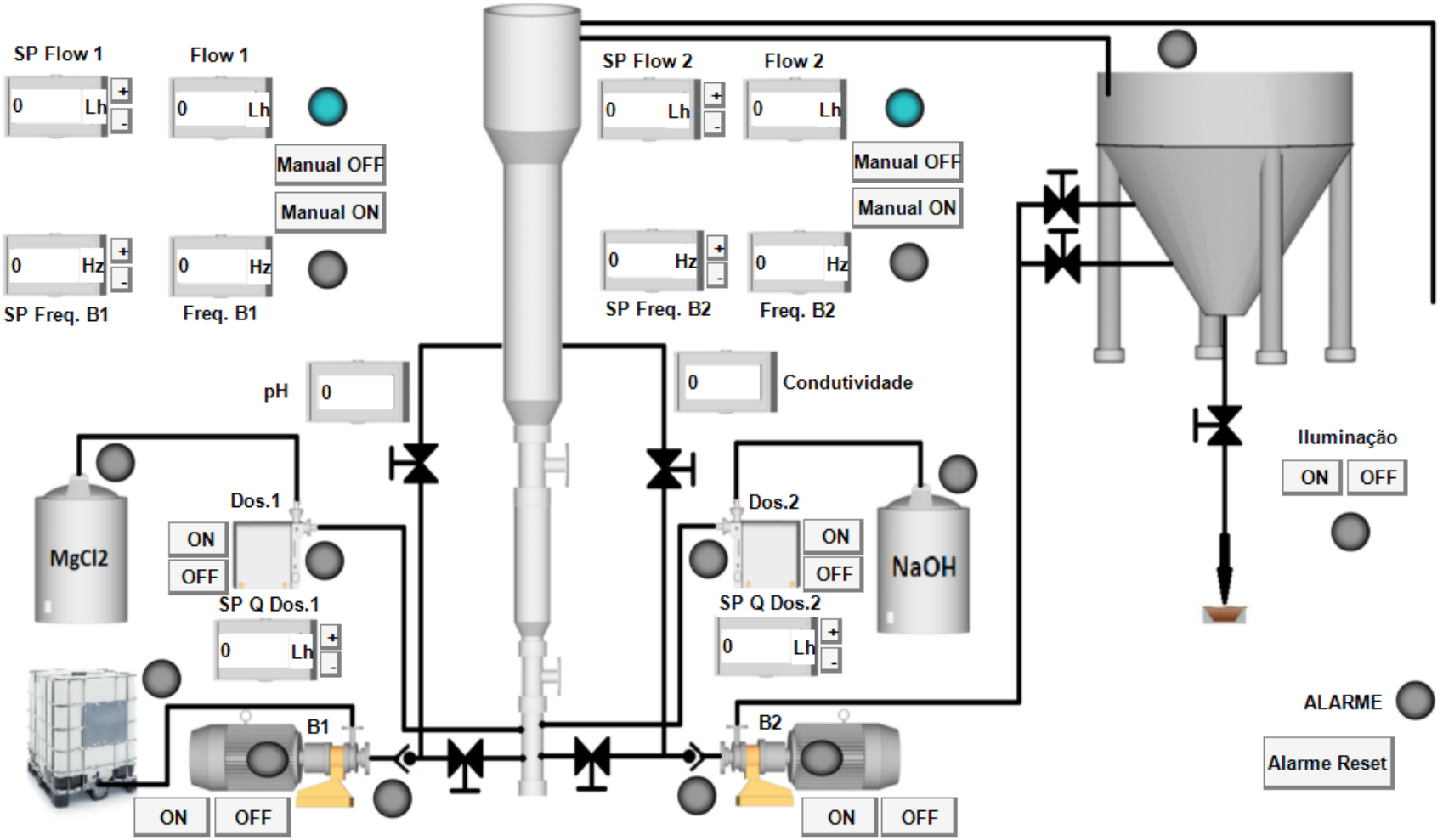

User interface of the reactors' programmable logic controller.